Time-Delay Estimation in Cognitive Radio and MIMO Systems

A THESIS

SUBMITTED TO THE DEPARTMENT OF ELECTRICAL AND

ELECTRONICS ENGINEERING

AND THE INSTITUTE OF ENGINEERING AND SCIENCES

OF BILKENT UNIVERSITY

IN PARTIAL FULFILLMENT OF THE REQUIREMENTS

FOR THE DEGREE OF

MASTER OF SCIENCE

By

Fatih Koçak

July 2010

I certify that I have read this thesis and that in my opinion it is fully adequate, in scope and in quality, as a thesis for the degree of Master of Science.

Asst. Prof. Dr. Sinan Gezici (Supervisor)

I certify that I have read this thesis and that in my opinion it is fully adequate, in scope and in quality, as a thesis for the degree of Master of Science.

Assoc. Prof. Dr. Ezhan Karaşan

I certify that I have read this thesis and that in my opinion it is fully adequate, in scope and in quality, as a thesis for the degree of Master of Science.

Asst. Prof. Dr. İbrahim Körpeoğlu

Approved for the Institute of Engineering and Sciences:

Prof. Dr. Levent Onural
Director of Institute of Engineering and Sciences

ABSTRACT

Time-Delay Estimation in Cognitive Radio and MIMO Systems

Fatih Koçak
M.S. in Electrical and Electronics Engineering
Supervisor: Asst. Prof. Dr. Sinan Gezici
July 2010

In this thesis, the time-delay estimation problem is studied for cognitive radio systems, multiple-input single-output (MISO) systems, and cognitive single-input multiple-output (SIMO) systems. A two-step approach is proposed for cognitive radio and cognitive SIMO systems in order to perform time-delay estimation with significantly lower computational complexity than the optimal maximum likelihood (ML) estimator. In the first step of this two-step approach, an ML estimator is used for each receiver branch in order to estimate the unknown parameters of the signal received via that branch. Then, in the second step, the estimates from the first step are combined in various ways in order to obtain the final time-delay estimate. The combining techniques that are used in the second step are called optimal combining, signal-to-noise ratio (SNR) combining, selection combining, and equal combining. It is shown that the performance of the optimal combining technique gets very close to the Cramer-Rao lower bound (CRLB) at high SNRs.

These combining techniques provide various mechanisms for diversity combining for time-delay estimation and extend the concept of diversity in communications systems to the time-delay estimation problem in cognitive radio and cognitive SIMO systems. Simulation results are presented to evaluate the performance of the proposed estimators and to verify the theoretical analysis. For the solution of the time-delay estimation problem in MISO systems, ML estimation based on a genetic global optimization algorithm, namely, differential evolution (DE), is proposed. This approach is proposed in order to decrease the computational complexity of the ML estimator, which results in a complex optimization problem in general. A theoretical analysis is carried out by deriving the CRLB. Simulation studies for Rayleigh and Rician fading scenarios are performed to investigate the performance of the proposed algorithm.

Keywords: Time-delay estimation, cognitive radio, multiple-input single-output (MISO) systems, cognitive single-input multiple-output (SIMO) systems, differential evolution (DE), maximum likelihood (ML) estimator, Cramer-Rao lower bound (CRLB).

ÖZET

BİLİŞSEL RADYO SİSTEMLERİNDE VE ÇOK GİRİŞLİ ÇOK ÇIKIŞLI SİSTEMLERDE ZAMAN GECİKMESİ KESTİRİMİ

Fatih Koçak
Elektrik ve Elektronik Mühendisliği Bölümü Yüksek Lisans
Tez Yöneticisi: Yrd. Doç. Dr. Sinan Gezici
Temmuz 2010

Bu tezde, bilişsel radyo sistemleri, çok girişli tek çıkışlı sistemler ve bilişsel tek girişli çok çıkışlı sistemlerde zaman gecikmesi kestirimi problemi çalışılmaktadır. Bilişsel radyo sistemlerinde ve bilişsel tek girişli çok çıkışlı sistemlerde ideal en büyük olabilirlik kestiricisinden önemli derecede daha düşük bir berimsel karmaşıklıkla zaman gecikmesi kestirimi yapmak amacıyla iki aşamalı bir yaklaşım önerilmektedir. Bu önerilen iki aşamalı yaklaşımın ilk aşamasında, her alıcı dalı için o dal yoluyla alınan sinyale ait bilinmeyen parametreleri kestirmek amacıyla bir en büyük olabilirlik kestiricisi kullanılmaktadır. Sonra, ikinci aşamada, birinci aşamada elde edilen tahminler son zaman gecikmesi tahminini elde etmek amacıyla çeşitli yollarla birleştirilmektedir. İdeal birleştirme, sinyal gürültü oranlı birleştirme, seçici birleştirme ve eşit birleştirme ikinci aşamada kullanılan birleştirme teknikleridir. İdeal birleştirme tekniğinin performansının yüksek sinyal gürültü oranlarında Cramer-Rao alt sınırına çok yaklaştığı gösterilmektedir. Bu

birleştirme teknikleri zaman gecikmesi kestirimine yönelik çeşitleme birleştirme için birçok mekanizma sunmaktadır ve haberleşme sistemlerindeki çeşitlilik konseptini bilişsel radyo sistemlerinde ve bilişsel tek girişli çok çıkışlı sistemlerde zaman gecikmesi kestirimi problemine genişletmektedir. Önerilen kestiricilerin performansını değerlendirmek ve teorik analizi doğrulamak amacıyla benzetim sonuçları sunulmaktadır. Çok girişli tek çıkışlı sistemlerdeki zaman gecikmesi kestirimi probleminin çözümü için bir global eniyileme algoritması olan diferansiyel gelişim tabanlı en büyük olabilirlik kestirimi öne sürülmektedir. Bu yaklaşım, genelde karmaşık bir eniyileme problemiyle sonuçlanan en büyük olabilirlik kestiricisinin berimsel karmaşıklığını azaltmak amacıyla öne sürülmektedir. Cramer-Rao alt sınırı türetilerek bir teorik analiz yapılmaktadır. Önerilen algoritmanın performansını incelemek amacıyla Rayleigh ve Rician sönümlenme senaryoları için benzetim çalışmaları yapılmaktadır.

Anahtar Kelimeler: Zaman gecikmesi kestirimi, bilişsel radyo, çok girişli tek çıkışlı sistemler, bilişsel tek girişli çok çıkışlı sistemler, diferansiyel gelişim, en büyük olabilirlik kestirimi, Cramer-Rao alt sınırı.

ACKNOWLEDGMENTS

I would like to express my special thanks to my supervisor Asst. Prof. Dr. Sinan Gezici whose guidance became a torch in my hands that enlightened my research path and who turned the preparation of this thesis into fun.

I am grateful to Assoc. Prof. Dr. Ezhan Karaşan and Asst. Prof. Dr. İbrahim Körpeoğlu for their valuable contributions by taking place in my thesis defense committee.

I would also like to thank Prof. H. Vincent Poor, Dr. Hasari Celebi, Prof. Dr. Khalid A. Qaraqe, Prof. Dr. Huseyin Arslan, and Dr. Onay Urfalıoğlu for their precious contributions to my thesis.

My final gratitude is to my family, who did not hesitate to support me during the preparation of this thesis, like in every step of my life.

Contents

List of Figures

To Science and Scientists ...

Chapter 1

Introduction

1.2 Background

1.2.1 Cognitive Radio Systems

Cognitive radio is a promising approach to implement intelligent wireless communications systems [1]-[8]. Cognitive radios can be perceived as more capable versions of software defined radios in the sense that they have sensing, awareness, learning, adaptation, goal driven autonomous operation and reconfigurability features [9], [10]. In Figure 1.1, the basic functional blocks of a cognitive radio are illustrated [11].

As a result of the aforementioned features of cognitive radio systems, radio resources, such as power and bandwidth, can be used more efficiently [1]. Especially since the electromagnetic spectrum is a precious resource, it must not be wasted. The recent spectrum measurement campaigns in the United States [12] and Europe [13] show that the spectrum is under-utilized; hence, opportunistic use of unoccupied frequency bands is highly desirable.

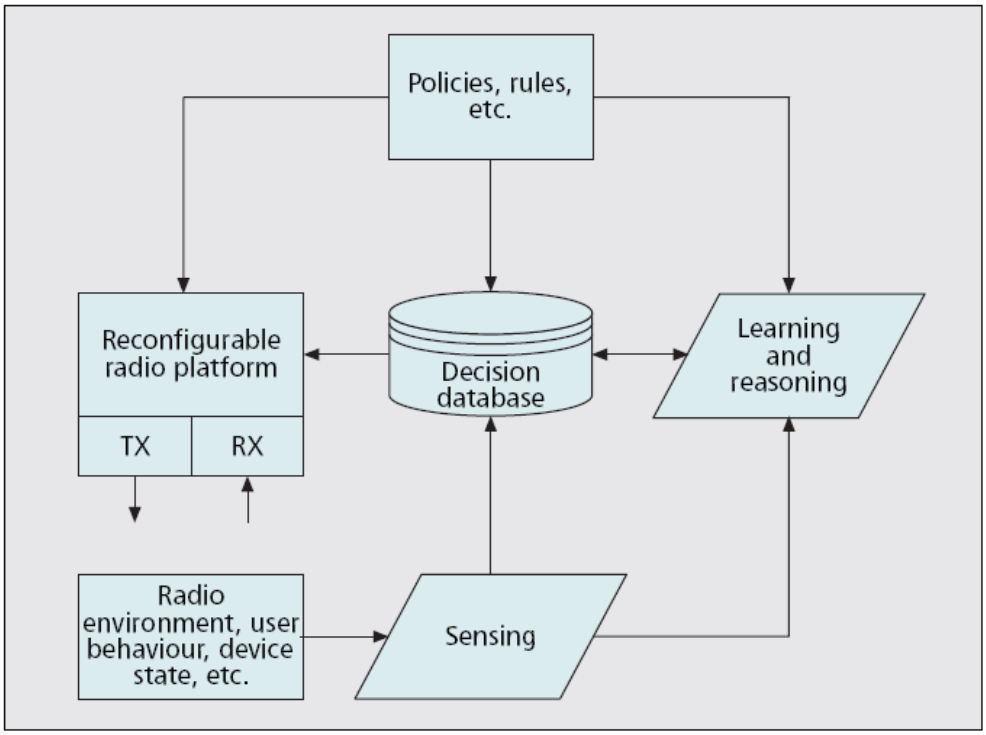

Figure 1.1: The structure of a cognitive radio system [11].

Cognitive radio provides a solution to the problem of inefficient spectrum utilization by using the vacant frequency spectrum over time in a certain geographical region. In other words, a cognitive radio system can opportunistically use the available spectrum of a legacy system without interfering with the licensed users of that spectrum [2, 3]. An example of spectrum usage in a cognitive radio network can be seen in Figure 1.2 [14].

1.2.2 Multiple-Input Multiple-Output Systems

A multiple-input multiple-output (MIMO) system uses multiple antennas at the transmitter and the receiver in order to provide space diversity [15]. MIMO

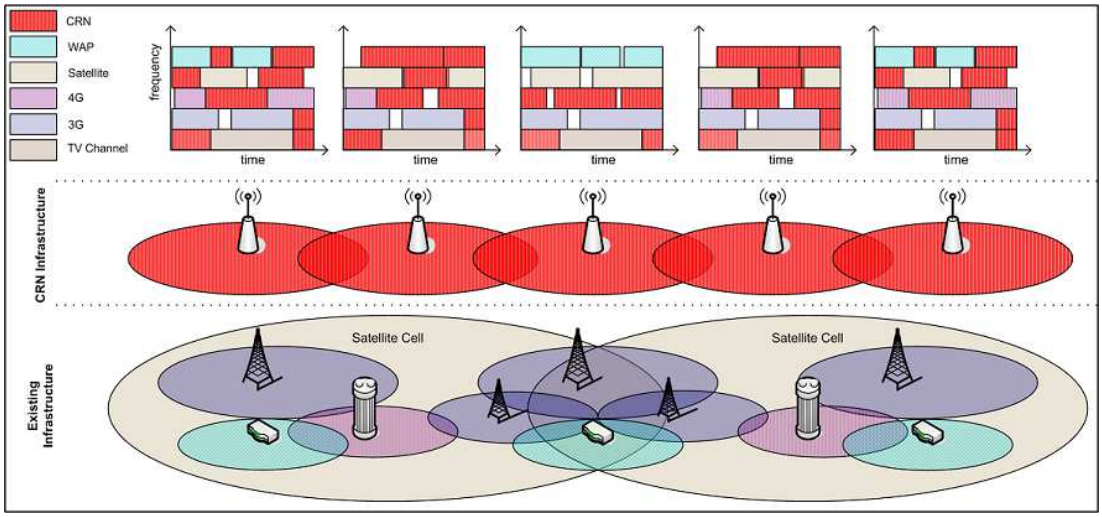

Figure 1.2: An example of opportunistic spectrum usage in a cognitive radio network [14].

systems will be used very widely in future communications systems since they provide advantages in terms of quality, reliability and capacity [15], [16]. An example of a MIMO structure is depicted in Figure 1.3.

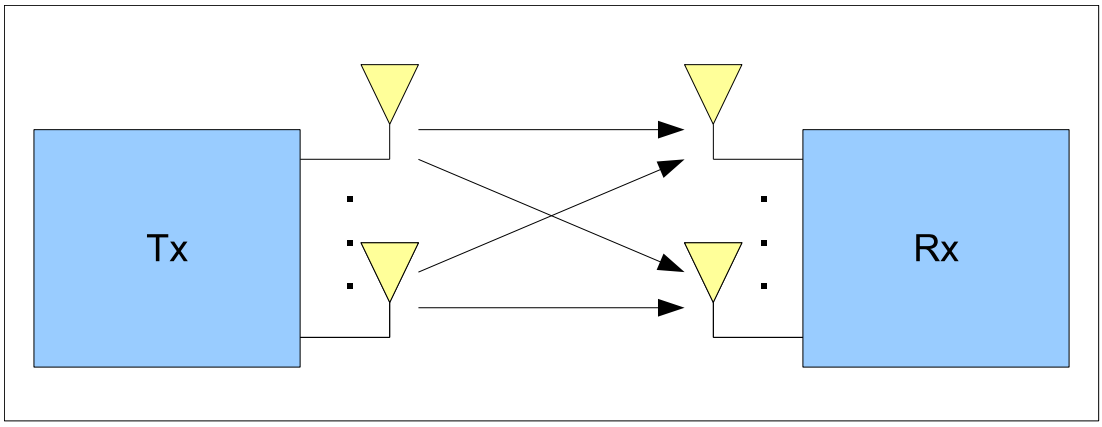

Figure 1.3: An example of a MIMO system.

Multiple-input single-output (MISO) systems, which are special cases of MIMO

systems, have multiple antennas at the transmitter but have a single antenna at the receiver. In this case, the space diversity can be called as the transmit diversity. Similarly, single-input multiple-output (SIMO) systems have a single antenna at the transmitter side and multiple antennas at the receiver side. SIMO systems also have space diversity, which can be called as receive diversity, since their multiple antenna structure is at the receiver side.

1.2.3 Cognitive Multiple-Input Multiple-Output Systems

Employment of the MIMO structure in cognitive radio systems brings the space diversity advantages of MIMO to cognitive radio networks [17], [18]. The resulting system can be called a cognitive MIMO radio [19], [20]. There are a few studies on cognitive radio MIMO networks, such as [21], since it is a relatively new topic resulting from the mergence of two hot research topics.

In cognitive MIMO radio systems, diversity is utilized in 2 dimensions, which are space and frequency. Space diversity results from the MIMO structure as mentioned before. Frequency diversity is a consequence of the dispersed spectrum utilization feature of cognitive radios. A cognitive radio can detect the vacant spectral bands at an arbitrary time and place. It can use multiple of those frequency bands if they are available. Therefore, using multiple dispersed frequency bands introduces frequency diversity to the cognitive radio system [22].

1.2.4 Positioning

Facilitating wireless networks in positioning applications besides the communications applications has been getting a growing attention recently [23]. There are a lot of application areas and services that make use of positioning techniques.

The typical examples for outdoor systems are enhanced 911 (E911), improved fraud detection, cellular system design and management, mobile yellow pages, location-based billing, intelligent transport systems, improved transport systems and the global positioning system (GPS) [24], [25]. For short-range networks and indoor positioning systems, inventory tracking, intruder detection, tracking of fire-fighters and miners, home automation and patient monitoring applications are examples that employ wireless positioning techniques [26].

Since positioning is an important application area of wireless systems, it is important to quantify the advantages of space diversity, which is utilized in MIMO systems, for positioning applications. Although the advantages of space diversity are investigated thoroughly for communications purposes [27] and radar systems [28], [29], [30], there are a few studies in the literature that investigate the effects of space diversity for positioning purposes. For example, [31] studies the space diversity that can be obtained via the use of multiple receive antennas. Mainly, it obtains the theoretical limits, in terms of the Cramer-Rao lower bound (CRLB), on range (equivalently, time-delay) estimation, and proposes a two-step asymptotically optimal range estimator.

It is mentioned in Section 1.2.1 that cognitive radios are able to facilitate opportunistic spectrum utilization. Therefore, it is important that cognitive radio devices are aware of their positions and monitor the environment continuously. These location and environmental awareness features of cognitive radios have been studied extensively in the literature [10], [32]-[38]. In [32], the concept of cognitive radar is introduced, which provides information related to the objects in an environment; i.e., it performs environmental sensing. In [33], a radio environment mapping method for cognitive radio networks is studied. Conceptual

models for location and environmental awareness engines and cycles are proposed in [10], [34] and [35] for cognitive radio systems. Also, [37] introduces the concept of a topology engine for cognitive radios by studying topology information characterization and its applications to cognitive radio networks. The location awareness feature of cognitive radios can also be used in many network optimization applications, such as location-assisted spectrum management, network planning, handover, routing, dynamic channel allocation and power control [8], [39].

1.3 Thesis Outline

In Chapter 2, the time-delay estimation problem in cognitive radio systems is analyzed. In Section 2.1, the signal model is introduced and the signal at each branch of the receiver is described. In Section 2.2, the optimal ML receiver is obtained, and the CRLBs on time delay estimation in dispersed spectrum cognitive radio systems are described. The proposed two-step time delay estimation approach is studied in Section 2.3. Then, in Section 2.4, the optimality properties of the proposed time delay estimators are investigated. Finally, simulation results are presented in Section 2.5.

In Chapter 3, the analysis of the time-delay estimation problem in MISO systems is performed. First, the signal model is constructed in Section 3.1. Then, the maximum likelihood (ML) time-delay estimator is provided and a theoretical analysis is performed in Section 3.2 by deriving the CRLB on time-delay estimation in a MISO system. In Section 3.3, a genetic global optimization algorithm, called differential evolution (DE), is used to estimate the time-delay parameter

from the ML estimator formulation. In that way, the CRLB can be achieved at high SNRs with a significantly lower computational complexity than the direct solution of the ML estimator via an exhaustive search. In DE, a number of parameter vectors are generated and updated at each generation in order to reach the global optimum [40], and these vectors encounter mutation, crossover, and selection steps at each generation [41]. Finally, simulation results are presented.

In Chapter 4, the time-delay estimation problem in cognitive SIMO systems is analyzed. This part of the thesis starts with the signal model in Section 4.1. Then, in Section 4.2, the theoretical bound for the estimation of the time-delay parameter after determining the log-likelihood function and the unknown parameters. Next, a two-step time-delay estimation algorithm is proposed, which is similar to the one proposed for cognitive radio systems in Chapter 2. This two-step approach includes ML estimation in every receiver branch and combination of the time-delay estimates of each branch in various ways in order to find the final time-delay estimate. In Section 4.6, the simulation results are provided.

Chapter 2

TIME-DELAY ESTIMATION IN DISPERSED SPECTRUM COGNITIVE RADIO SYSTEMS

Location awareness requires that a cognitive radio device performs accurate estimation of its position. One possible way of obtaining position information is to use the Global Positioning System (GPS) technology in cognitive radio systems. However, this is not a very efficient or cost-effective solution [36]. As another approach, cognitive radio devices can estimate position related parameters of signals traveling between them in order to estimate their positions [36], [23]. Among various position related parameters, the time-delay parameter commonly provides accurate position information with reasonable complexity [23], [42]. The main focus of Chapter 2 is time-delay estimation in cognitive radio systems. In other words, the aim is to propose techniques for accurate time-delay estimation in dispersed spectrum systems in order to provide accurate location information to

cognitive users. Since the accuracy of location estimation increases as the accuracy of time-delay estimation increases, design of time-delay estimators with high accuracy and reasonable complexity is crucial for the location awareness feature of a cognitive radio system [23].

Time-delay estimation in cognitive radio systems differs from conventional time-delay estimation mainly due to the fact that a cognitive radio system can transmit and receive over multiple dispersed bands. In other words, since a cognitive radio device can utilize the spectral holes of a legacy system, it can have a spectrum that consists of multiple bands that are dispersed over a wide range of frequencies (cf. Figure 2.1). In [43], the theoretical limits on time-delay estimation are studied for dispersed spectrum cognitive radio systems, and the effects of carrier frequency offset (CFO) and modulation schemes of training signals on the accuracy of time-delay estimation are quantified. The expressions for the theoretical limits indicate that frequency diversity can be utilized in time-delay estimation. Similarly, the effects of spatial diversity on time-delay estimation are studied in [31] for single-input multiple-output (SIMO) systems. In addition, the effects of multiple antennas on time-delay estimation and synchronization problems are investigated in [44].

In this chapter, time-delay estimation is studied for dispersed spectrum cognitive radio systems. First, it is observed that maximum likelihood (ML) estimation is not very practical for time-delay estimation in such systems. Then, a two-step time-delay estimation approach is proposed in order to provide accurate time-delay estimation with significantly lower computational complexity than that of the optimal ML estimator. In the proposed scheme, the receiver consists of multiple branches and each branch processes the part of the received signal

that occupies the corresponding frequency band. An ML estimator is used in each branch in order to estimate the unknown parameters of the signal observed in that branch. Then, in the second step, the estimates from all the branches are combined to obtain the final time-delay estimate. Various techniques are proposed for the combining operation in the second step: Optimal combining, signal-to-noise ratio (SNR) combining, selection combining, and equal combining. The biases and variances of the time-delay estimators that employ these combining techniques are investigated. It is shown that the optimal combining technique results in a mean-squared error (MSE) that approximates the Cramer-Rao lower bound (CRLB) at high SNRs. Simulation results are provided in order to compare the performance of the proposed time-delay estimators. In a more generic perspective, this study focuses on the utilization of frequency diversity for a parameter estimation problem. Therefore, the proposed estimators can be applied to other systems that have frequency diversity as well.

2.1 Signal Model

A cognitive radio system that occupies K dispersed frequency bands is considered as shown in Figure 2.1. The transmitter sends a signal occupying all the K bands simultaneously, and the receiver aims to calculate the time-delay of the incoming signal [45].

One approach for designing such a system involves the use of orthogonal frequency division multiplexing (OFDM). In this approach, the received signal is considered as a single OFDM signal with zero coefficients at the sub-carriers

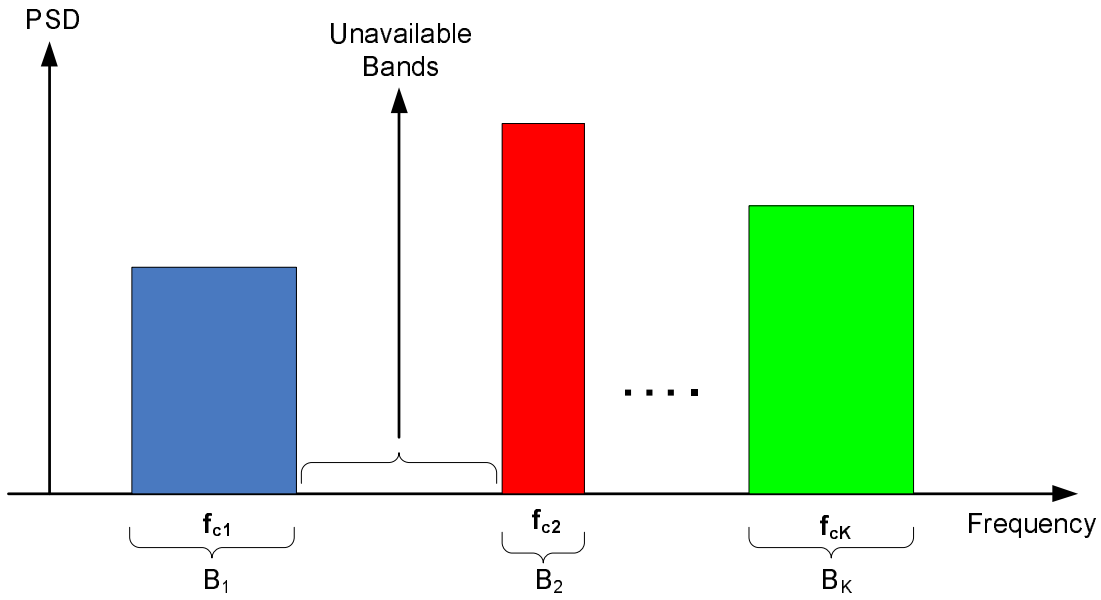

Figure 2.1: Illustration of dispersed spectrum utilization in cognitive radio systems [22].

corresponding to the unavailable bands [46]-[48]. Then, the signal can be processed as in conventional OFDM receivers. The main drawback of this approach is that it requires processing of very large bandwidths when the available spectrum is dispersed over a wide range of frequencies. Therefore, the design of RF components, such as filters and low-noise amplifiers (LNAs) can become very complex and costly, and result in components with high power consumption [25]. In such scenarios, it can be more practical to process the received signal in multiple branches, as shown in Figure 2.2. In that case, each branch processes one available band, and down-converts the signal according to the center frequency of that band. Therefore, signals with narrower bandwidths can be processed at each branch [22].

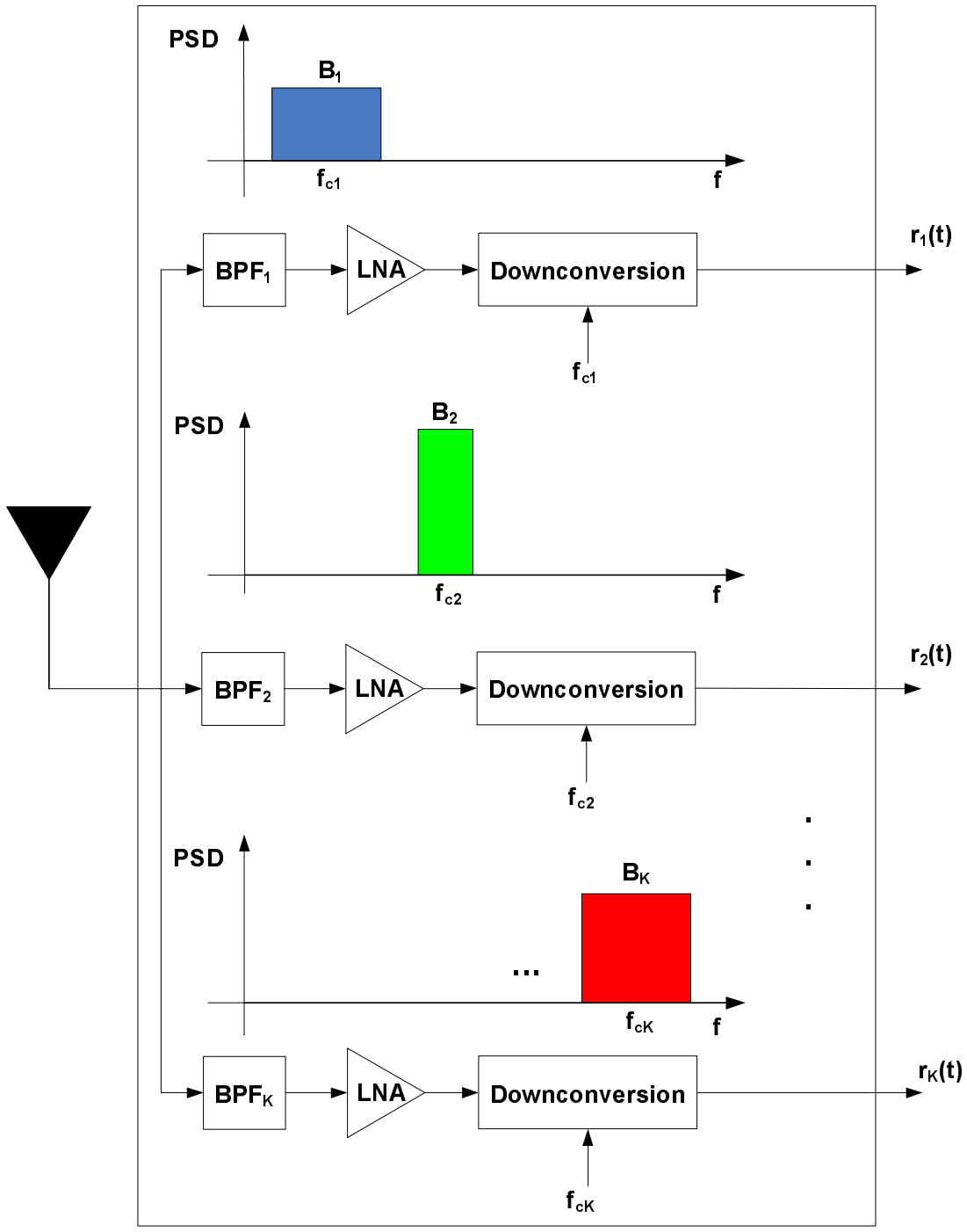

Figure 2.2: Block diagram of the front-end of a cognitive radio receiver, where BPF and LNA refer to band-pass filter and low-noise amplifier, respectively [22].

For the receiver model in Figure 2.2, the baseband representation of the received signal in the ith branch can be modeled as

$$r_i(t) = \alpha_i \, \mathrm{e}^{j\omega_i t} s_i(t-\tau) + n_i(t) \ , \tag{2.1}$$

for $i = 1, \ldots, K$, where τ is the time-delay of the signal, $\alpha_i = a_i \, \mathrm{e}^{j\phi_i}$ and ω_i represent, respectively, the channel coefficient and the CFO for the signal in the ith branch, $s_i(t)$ is the baseband representation of the transmitted signal in the ith band, and $n_i(t)$ is modeled as complex white Gaussian noise with independent components, each having spectral density σ_i^2.

The signal model in (2.1) assumes that the signal in each branch can be modeled as a narrowband signal. Hence, a single complex channel coefficient is used to represent the fading of each signal.

The system model considered in this study falls within the framework of cognitive radio systems, since the cognitive user first needs to detect the available frequency bands, and then to adapt its receiver parameters accordingly. Therefore, the spectrum sensing and adaptation features of cognitive systems are assumed for the considered system in this study [9], [10].

2.2 Optimal Time-Delay Estimation and Theoretical Limits

Accurate estimation of the time-delay parameter τ in (2.1) is quite challenging due to the presence of unknown channel coefficients and CFOs. For a system with K bands, there are $3K$ nuisance parameters. In other words, the vector $\boldsymbol{\theta}$

of unknown parameters can be expressed as

$$\boldsymbol{\theta} = [\tau \; a_1 \cdots a_K \; \phi_1 \cdots \phi_K \; \omega_1 \cdots \omega_K] \; . \tag{2.2}$$

When the signals in (2.1) are observed over the interval $[0, T]$, the log-likelihood function for $\boldsymbol{\theta}$ is given by [49]

$$\Lambda(\boldsymbol{\theta}) = c - \sum_{i=1}^{K} \frac{1}{2\sigma_i^2} \int_0^T \left| r_i(t) - \alpha_i \, \mathrm{e}^{j\omega_i t} s_i(t-\tau) \right|^2 \mathrm{d}t \; , \tag{2.3}$$

where c is a constant that is independent of $\boldsymbol{\theta}$ (the unknown parameters are assumed to be constant during the observation interval). Then, the ML estimate for $\boldsymbol{\theta}$ can be obtained from (2.3) as [43]

$$\hat{\boldsymbol{\theta}}_{\mathrm{ML}} = \arg\max_{\boldsymbol{\theta}} \left\{ \sum_{i=1}^{K} \frac{1}{\sigma_i^2} \int_0^T \mathcal{R}\left\{ \alpha_i^* \mathrm{e}^{-j\omega_i t} r_i(t) s_i^*(t-\tau) \right\} \mathrm{d}t - \sum_{i=1}^{K} \frac{E_i |\alpha_i|^2}{2\sigma_i^2} \right\} \; , \tag{2.4}$$

where $E_i = \int_0^T |s_i(t-\tau)|^2 \mathrm{d}t$ is the signal energy, and $\mathcal{R}$ represents the operator that selects the real-part of its argument.

It is observed from (2.4) that the ML estimator requires an optimization over a $(3K+1)$-dimensional space, which is quite challenging in general. Therefore, the aim of this study is to propose low-complexity time-delay estimation algorithms with comparable performance to that of the ML estimator in (2.4). In other words, accurate time-delay estimation algorithms are studied under practical constraints on the processing power of the receiver. Since the ML estimator is difficult to implement, the performance comparisons will be performed with respect to the theoretical limits on time-delay estimation (of course, an ML estimator achieves the CRLB asymptotically under certain conditions [49]). In [43], the CRLBs on the mean-squared errors (MSEs) of unbiased time-delay estimators

are obtained for the signal model in (2.1). When the baseband representation of the signals in different branches are of the form $s_i(t) = \sum_l d_{i,l} p_i(t - lT_i)$, where $d_{i,l}$ denotes the complex training data and $p_i(t)$ is a pulse with duration T_i, the CRLB is expressed as

$$\mathrm{E}\{(\hat{\tau} - \tau)^2\} \geq \left(\sum_{i=1}^{K} \frac{a_i^2}{\sigma_i^2} \left(\tilde{E}_i - (\hat{E}_i^{\mathrm{R}})^2 / E_i \right) \right)^{-1} , \tag{2.5}$$

where

$$\tilde{E}_i = \int_0^T |s_i'(t - \tau)|^2 \mathrm{d}t \ , \tag{2.6}$$

and

$$\hat{E}_i^{\mathrm{R}} = \int_0^T \mathcal{R}\{s_i'(t - \tau_i) s_i^*(t - \tau_i)\} \mathrm{d}t \ , \tag{2.7}$$

with $s'(t)$ representing the first derivative of $s(t)$. In the special case of $|d_{i,l}| = |d_i|$ $\forall l$ and $p_i(t)$ satisfying $p_i(0) = p_i(T_i)$ for $i = 1, \ldots, K$, (2.5) becomes [43]

$$\mathrm{E}\{(\hat{\tau} - \tau)^2\} \geq \left(\sum_{i=1}^{K} \frac{\tilde{E}_i \, a_i^2}{\sigma_i^2} \right)^{-1} . \tag{2.8}$$

It is observed from (2.5) and (2.8) that frequency diversity can be useful in time-delay estimation. For example, when one of the bands is in a deep fade (i.e., small a_i^2), some other bands can still be in good condition to facilitate accurate time-delay estimation.

2.3 Two-Step Time-Delay Estimation and Diversity Combining

Due to the complexity of the ML estimator in (2.4), a two-step time-delay estimation approach is proposed in this study, as shown in Figure 2.3. Two-step

approaches are commonly used in optimization/estimation problems in order to provide suboptimal solutions with reduced computational complexity [50, 51]. In the proposed estimator, each branch of the receiver performs estimation of the time-delay, the channel coefficient and the CFO related to the signal in that branch. Then, the estimates from all the branches are used to obtain the final time-delay estimate as shown in Figure 2.3. In the following sections, the details of the proposed approach are explained, and the utilization of frequency diversity in time-delay estimation is explained.

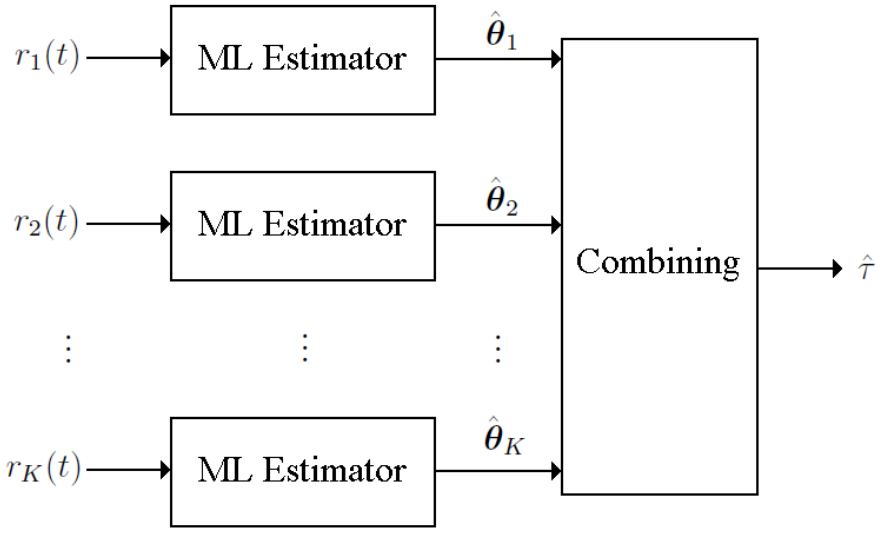

Figure 2.3: The block diagram of the proposed time-delay estimation approach. The signals $r_1(t), \ldots, r_K(t)$ are obtained at the front-end of the receiver as shown in Figure 2.2.

2.3.1 First Step: Parameter Estimation at Different Branches

In the first step of the proposed approach, the unknown parameters of each received signal are estimated at the corresponding receiver branch according to the

ML criterion (cf. Figure 2.3). Based on the signal model in (2.1), the likelihood function at branch i can be expressed as

$$\Lambda_i(\boldsymbol{\theta}_i) = c_i - \frac{1}{2\sigma_i^2} \int_0^T \left| r_i(t) - \alpha_i \, \mathrm{e}^{j\omega_i t} s_i(t-\tau) \right|^2 \mathrm{d}t \ , \tag{2.9}$$

for $i = 1, \ldots, K$, where $\boldsymbol{\theta}_i = [\tau \ a_i \ \phi_i \ \omega_i]$ represents the vector of unknown parameters related to the signal at the ith branch, $r_i(t)$, and c_i is a constant that is independent of $\boldsymbol{\theta}_i$.

From (2.9), the ML estimator at branch i can be stated as

$$\hat{\boldsymbol{\theta}}_i = \arg\min_{\boldsymbol{\theta}_i} \int_0^T \left| r_i(t) - \alpha_i \, \mathrm{e}^{j\omega_i t} s_i(t-\tau) \right|^2 \mathrm{d}t \ , \tag{2.10}$$

where $\hat{\boldsymbol{\theta}}_i = [\hat{\tau}_i \ \hat{a}_i \ \hat{\phi}_i \ \hat{\omega}_i]$ is the vector of estimates at the ith branch. After some manipulation, the solution of (2.10) can be obtained as

$$\left[\hat{\tau}_i \ \hat{\phi}_i \ \hat{\omega}_i \right] = \arg \max_{\phi_i, \omega_i, \tau_i} \left| \int_0^T \mathcal{R} \left\{ r_i(t) \, \mathrm{e}^{-j(\omega_i t + \phi_i)} s_i^*(t-\tau_i) \right\} \mathrm{d}t \right| \tag{2.11}$$

and

$$\hat{a}_i = \frac{1}{E_i} \int_0^T \mathcal{R} \left\{ r_i(t) \, \mathrm{e}^{-j(\hat{\omega}_i t + \hat{\phi}_i)} s_i^*(t-\hat{\tau}_i) \right\} \mathrm{d}t \ . \tag{2.12}$$

In other words, at each branch, optimization over a three-dimensional space is required to obtain the unknown parameters. Compared to the ML estimator in Section 2.2, the optimization problem in (2.4) over $(3K+1)$ variables is reduced to K optimization problems over three variables, which results in a significant amount of reduction in the computational complexity.

In the absence of CFO; i.e., $\omega_i = 0 \ \forall i$, (2.11) and (2.12) reduce to

$$\left[\hat{\tau}_i \ \hat{\phi}_i \right] = \arg \max_{\phi_i, \tau_i} \left| \int_0^T \mathcal{R} \left\{ r_i(t) \, \mathrm{e}^{-j\phi_i} s_i^*(t-\tau_i) \right\} \mathrm{d}t \right| \tag{2.13}$$

and

$$\hat{a}_i = \frac{1}{E_i} \int_0^T \mathcal{R}\left\{ r_i(t)\, \mathrm{e}^{-j\hat{\phi}_i} s_i^*(t - \hat{\tau}_i) \right\} \mathrm{d}t \ . \tag{2.14}$$

In that case, the optimization problem at each branch is performed over only two dimensions. This scenario is valid when the carrier frequency of each band is known accurately.

2.3.2 Second Step: Combining Estimates from Different Branches

After obtaining K different time-delay estimates, $\hat{\tau}_1, \ldots, \hat{\tau}_K$, in (2.11), the second step combines those estimates according to one of the criteria below and makes the final time-delay estimate (cf. Figure 2.3).

Optimal Combining

According to the "optimal" combining criterion (the optimality properties of this combining technique are investigated in Section 2.4), the time-delay estimate is obtained as

$$\hat{\tau} = \frac{\sum_{i=1}^{K} \kappa_i \, \hat{\tau}_i}{\sum_{i=1}^{K} \kappa_i} \ , \tag{2.15}$$

where $\hat{\tau}_i$ is the time-delay estimate of the ith branch, which is obtained from (2.11), and

$$\kappa_i = \frac{\hat{a}_i^2 \tilde{E}_i}{\sigma_i^2} \ , \tag{2.16}$$

with $\tilde{E}_i$ being defined in (2.6). In other words, the optimal combining technique estimates the time-delay as a weighted average of the time-delays of different

branches, where the weights are chosen as proportional to the multiplication of the SNR estimate, $E_i\hat{a}_i^2/\sigma_i^2$, and $\tilde{E}_i/E_i$. Since $\tilde{E}_i$ is defined as the energy of the first derivative of $s_i(t)$ as in (2.6), $\tilde{E}_i/E_i$ can be expressed, using Parseval's relation, as $\tilde{E}_i/E_i = 4\pi^2\beta_i^2$, where β_i is the effective bandwidth of $s_i(t)$, which is defined as [49]

$$\beta_i^2 = \frac{1}{E_i}\int_{-\infty}^{\infty} f^2|S_i(f)|^2\mathrm{d}f \ , \tag{2.17}$$

with $S_i(f)$ denoting the Fourier transform of $s_i(t)$. Therefore, it is concluded that the optimal combining technique assigns a weight to the time-delay estimate of a given branch in proportion to the product of the SNR estimate and the effective bandwidth related to that branch. The intuition behind this combining technique is the fact that signals with larger effective bandwidths and/or larger SNRs facilitate more accurate time-delay estimation [49]; hence, their weights should be larger in the combining process. This intuition is verified theoretically in Section 2.4.

SNR Combining

The second technique combines the time-delay estimates in the first step according to the SNR estimates at the respective branches. In other words, the time-delay estimate is obtained as

$$\hat{\tau} = \frac{\sum_{i=1}^{K}\gamma_i\,\hat{\tau}_i}{\sum_{i=1}^{K}\gamma_i} \ , \tag{2.18}$$

where

$$\gamma_i = \frac{\hat{a}_i^2 E_i}{\sigma_i^2} \ . \tag{2.19}$$

Note that γ_i defines the SNR estimate at branch i. In other words, this technique considers only the SNR estimates at the branches in order to determine the combining coefficients, and does not take the signal bandwidths into account.

It is observed from (2.15)-(2.19) that the optimal combining and the SNR combining techniques become equivalent if $\tilde{E}_1/E_1 = \cdots = \tilde{E}_K/E_K$. Since $\tilde{E}_i/E_i = 4\pi^2\beta_i^2$, where β_i is the effective bandwidth defined in (2.17), the two techniques are equivalent when the effective bandwidths of the signals at different branches are all equal.

Selection Combining-1 (SC-1)

Another technique for obtaining the final time-delay estimate is to determine the "best" branch and to use its estimate as the final time-delay estimate. According to SC-1, the best branch is defined as the one that has the maximum value of $\kappa_i = \hat{a}_i^2\tilde{E}_i/\sigma_i^2$ for $i = 1, \ldots, K$. In other words, the branch with the maximum multiplication of the SNR estimate and the effective bandwidth is determined as the best branch and its estimate is used as the final one. That is,

$$\hat{\tau} = \hat{\tau}_m \ , \qquad m = \arg \max_{i \in \{1,\ldots,K\}} \left\{ \hat{a}_i^2 \tilde{E}_i/\sigma_i^2 \right\} \ , \tag{2.20}$$

where $\hat{\tau}_m$ represents the time-delay estimate at the mth branch.

Selection Combining-2 (SC-2)

Similar to SC-1, SC-2 selects the "best" branch and uses its estimate as the final time-delay estimate. However, according to SC-2, the best branch is defined as the one with the maximum SNR. Therefore, the time-delay estimate is obtained

as follows according to SC-2:

$$\hat{\tau} = \hat{\tau}_m \ , \qquad m = \arg \max_{i \in \{1,\ldots,K\}} \left\{ \hat{a}_i^2 E_i / \sigma_i^2 \right\} \ , \tag{2.21}$$

where $\hat{\tau}_m$ represents the time-delay estimate at the mth branch.

SC-1 and SC-2 become equivalent when the effective bandwidths of the signals at different branches are all equal.

Equal Combining

The equal combining technique assigns equal weights to the estimates from different branches and obtains the time-delay estimate as follows:

$$\hat{\tau} = \frac{1}{K} \sum_{i=1}^{K} \hat{\tau}_i \ . \tag{2.22}$$

Considering the proposed combining techniques above, it is observed that they are similar to diversity combining techniques in communications systems [52]. However, the main difference is the following. The aim is to maximize the SNR or to reduce the probability of symbol error in communications systems [52], whereas, in the current problem, it is to reduce the MSE of time-delay estimation. In other words, this study considers diversity combining for time-delay estimation, where the diversity results from the dispersed spectrum utilization of the cognitive radio system [22].

2.4 On the Optimality of Two-Step Time-Delay Estimation

In this section, the asymptotic optimality properties of the two-step time-delay estimators proposed in the previous section are investigated. In order to analyze

the performance of the estimators at high SNRs, the result in [31] for time-delay estimation at multiple receive antennas is extended to the scenario in this study.

Lemma 1: *Consider any linear modulation of the form* $s_i(t) = \sum_l d_{i,l} p_i(t - lT_i)$*, where* $d_{i,l}$ *denotes the complex data for the* l*th symbol of signal* i*, and* $p_i(t)$ *represents a pulse with duration* T_i*. Assume that* $\int_{-\infty}^{\infty} s_i'(t-\tau) s_i^*(t-\tau) \mathrm{d}t = 0$ *for* $i = 1, \ldots, K$*. Then, for the signal model in (2.1), the delay estimate in (2.11) and the channel amplitude estimate in (2.12) can be modeled, at high SNR, as*

$$\hat{\tau}_i = \tau + \nu_i \ , \tag{2.23}$$

$$\hat{a}_i = a_i + \eta_i \ , \tag{2.24}$$

for $i = 1, \ldots, K$*, where* ν_i *and* η_i *are independent zero mean Gaussian random variables with variances* $\sigma_i^2/(\tilde{E}_i\, a_i^2)$ *and* σ_i^2/E_i*, respectively. In addition,* ν_i *and* ν_j *(*η_i *and* η_j*) are independent for* $i \neq j$*.*

Proof: The proof uses the derivations in [43] in order to extend Lemma 1 in [31] to the cases with CFO. At high SNRs, the ML estimate $\hat{\boldsymbol{\theta}}_i$ of $\boldsymbol{\theta}_i = [\tau \ a_i \ \phi_i \ \omega_i]$ in (2.11) and (2.12) is approximately distributed as a jointly Gaussian random variable with the mean being equal to $\boldsymbol{\theta}_i$ and the covariance matrix being given by the inverse of the Fisher information matrix (FIM) for observation $r_i(t)$ in (2.1) over $[0, T]$. Then, the results in [43] can be used to show that, under the conditions in the lemma, the first 2×2 block of the covariance matrix can be obtained as $\mathrm{diag}\{\sigma_i^2/(\tilde{E}_i a_i^2), \sigma_i^2/E_i\}$. Therefore, $\hat{\tau}_i$ and $\hat{a}_i$ can be modeled as in (2.23) and (2.24). In addition, since the noise at different branches are independent, the estimates are independent for different branches. □

Based on Lemma 1, the asymptotic unbiasedness properties of the estimators in Section 2.3 can be verified. First, it is observed from Lemma 1 that $\mathrm{E}\{\hat{\tau}_i\} = \tau$. Considering the optimal combining technique in (2.15) as example,

the unbiasedness property can be shown as

$$\mathrm{E}\{\hat{\tau}|\hat{a}_1,\ldots,\hat{a}_K\} = \frac{\sum_{i=1}^{K}\kappa_i\,\mathrm{E}\{\hat{\tau}_i|\hat{a}_1,\ldots,\hat{a}_K\}}{\sum_{i=1}^{K}\kappa_i} = \frac{\sum_{i=1}^{K}\kappa_i\,\mathrm{E}\{\hat{\tau}_i|\hat{a}_i\}}{\sum_{i=1}^{K}\kappa_i} = \tau\ , \quad (2.25)$$

where $\kappa_i = \hat{a}_i^2\tilde{E}_i/\sigma_i^2$. Since $\mathrm{E}\{\hat{\tau}|\hat{a}_1,\ldots,\hat{a}_K\}$ does not depend on $\hat{a}_1,\ldots,\hat{a}_K$, $\mathrm{E}\{\hat{\tau}\} = \mathrm{E}\{\mathrm{E}\{\hat{\tau}|\hat{a}_1,\ldots,\hat{a}_K\}\} = \tau$. In other words, since for each specific value of $\hat{a}_i$, $\hat{\tau}_i$ is unbiased ($i = 1,\ldots,K$), the weighted average of $\hat{\tau}_1,\ldots,\hat{\tau}_K$ is also unbiased. Similar arguments can be used to show that all the two-step estimators described in Section 2.3 are asymptotically unbiased.

Regarding the variance of the estimators, it can be shown that the optimal combining technique has a variance that is approximately equal to the CRLB at high SNRs (in fact, this is the main reason why this combining technique is called *optimal*). To that aim, the conditional variance of $\hat{\tau}$ in (2.15) given $\hat{a}_1,\ldots,\hat{a}_K$ is obtained as follows:

$$\mathrm{Var}\{\hat{\tau}|\hat{a}_1,\ldots,\hat{a}_K\} = \frac{\sum_{i=1}^{K}\kappa_i^2\,\mathrm{Var}\{\hat{\tau}_i|\hat{a}_1,\ldots,\hat{a}_K\}}{\left(\sum_{i=1}^{K}\kappa_i\right)^2}\ , \quad (2.26)$$

where the independence of the time-delay estimates is used to obtain the result (cf. Lemma 1). Since $\mathrm{Var}\{\hat{\tau}_i|\hat{a}_1,\ldots,\hat{a}_K\} = \mathrm{Var}\{\hat{\tau}_i|\hat{a}_i\} = \sigma_i^2/(\tilde{E}_i\,a_i^2)$ from Lemma 1 and $\kappa_i = \hat{a}_i^2\tilde{E}_i/\sigma_i^2$, (2.26) can be expressed as

$$\begin{aligned}\mathrm{Var}\{\hat{\tau}|\hat{a}_1,\ldots,\hat{a}_K\} &= \frac{\sum_{i=1}^{K}\frac{\hat{a}_i^4\tilde{E}_i^2}{\sigma_i^4}\frac{\sigma_i^2}{\tilde{E}_i a_i^2}}{\left(\sum_{i=1}^{K}\frac{\hat{a}_i^2\tilde{E}_i}{\sigma_i^2}\right)^2} \\ &= \sum_{i=1}^{K}\frac{\hat{a}_i^4\tilde{E}_i}{a_i^2\sigma_i^2}\left(\sum_{i=1}^{K}\frac{\hat{a}_i^2\tilde{E}_i}{\sigma_i^2}\right)^{-2}\ . \end{aligned} \quad (2.27)$$

Lemma 1 states that at high SNRs, $\hat{a}_i$ is distributed as a Gaussian random variable with mean a_i and variance σ_i^2/E_i. Therefore, for sufficiently large values

of $\frac{E_i}{\sigma_i^2}, \ldots, \frac{E_K}{\sigma_K^2}$, (2.27) can be approximated by

$$\mathrm{Var}\{\hat{\tau}|\hat{a}_1, \ldots, \hat{a}_K\} \approx \left(\sum_{i=1}^{K} \frac{\tilde{E}_i \, a_i^2}{\sigma_i^2} \right)^{-1} , \tag{2.28}$$

which is equal to CRLB expression in (2.8). Therefore, the optimal combining technique in (2.15) results in an approximately optimal estimator at high SNRs.

The variances of the other combining techniques in Section 2.3 can be obtained in a straightforward manner and it can be shown that the asymptotic variances are larger than the CRLB in general. For example, for the SNR combining technique in (2.18), the conditional variance can be calculated as

$$\begin{aligned} \mathrm{Var}\{\hat{\tau}|\hat{a}_1, \ldots, \hat{a}_K\} &= \frac{\sum_{i=1}^{K} \frac{\hat{a}_i^4 E_i^2}{\sigma_i^4} \frac{\sigma_i^2}{\tilde{E}_i a_i^2}}{\left(\sum_{i=1}^{K} \frac{\hat{a}_i^2 E_i}{\sigma_i^2} \right)^2} \\ &= \sum_{i=1}^{K} \frac{\hat{a}_i^4 E_i^2}{a_i^2 \tilde{E}_i \sigma_i^2} \left(\sum_{i=1}^{K} \frac{\hat{a}_i^2 E_i}{\sigma_i^2} \right)^{-2} , \end{aligned} \tag{2.29}$$

which, for sufficiently large SNRs, becomes

$$\mathrm{Var}\{\hat{\tau}|\hat{a}_1, \ldots, \hat{a}_K\} \approx \sum_{i=1}^{K} \frac{a_i^2 E_i^2}{\tilde{E}_i \sigma_i^2} \left(\sum_{i=1}^{K} \frac{a_i^2 E_i}{\sigma_i^2} \right)^{-2} . \tag{2.30}$$

Then, from the Cauchy-Schwarz inequality, the following condition is obtained:

$$\mathrm{Var}\{\hat{\tau}|\hat{a}_1, \ldots, \hat{a}_K\} \approx \frac{\sum_{i=1}^{K} \frac{a_i^2 E_i^2}{\tilde{E}_i \sigma_i^2}}{\left(\sum_{i=1}^{K} \frac{a_i E_i}{\sigma_i \sqrt{\tilde{E}_i}} \frac{a_i \sqrt{\tilde{E}_i}}{\sigma_i} \right)^2} \geq \frac{\sum_{i=1}^{K} \frac{a_i^2 E_i^2}{\tilde{E}_i \sigma_i^2}}{\sum_{i=1}^{K} \frac{a_i^2 E_i^2}{\tilde{E}_i \sigma_i^2} \sum_{i=1}^{K} \frac{a_i^2 \tilde{E}_i}{\sigma_i^2}} = \mathrm{CRLB} , \tag{2.31}$$

which holds with equality if and only if $\frac{\tilde{E}_1}{E_1} = \cdots = \frac{\tilde{E}_K}{E_K}$ (or, $\beta_1 = \cdots = \beta_K$). In fact, under that condition, the optimal combining and the SNR combining techniques become identical as mentioned in Section 2.3, since $\kappa_i = \hat{a}_i^2 \tilde{E}_i / \sigma_i^2 = (\tilde{E}_i / E_i)(E_i \hat{a}_i^2 / \sigma_i^2) = (\tilde{E}_i / E_i)\gamma_i$ (cf. (2.16) and (2.19)). In other words, when

the effective bandwidths of the signals at different branches are not equal, the asymptotic variance of the SNR combining technique is strictly larger than the CRLB.

Regarding the selection combining approaches in (2.20) and (2.21), similar conclusions as for the diversity combining techniques in communications systems can be made [52]. Specifically, SC-1 and SC-2 perform worse than the optimal combining and the SNR combining techniques, respectively, in general. However, when the estimate of a branch is significantly more accurate than the others, the performance of the selection combining approach can get very close to the optimal combining or the SNR combining technique. However, when the branches have similar estimation accuracies, the selection combining techniques can perform significantly worse. The conditional variances of the selection combining techniques can be approximated at high SNR as

$$\mathrm{Var}\{\hat{\tau}|\hat{a}_1,\ldots,\hat{a}_K\} \approx \min\left\{\frac{\sigma_1^2}{\tilde{E}_1 a_1^2},\ldots,\frac{\sigma_K^2}{\tilde{E}_K a_K^2}\right\}\ , \tag{2.32}$$

for SC-1, and

$$\mathrm{Var}\{\hat{\tau}|\hat{a}_1,\ldots,\hat{a}_K\} \approx \frac{E_m}{\tilde{E}_m}\min\left\{\frac{\sigma_1^2}{E_1 a_1^2},\ldots,\frac{\sigma_K^2}{E_K a_K^2}\right\}\ , \tag{2.33}$$

for SC-2, where $m = \arg\min_{i\in\{1,\ldots,K\}} \{\sigma_i^2/(E_i\hat{a}_i^2)\}$. From (2.32) and (2.33), it is observed that if $\frac{\tilde{E}_1}{E_1} = \cdots = \frac{\tilde{E}_K}{E_K}$ $(\beta_1 = \cdots = \beta_K)$, then the asymptotic variances of the SC-1 and SC-2 techniques become equivalent.

Finally, for the equal combining technique, the variance can be obtained from (2.22) as

$$\mathrm{Var}\{\hat{\tau}\} = \frac{1}{K^2}\sum_{i=1}^{K}\frac{\sigma_i^2}{\tilde{E}_i a_i^2}\ . \tag{2.34}$$

In general, the equal combining technique is expected to have the worst performance since it does not make use of any information about the SNR or the signal bandwidths in the estimation of the time-delay.

2.5 Simulation Results

In this section, simulations are performed in order to evaluate the performance of the proposed time-delay estimators and compare them with each other and against the CRLBs. The signal $s_i(t)$ in (2.1) corresponding to each branch is modeled by the Gaussian doublet given by

$$s_i(t) = A_i \left(1 - \frac{4\pi(t - 1.25\,\zeta_i)^2}{\zeta_i^2}\right) e^{-2\pi(t-1.25\zeta_i)^2/\zeta_i^2}\ , \tag{2.35}$$

where A_i and ζ_i are the parameters that are used to adjust the pulse energy and the pulse width, respectively. The bandwidth of $s_i(t)$ in (2.35) can approximately be expressed as $B_i \approx 1/(2.5\,\zeta_i)$ [25]. For the following simulations, A_i values are adjusted to generate unit-energy pulses.

For all the simulations, the spectral densities of the noise at different branches are assumed to be equal; that is, $\sigma_i^2 = \sigma^2$ for $i = 1, \ldots, K$. In addition, the SNR of the system is defined with respect to the total energy of the signals at different branches; i.e., $\text{SNR} = 10\log_{10}\left(\frac{\sum_{i=1}^{K} E_i}{2\,\sigma^2}\right)$.

In assessing the root-mean-squared errors (RMSEs) of the different estimators, a Rayleigh fading channel is assumed. Namely, the channel coefficient $\alpha_i = a_i\,\mathrm{e}^{j\phi_i}$ in (2.1) is modeled as a_i being a Rayleigh distributed random variable and ϕ_i being uniformly distributed in $[0, 2\pi)$. Also, the same average power is assumed for all the bands; namely, $\mathrm{E}\{|\alpha_i|^2\} = 1$ is used. The time-delay τ in (2.1) is uniformly distributed over the observation interval. In addition, it is assumed that there is

no CFO in the system.

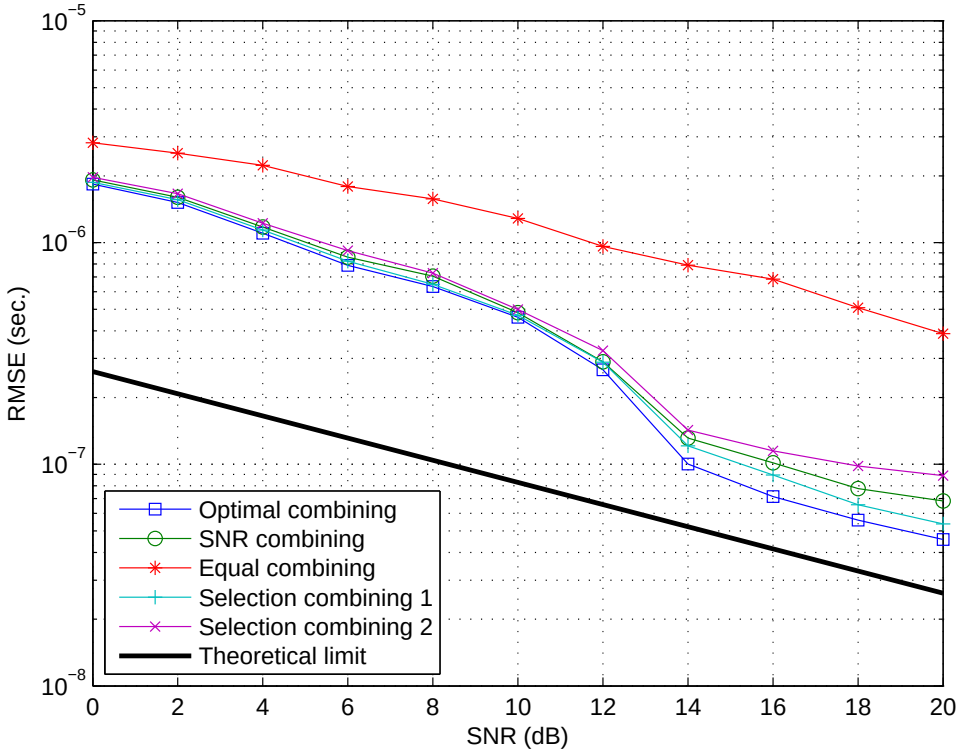

Figure 2.4: RMSE versus SNR for the proposed algorithms, and the theoretical limit (CRLB). The signal occupies three dispersed bands with bandwidths $B_1 = 200$ kHz, $B_2 = 100$ kHz and $B_3 = 400$ kHz.

First, the performance of the proposed estimators is evaluated with respect to the SNR for a system with $K = 3$, $B_1 = 200$ kHz, $B_2 = 100$ kHz and $B_3 = 400$ kHz. The results in Figure 2.4 indicate that the optimal combining technique has the best performance as expected from the theoretical analysis, and SC-1, which estimates the delay according to (2.20), has performance close to that of the optimal combining technique. The SNR combining and SC-2 techniques have

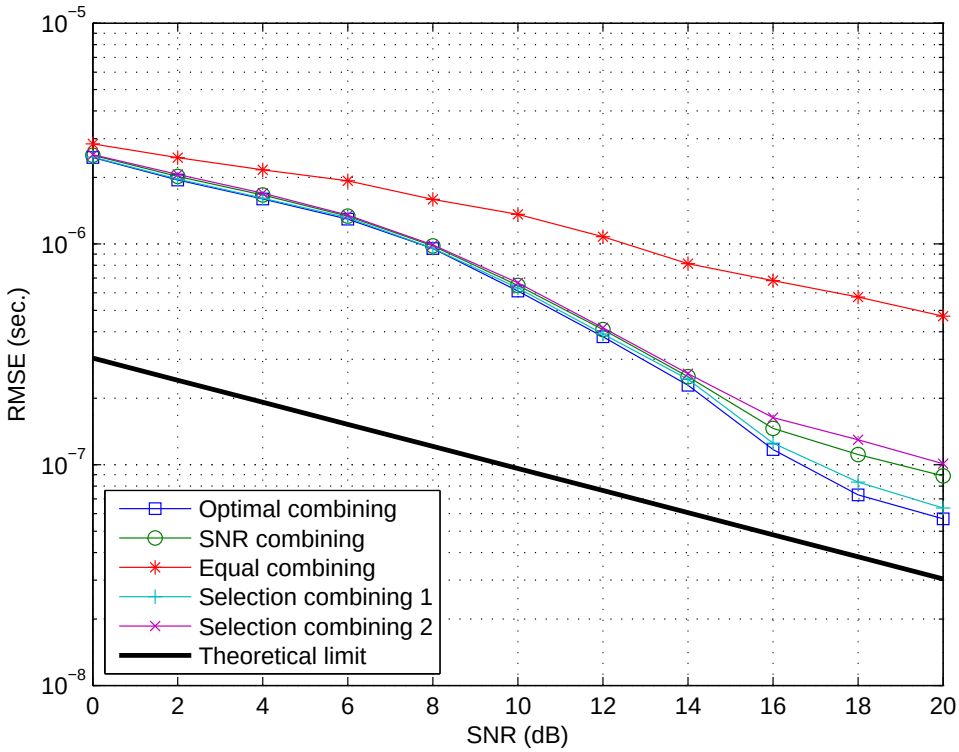

Figure 2.5: RMSE versus SNR for the proposed algorithms, and the theoretical limit (CRLB). The signal occupies two dispersed bands with bandwidths $B_1 = 100$ kHz and $B_2 = 400$ kHz.

worse performance than the optimal and SC-1 techniques, respectively. In addition, SC-1 has better performance than the SNR combining technique in this scenario, which indicates that selecting the delay estimate corresponding to the largest $\tilde{E}_i \hat{a}_i^2/\sigma_i^2$ value is closer to optimal than combining the delay estimates of the different branches according to the SNR combining criterion in (2.18) for the considered scenario. The main reason for this is related to the large variability of the channel amplitudes due to the nature of the Rayleigh distribution. Since the channel amplitude levels are expected to be quite different for most of the

time, using the delay estimate of the best one yields a more reliable estimate than combining the delay estimates according to the *suboptimal* SNR combining technique (since the signal bandwidths are different, the SNR combining technique is suboptimal as studied in Section 2.4). Regarding the equal combining technique, it has significantly worse performance than the others, since it combines all the delay estimates equally. Since the delay estimates of some branches can have very large errors due to fading, the RMSEs of the equal combining technique become significantly larger. For example, when converted to distance estimates, an RMSE of about 120 meters is achieved by this technique, whereas the optimal combining technique results in an RMSE of less than 15 meters. Finally, it is observed that the performance of the optimal combining technique gets very close to the CRLB at high SNRs, which is expected from the asymptotic arguments in Section 2.4.

Next, similar performance comparisons are performed for a signal with $K = 2$, $B_1 = 100$ kHz, and $B_2 = 400$ kHz, as shown in Figure 2.5. Again similar observations as for Figure 2.4 are made. In addition, since there are only two bands ($K = 2$) and the signal bandwidths are quite different, the selection combining techniques, SC-1 and SC-2, get very close to the optimal combining and the SNR combining techniques, respectively.

In addition, the equivalence of the optimal combining and the SNR combining techniques and that of SC-1 and SC-2 are illustrated in Figure 2.6, where $K = 2$, and $B_1 = B_2 = 400$ kHz are used. In other words, the signal consists of two dispersed bands with 400 kHz bandwidths, and in each band, the same signal described by (2.35) is used. Therefore, $\tilde{E}_1/E_1 = \tilde{E}_2/E_2$ is satisfied, which results in the equivalence of the optimal combining and the SNR combining techniques,

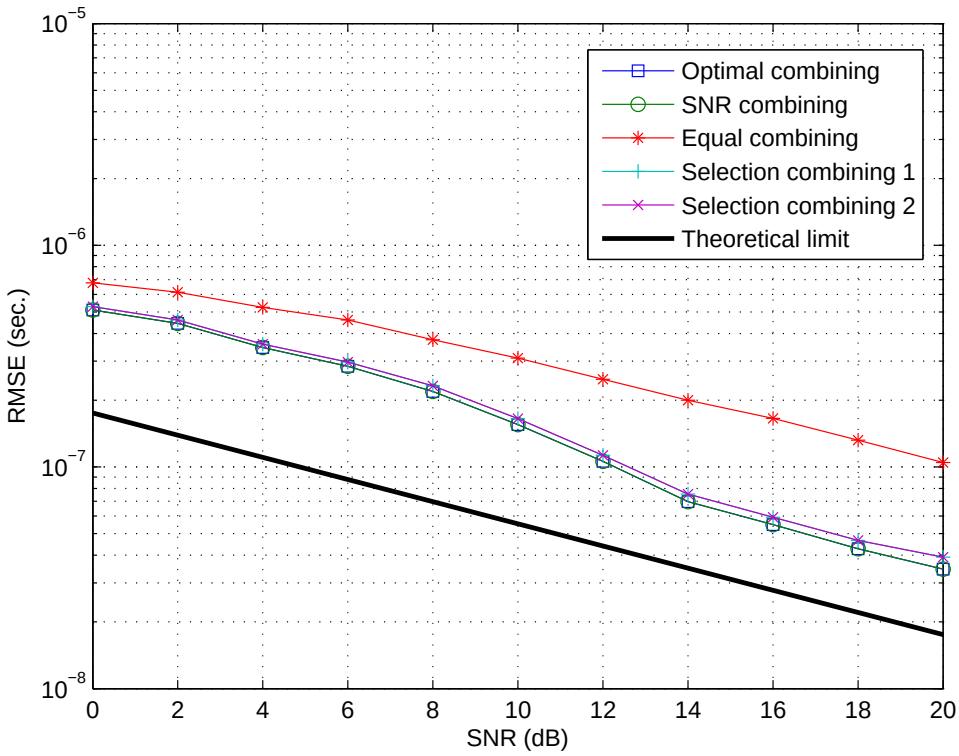

Figure 2.6: RMSE versus SNR for the proposed algorithms, and the theoretical limit (CRLB). The signal occupies two dispersed bands with equal bandwidths of 400 kHz.

as well as that of the SC-1 and SC-2 techniques, as discussed in Section 2.3. Also, since there are only two bands ($K = 2$), the selection combining techniques get very close to the optimal combining and the SNR combining techniques.

In Figure 2.7, the RMSEs of the proposed estimators are plotted against the number of bands, where each band is assumed to have 100 kHz bandwidth. The spectral densities are set to $\sigma_i^2 = \sigma^2 = 0.1\ \forall i$. Since the same signals are used in each band, the optimal combining and the SNR combining techniques become identical; hence, only one of them is marked in the figure. Similarly, since SC-1

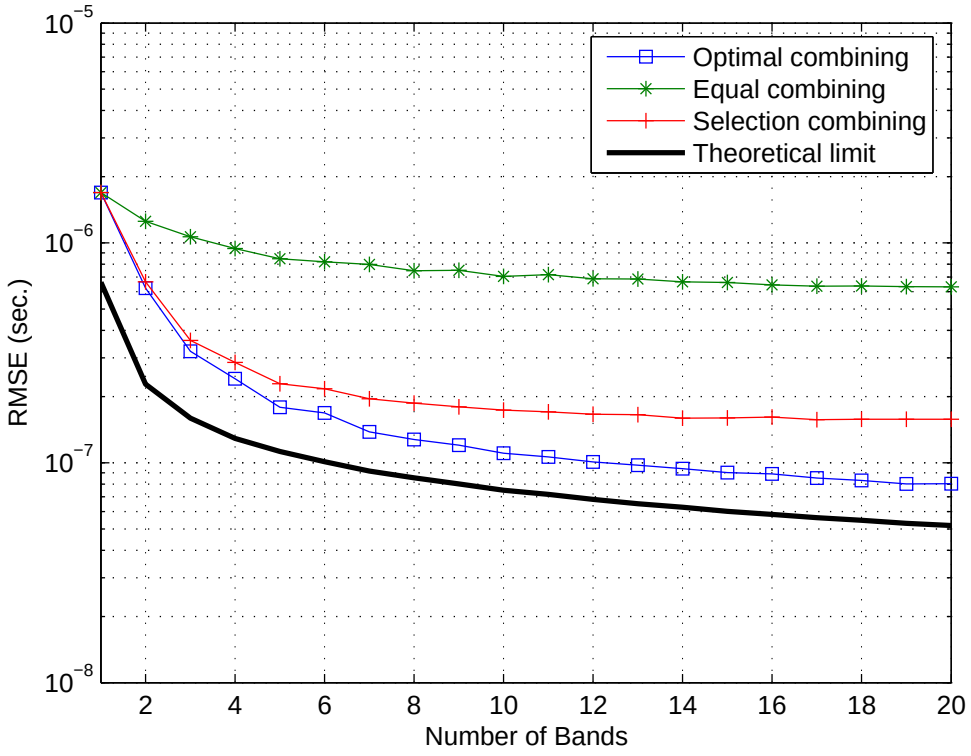

Figure 2.7: RMSE versus the number of bands for the proposed algorithms, and the theoretical limit (CRLB). Each band occupies 100 kHz, and $\sigma_i^2 = 0.1\ \forall i$.

and SC-2 are identical in this scenario, they are referred to as "selection combining" in the figure. It is observed from Figure 2.7 that the optimal combining has better performance than the selection combining and the equal combining techniques. In addition, as the number of bands increases, the amount of reduction in the RMSE per additional band decreases (i.e., diminishing return). In fact, the selection combining technique seems to converge to an almost constant value for large numbers of bands. This is intuitive since the selection combining technique always uses the estimate from one of the branches; hence, in the presence of a sufficiently large number of bands, additional bands do not cause a significant

increase in the diversity. On the other hand, the optimal combining technique has a slope that is quite similar to that of the CRLB; that is, it makes an efficient use of the frequency diversity.

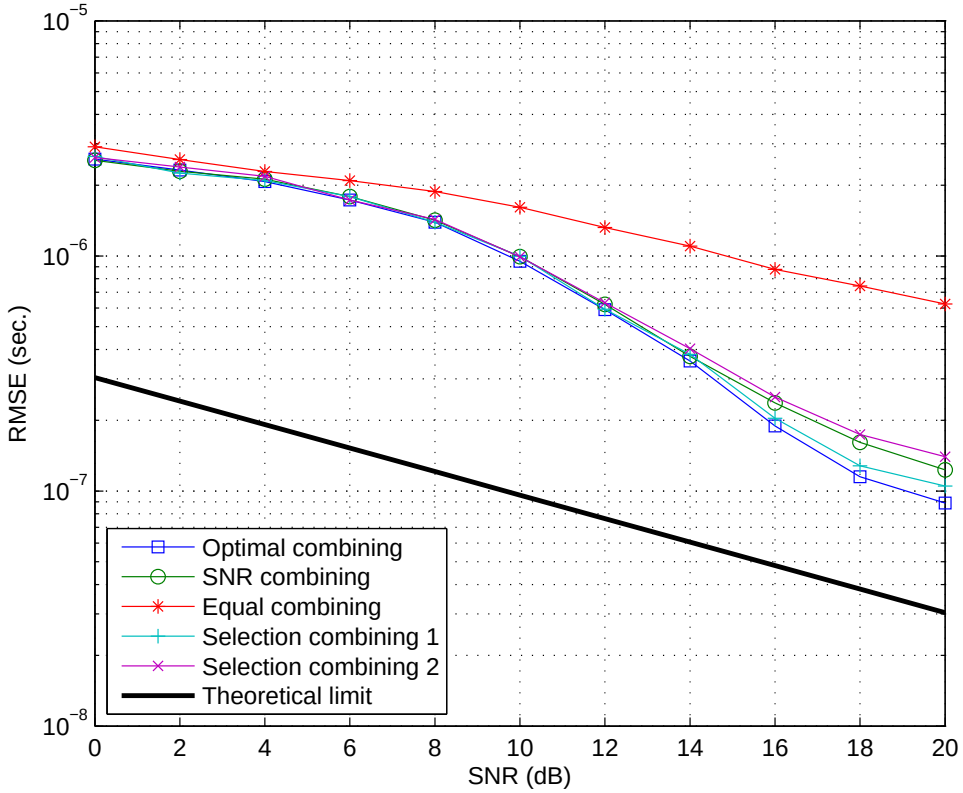

Figure 2.8: RMSE versus SNR for the proposed algorithms, and the theoretical limit (CRLB) in the presence of CFO. The signal occupies two dispersed bands with bandwidths $B_1 = 100$ kHz and $B_2 = 400$ kHz.

Finally, the performance of the proposed algorithms is investigated in the presence of CFO in Figure 2.8. The CFOs at different branches are modeled by independent uniform random variables over $[-100, 100]$ Hz, and the RMSEs are obtained for the system parameters that are considered for Figure 2.5. Again

similar observations as for Figure 2.4 and Figure 2.5 are made. In addition, the comparison of Figure 2.5 and Figure 2.8 reveals that the RMSE values slightly increase in the presence of CFOs, although the theoretical limit stays the same [43].

Chapter 3

TIME-DELAY ESTIMATION IN MULTIPLE-INPUT SINGLE-OUTPUT SYSTEMS

In this chapter, the time-delay estimation problem in MISO systems is investigated. Because of the aforementioned importance of positioning in wireless systems and time-delay estimation in positioning, this problem comes out as a significant research problem to be solved.

Although the effects of receive diversity are studied in [31], no studies have quantified the effects of transmit diversity, which is present in MISO systems, for time-delay estimation and investigated optimal estimation. The study in this chapter analyzes the time-delay estimation problem in MISO that facilitates the transmit diversity.

In this chapter, the ML time-delay estimator is provided after the signal model is constructed. Because of the computational complexity of the ML estimator,

an alternative solution by DE is proposed and the performance of this solution is compared to the CRLB in the simulations.

3.1 Signal Model

Consider a MISO system with M antennas at the transmitter and a single antenna at the receiver, as shown in Figure 3.1. The baseband received signal at the

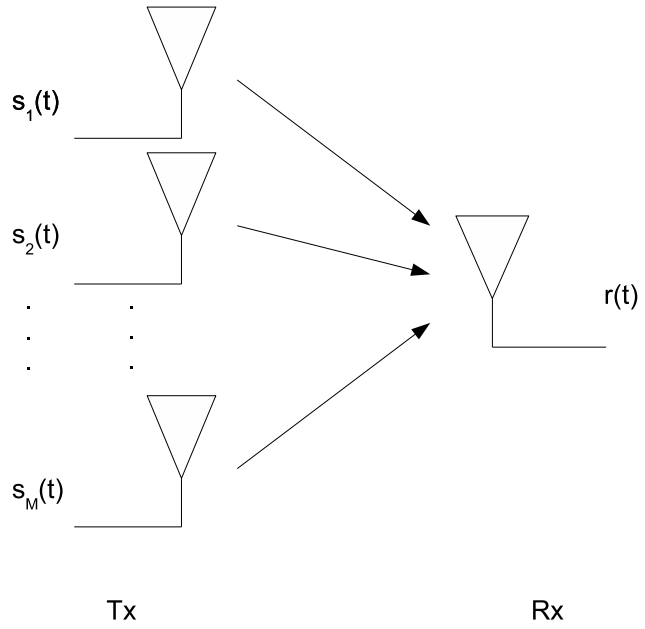

Figure 3.1: A MISO system with M transmitter antennas.

receiver antenna can be modeled as follows:

$$r(t) = \sum_{i=1}^{M} \alpha_i s_i(t-\tau) + n(t) \ , \tag{3.1}$$

where $\alpha_i = a_i e^{j\phi_i}$ is the channel coefficient of the ith transmitter branch, τ is the time-delay, $s_i(t)$ is the baseband representation of the transmitted signal from the ith transmitter antenna, and $n(t)$ denotes the complex additive white Gaussian

noise with independent components each having mean zero and spectral density σ^2.

For the signal model in (3.1), it is assumed that the signals $s_1(t), \ldots, s_M(t)$ are narrowband signals. Hence, the differences in the time-delays of the signals coming from different antennas are very small compared to the duration of the signals. Hence, the time-delay parameter can be modeled by a single parameter τ as in (3.1). In addition, the transmit antennas are assumed to be separated sufficiently (on the order of signal wavelength) in such a way that the channel coefficients for signals coming from different antennas are independent, which is the main source of transmit diversity in the system.

3.2 Theoretical Limits

The time-delay estimation problem involves the joint estimation of τ and the other unknown parameters of the receiver signal in (3.1). The unknown signal parameters are given by vector $\boldsymbol{\lambda}$ that is expressed as

$$\boldsymbol{\lambda} = \begin{bmatrix} \tau & a_1 & \cdots & a_M & \phi_1 & \cdots & \phi_M \end{bmatrix} . \tag{3.2}$$

If the received signal is observed over the time interval [0, T], then the log-likelihood function for $\boldsymbol{\lambda}$ can be expressed as [49]

$$\Lambda(\boldsymbol{\lambda}) = k - \frac{1}{2\sigma^2} \int_0^T \left| r(t) - \sum_{i=1}^{M} \alpha_i s_i(t-\tau) \right|^2 dt \tag{3.3}$$

where k is a term independent of $\boldsymbol{\lambda}$.

After some manipulation, we obtain the Fisher information matrix (FIM) [49]

from (3.3) as

$$\mathbf{I} = \begin{bmatrix} \mathrm{I}_{\tau\tau} & \mathbf{I}_{\tau a} & \mathbf{I}_{\tau\phi} \\ \mathbf{I}_{\tau a}^T & \mathbf{I}_{aa} & \mathbf{I}_{a\phi} \\ \mathbf{I}_{\tau\phi}^T & \mathbf{I}_{a\phi}^T & \mathbf{I}_{\phi\phi} \end{bmatrix} , \tag{3.4}$$

where the submatrices of the FIM are given by[1]

$$\begin{aligned} \mathrm{I}_{\tau\tau} &= \mathrm{E}\left\{ \left(\frac{\partial \Lambda(\lambda)}{\partial \tau} \right)^2 \right\} \\ &= \frac{1}{\sigma^2} \int_0^T \left| \sum_{i=1}^{M} \alpha_i s_i'(t-\tau) \right|^2 dt = \frac{\hat{E}_s}{\sigma^2} , \end{aligned} \tag{3.5}$$

$$\begin{aligned} [\mathbf{I}_{aa}]_{kk} &= \mathrm{E}\left\{ \left(\frac{\partial \Lambda(\lambda)}{\partial a_k} \right)^2 \right\} \\ &= \frac{1}{\sigma^2} \int_0^T |s_k(t-\tau)|^2 \, dt = \frac{E_k}{\sigma^2} , \end{aligned} \tag{3.6}$$

$$[\mathbf{I}_{aa}]_{kn} = \mathrm{E}\left\{ \frac{\partial \Lambda(\lambda)}{\partial a_k} \frac{\partial \Lambda(\lambda)}{\partial a_n} \right\} = \frac{P_{k,n}}{\sigma^2}, \quad \text{if } k \neq n , \tag{3.7}$$

$$\begin{aligned} [\mathbf{I}_{\phi\phi}]_{kk} &= \mathrm{E}\left\{ \left(\frac{\partial \Lambda(\lambda)}{\partial \phi_k} \right)^2 \right\} \\ &= \frac{a_k^2}{\sigma^2} \int_0^T |s_k(t-\tau)|^2 \, dt = \frac{a_k^2 E_k}{\sigma^2} , \end{aligned} \tag{3.8}$$

$$[\mathbf{I}_{\phi\phi}]_{kn} = \mathrm{E}\left\{ \frac{\partial \Lambda(\lambda)}{\partial \phi_k} \frac{\partial \Lambda(\lambda)}{\partial \phi_n} \right\} = \frac{R_{k,n}}{\sigma^2} , \quad \text{if } k \neq n \tag{3.9}$$

$$[\mathbf{I}_{\tau a}]_k = \mathrm{E}\left\{ \frac{\partial \Lambda(\lambda)}{\partial \tau} \frac{\partial \Lambda(\lambda)}{\partial a_k} \right\} = \frac{-F_k}{\sigma^2} , \tag{3.10}$$

$$[\mathbf{I}_{\tau\phi}]_k = \mathrm{E}\left\{ \frac{\partial \Lambda(\lambda)}{\partial \tau} \frac{\partial \Lambda(\lambda)}{\partial \phi_k} \right\} = \frac{-G_k}{\sigma^2} , \tag{3.11}$$

$$[\mathbf{I}_{a\phi}]_{kn} = \mathrm{E}\left\{ \frac{\partial \Lambda(\lambda)}{\partial a_k} \frac{\partial \Lambda(\lambda)}{\partial \phi_n} \right\} = \frac{-H_{k,n}}{\sigma^2} , \quad \text{if } k \neq n \tag{3.12}$$

$$[\mathbf{I}_{a\phi}]_{kk} = \mathrm{E}\left\{ \frac{\partial \Lambda(\lambda)}{\partial a_k} \frac{\partial \Lambda(\lambda)}{\partial \phi_n} \right\} = 0 , \quad \text{if } k = n \tag{3.13}$$

[1] $[\mathbf{X}]_{kn}$ denotes the element of matrix $\mathbf{X}$ in row k and column n.

with

$$E_k \triangleq \int_0^T |s_k(t-\tau)|^2 \, dt \ , \tag{3.14}$$

$$\hat{E}_s \triangleq \int_0^T \left| \sum_{i=1}^{M} \alpha_i s_i'(t-\tau) \right|^2 dt \ , \tag{3.15}$$

$$P_{k,n} \triangleq \int_0^T Re\left\{ s_k^*(t-\tau) s_n(t-\tau) e^{j(\phi_n - \phi_k)} \right\} dt \ , \tag{3.16}$$

$$R_{k,n} \triangleq \int_0^T Re\left\{ \alpha_k^* \alpha_n s_k^*(t-\tau) s_n(t-\tau) \right\} dt \ , \tag{3.17}$$

$$F_k \triangleq \int_0^T Re\left\{ e^{-j\phi_k} s_k^*(t-\tau) \sum_{i=1}^{M} \alpha_i s_i'(t-\tau) \right\} dt \ , \tag{3.18}$$

$$G_k \triangleq \int_0^T Im\left\{ \alpha_k^* s_k^*(t-\tau) \sum_{i=1}^{M} \alpha_i s_i'(t-\tau) \right\} dt \ , \tag{3.19}$$

and

$$H_{k,n} \triangleq \int_0^T Im\left\{ a_n e^{j(\phi_n - \phi_k)} s_k^*(t-\tau) s_n(t-\tau) \right\} dt \ . \tag{3.20}$$

Since the CRLB for the time-delay parameter is given by the first element of the inverse of the FIM, namely, $[\mathbf{I}^{-1}]_{11}$, the expressions above should be used to obtain the result numerically in general. However, under certain assumptions, closed-form CRLB expressions can also be obtained as shown below.

Condition 1. *Assume* $\int_0^T s_k^*(t) s_n'(t)\, dt = 0$ *for* $\forall k \neq n$.

Under this assumption, $\mathbf{I}_{\tau a}$ and $\mathbf{I}_{\tau\phi}$ become $\mathbf{0}$. Then, the CRLB for τ becomes

$$\text{CRLB} = \left[\mathbf{I}^{-1}\right]_{11} = \frac{\sigma^2}{\hat{E}_s} \ . \tag{3.21}$$

Condition 2. *Assume* $\int_0^T s_k(t)s_n^*(t)\,dt = 0$ *for* $\forall k \neq n$ *(orthogonality condition).*

Under this assumption, (3.7), (3.9), and (3.12) become 0. For an arbitrary matrix $\mathbf{E} = \begin{bmatrix} \mathbf{A} & \mathbf{B} \\ \mathbf{C} & \mathbf{D} \end{bmatrix}$, $\left[\mathbf{E}^{-1}\right]_{M\times M} = (\mathbf{A} - \mathbf{B}\mathbf{D}^{-1}\mathbf{C})^{-1}$ where $\mathbf{A}$ is an M-by-M matrix. If applied to the FIM provided in (4.7) as

$$A = \mathrm{I}_{\tau\tau} \tag{3.22}$$

$$\mathbf{B} = \begin{bmatrix} \mathbf{I}_{\tau a} & \mathbf{I}_{\tau\phi} \end{bmatrix} \tag{3.23}$$

$$\mathbf{C} = \mathbf{B}^T \tag{3.24}$$

$$\mathbf{D} = \begin{bmatrix} \mathbf{I}_{aa} & \mathbf{I}_{a\phi} \\ \mathbf{I}_{a\phi}^T & \mathbf{I}_{\phi\phi} \end{bmatrix} \tag{3.25}$$

then the CRLB, which is $[\mathbf{I^{-1}}]_{\mathbf{11}}$, can be calculated as follows:

$$\begin{aligned} \mathrm{CRLB} &= \left(\mathbf{I}_{\tau\tau} - \begin{bmatrix} \mathbf{I}_{\tau a} & \mathbf{I}_{\tau\phi} \end{bmatrix} \begin{bmatrix} \mathbf{I}_{aa} & \mathbf{I}_{a\phi} \\ \mathbf{I}_{a\phi}^T & \mathbf{I}_{\phi\phi} \end{bmatrix} \begin{bmatrix} \mathbf{I}_{\tau a}^T \\ \mathbf{I}_{\tau\phi}^T \end{bmatrix} \right)^{-1} \\ &= \left(\frac{\hat{E}_s}{\sigma^2} - \frac{1}{\sigma^2}\sum_{k=1}^{M} \frac{F_k^2}{E_k} - \frac{1}{\sigma^2}\sum_{k=1}^{M} \frac{G_k^2}{E_k a_k^2} \right)^{-1} \\ &= \frac{\sigma^2}{\hat{E}_s - \sum_{k=1}^{M} \left(\frac{F_k^2 a_k^2 + G_k^2}{E_k a_k^2} \right)} \end{aligned} \tag{3.26}$$

The CRLB must be minimized in order to maximize the time-delay estimation accuracy. From (3.21) and (3.26), it is observed that the maximization of $\hat{E}_s$ in (3.15) is critical in order to achieve the minimum CRLB. In order to provide intuition about how space diversity can be achieved in MISO systems, consider the following two cases:

- If $s_i(t) = s(t)$ for all i, then $\hat{E}_s$ will reduce to

$$\hat{E}_s = \left| \sum_{i=1}^{M} \alpha_i \right|^2 \int_0^T \left| s'(t-\tau) \right|^2 \, dt = |\alpha|^2 \hat{E} \tag{3.27}$$

where $\alpha = \sum_{i=1}^{M} \alpha_i$ and $\hat{E} = \int_0^T |s'(t-\tau)|^2 \, dt$. It is observed that when the signals are selected to be equal to each other, then $\hat{E}_s$ can be undesirably small due to fading and result in a large CRLB. In this case, no space diversity is available in the system.

- If $s_i'(t)$'s are orthogonal to each other, then

$$\begin{aligned} \hat{E}_s &= \int_0^T \left\{ \sum_{i=1}^{M} \sum_{j=1}^{M} \alpha_i \alpha_j^* s_i'(t-\tau) s_j'^*(t-\tau) \right\} dt \\ &= \sum_{i=1}^{M} |\alpha_i|^2 \int_0^T \left| s_i'(t-\tau) \right|^2 \, dt = \sum_{i=1}^{M} |\alpha_i|^2 \hat{E}_i \end{aligned} \tag{3.28}$$

where $\hat{E}_i = \int_0^T \left| s_i'(t-\tau) \right|^2 \, dt$. In this case, the signals are selected so that their derivatives are orthogonal. Such a signal design results in a more robust CRLB by utilizing the transmit diversity in the system. Specifically, even if some of the signals are under deep fades, the other signals can still have reasonably large channel coefficients and can provide a reasonably large $\hat{E}_s$ value. Hence, the CRLB will stay reasonably low, which means that accurate time-delay estimation can still be possible in those scenarios. Therefore, the space diversity is utilized in that case.

3.3 ML Estimation Based On Differential Evolution

3.3.1 ML Estimator

From (3.3), the maximum likelihood (ML) estimator for $\boldsymbol{\lambda}$ can be obtained as

$$\Lambda(\boldsymbol{\lambda}) = \arg\max_{\boldsymbol{\lambda}} \frac{1}{2\sigma^2} \int_0^T \Bigg\{ r(t) \sum_{i=1}^{M} \alpha_i^* s_i^*(t-\tau) + r^*(t) \sum_{i=1}^{M} \alpha_i s_i(t-\tau) - \sum_{i=1}^{M} \alpha_i s_i(t-\tau) \sum_{i=1}^{M} \alpha_i^* s_i^*(t-\tau) \Bigg\} dt \ . \tag{3.29}$$

Under certain conditions, the ML estimator achieves the CRLB asymptotically [49]. However, an exhaustive search approach to find the ML solution for this estimation problem introduces tremendous computational overhead in the presence of multiple transmit antennas. Therefore, there exists a need for finding an algorithm that will obtain the ML solution (approximately) with a low computational load. For that purpose, first, the particle swarm optimization (PSO) approach is tested, which is a renown global optimization algorithm [53]. Despite the general success of the algorithm, it occasionally gets trapped in local minima and does not provide similar results on different trials for the time-delay estimation in MISO systems. Such a problem of PSO is also highlighted in [54], and it is also mentioned that DE is more efficient and robust than PSO in certain cases.

3.3.2 Differential Evolution (DE)

DE is a global optimization algorithm with simplicity, reliability, and high performance features. It is proposed by Storn and Price [55], and intended especially

for usage in continuous optimization [56]. It is similar to the evolutionary algorithms, but in terms of new candidate set generation and selection scheme, it differs from them. It does not recombine the solutions using probabilistic schemes but uses the differences of the population members [56]. The basic steps of DE are as follows [41], [54], [56]:

- Initialization: For a global optimization problem with D parameters, a population comprised of NP individuals, which are D-dimensional vectors, is generated. The individuals are uniformly distributed all over the optimization space. At each generation, the population is updated according to the update rules used in the next steps. (The parameter vectors at generation G are denoted by $x_{i,G}$ for $i = 1, 2, \ldots, NP$.)

- Mutation: In this step, for each individual (target vector ($x_{i,G}$)), three more individuals ($x_{r1,G}$, $x_{r2,G}$, $x_{r3,G}$) are randomly selected from the population so that all of the four individuals are different from each other. Then, a mutant vector $v_{i,G+1}$ is generated using $x_{r1,G}$, $x_{r2,G}$, $x_{r3,G}$ in the following way:

$$v_{i,G+1} = x_{r1,G} + F(x_{r2,G} - x_{r3,G}) \tag{3.30}$$

  where F is the amplification factor of the differential variation ($x_{r2,G} - x_{r3,G}$). Since the search is based on the difference between the individuals, at the beginning of the evolution, the search is distributed all over the search space. However, as the evolution continues, the search is concentrated in the neighborhood of the possible solution. As the difference between the individuals decreases, the step-size is automatically adapted to this situation and decreased.

- Crossover: A crossover between the target vector and the mutant vector is done, which means the elements of them are mixed according to the following rule:

$$u_{j,i,G} = \begin{cases} v_{i,G+1} \ , & \text{if rand}(0,1) < CR \\ x_{i,G} \ , & \text{otherwise} \end{cases} , \tag{3.31}$$

  where CR is the crossover probability for each element of $u_{j,i,G}$. If CR is 0, then no crossover is done, which means all of the elements of $u_{j,i,G}$ are taken from the target vector $x_{i,G}$. Conversely, if CR is 1, then the mutant vector is copied directly to $u_{j,i,G}$.

- Selection: The decision on the new population member is done greedily in DE. If $u_{j,i,G}$ has a better cost function value than $x_{i,G}$, then $u_{j,i,G}$ takes place of $x_{i,G}$ in generation $G+1$. If the reverse is valid, then $x_{i,G}$ retains its place in the next generation.

This is the standard version of DE, which is also known as "DE/rand/1". The general notation for representing the DE variants is "DE/x/y", where "x" denotes the selection method of the target vector and "y" denotes the number of difference vectors used. In the standard version, the target vector is chosen randomly, hence "x" is "rand". There is only one difference vector $(x_{r2,G} - x_{r3,G})$ used for improvement of the evolution, hence "y" is "1" [41], [56]. There are many variants of DE proposed in the literature, such as "DE/best/1", "DE/cur-to-best/1", "DE/best/2", "DE/rand/2", and "DE/rand-to-best/2" [57].

There are three parameters of DE as can be observed from above. They are the crossover probability (CR), the amplification factor for the differential variation (F) and the population size (NP). Finding the correct settings of

these parameters for a given problem may be a difficult and non-intuitive task [56]. Additionally, different problems may have very different parameter settings [58]. According to the No Free Lunch Theorems, if an algorithm performs well in some set of optimization problems, then it will perform bad for the other set of problems which means some other algorithms will perform well for the second set [59]. The reflection of this concept to the parameter setting problem of DE is finding different parameters that work well for different problems.

Although it is hard to find the optimum parameters for an arbitrary problem and general rules for these parameters, there are many studies on the parameter setting problem in DE. For example, in [40], it is suggested to use 10 times the dimensionality as the population size (NP). Increasing the population size will result in a more explorative and slower algorithm. In our trials on DE parameters, it is seen that with population size 50, which is 10 times the dimensionality of the problem (5 dimensions for two transmit antenna), the algorithm is not as successful as population size is 100 case. Therefore, 100 is preferred in this study. Generally, the recommendation for the CR value is 0.9 [60], [61]. So, we used 0.9 in our study. For the amplification factor (F), there are many recommended values. But, they are generally between 0.5 and 1. [60] The best performance in this optimization problem is obtained when F is selected as 0.5.

The stopping criterion for the algorithm is selected as the iteration count. Although it is observed that 100-150 iterations are generally seen to be sufficient, to be on the safe side, iteration count is selected as 200.

3.4 Simulation Results

In this section, simulations performed by using the DE algorithm studied in Section 3.3 are provided. The performance of DE is compared with the theoretical limit (CRLB) under different simulation scenarios. In the simulations, for $s_i(t)$, the modified Hermite pulses (MHPs) are used [62], [63]. $s_1(t)$ is the second order MHP and $s_2(t)$ is the third order MHP.

$$s_1(t) = \frac{e^{-t^2/4\beta^2}}{\beta^2}\left(\frac{t^2}{\beta^2} - 1\right) \ , \tag{3.32}$$

$$s_2(t) = \frac{e^{-t^2/4\beta^2}}{\beta^4}\left(\frac{t^3}{\beta^2} - 3t\right) \ , \tag{3.33}$$

where β is the parameter used for adjusting the pulse according to a given pulse width (PW). It is selected as $PW/15$ in the simulations. The MHPs are selected because of their orthogonality property. Since the orthogonality property of the signals satisfy Condition 2 provided in Section 3.2, the results of the simulations are compared to the square-root of the CRLB (theoretical bound) calculated under this assumption. The derivatives of MHPs are also approximately orthogonal, so the space diversity explained in Section 3.2 is present. The ML estimator reaches the theoretical bound under certain conditions. However, it is computationally very complex to obtain the exact ML solution via an exhaustive search compared to the ML solution by using DE. The simulations depict the performance of the DE based ML solution for different channel conditions.

The first simulation is performed under a Rayleigh fading channel condition, and the results are illustrated in Figure 3.2. For Rayleigh fading, the amplitudes of the channel coefficients ($\alpha_i = a_i e^{j\theta_i}$) can differ significantly. Therefore, the utilization of diversity is very important in this scenario. In the figure, the SNR

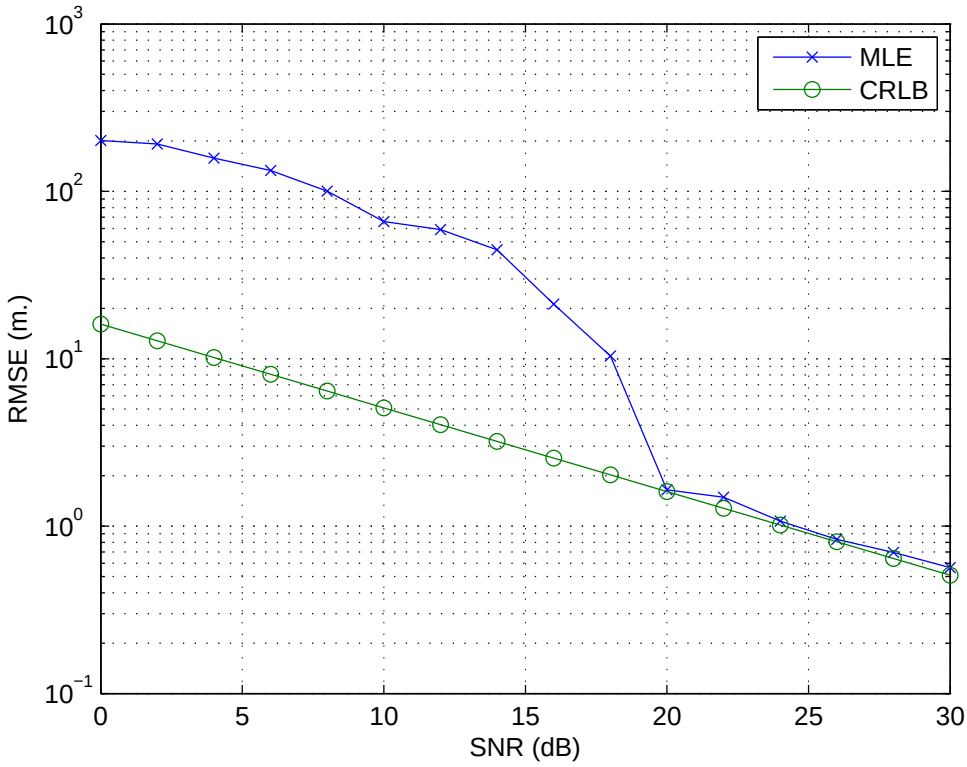

Figure 3.2: The RMSE of the MLE and the square-root of the CRLB for the Rayleigh fading channel.

of the system is defined as $\mathrm{SNR} = 10\log_{10}\left(\frac{E}{2\sigma^2}\right)$, where E is the energy of one of the signals transmitted from one antenna (all of the signal energies are set to 1 in the simulations). The channel coefficients (a_i) are Rayleigh distributed random variables with average power 1 ($\mathrm{E}\{a_i^2\} = 1$) and ϕ_i's are distributed as uniform random variables in the interval $[0, 2\pi)$. The time-delay τ is generated according to uniform distribution over the observation interval. The bandwidths of the signals are $B = 1$ MHz. The root mean-squared error (RMSE) is calculated over many channel realizations and this is compared to the square-root of the CRLB.

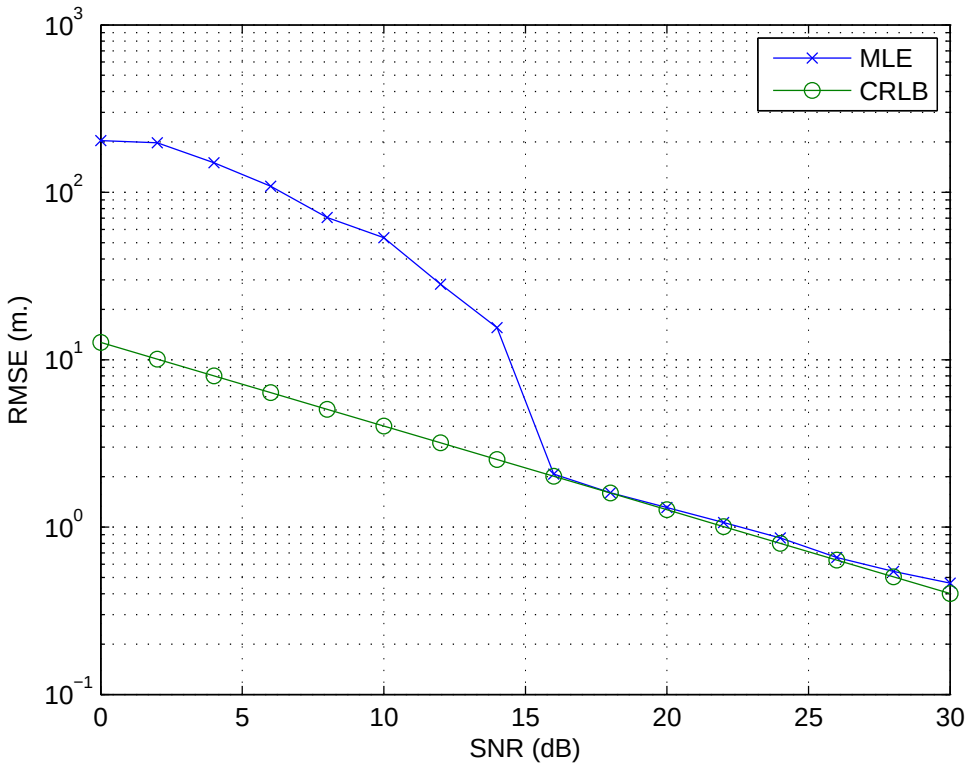

Figure 3.3: The RMSE of the MLE and the square-root of the CRLB for the Rician fading channel ($K = 5$).

The second simulation investigates the performance of the DE based ML algorithm under Rician fading with K factor 5 [64]. The SNR definition, the average power of channel coefficients, and the distribution of a_i's and ϕ_i's are the same as in the previous simulation. Figure 3.3 shows the performance of the algorithm in this scenario. If the two simulation results are compared, it can be observed that the presence of strong line-of-sight component in Rician fading causes the estimator to converge the bound ($\sqrt{\text{CRLB}}$) at lower SNRs compared to the Rayleigh fading scenario, which does not include a significant line-of-sight component. But, in both cases, the algorithm converges to the bound at sufficiently high SNRs by utilizing the space diversity introduced by the transmitter antennas.

Chapter 4

TIME-DELAY ESTIMATION IN COGNITIVE SINGLE-INPUT MULTIPLE-OUTPUT SYSTEMS

In this chapter, the time-delay estimation problem in cognitive SIMO systems is analyzed. In the previous chapters, the same problem is investigated in cognitive systems and MISO systems, which include frequency and space diversity, respectively. The study in this chapter focuses on facilitation of the combination of frequency and space diversity in time-delay estimation problem. It should be kept in mind that the space diversity here takes place as receive diversity.

In the rest of the chapter, the signal model is provided and afterwards the CRLB for the estimation of time-delay parameter is found. Then, the ML estimator is expressed and two-step approach similar to the one applied in Chapter

2 is used to propose an asymptotically optimal solution to the ML estimation. This solution consists of estimating the signal parameters at each receiver branch and combining the time-delay estimates at the second step. Various combination algorithms for combining these time-delay estimates are proposed and the performance analyses of them under various scenarios are provided in the simulations.

4.1 Signal Model

In a cognitive SIMO system, there are multiple antennas at the receiver and a single antenna at the transmitter side because of the SIMO structure. This structure is depicted in Figure 4.1.

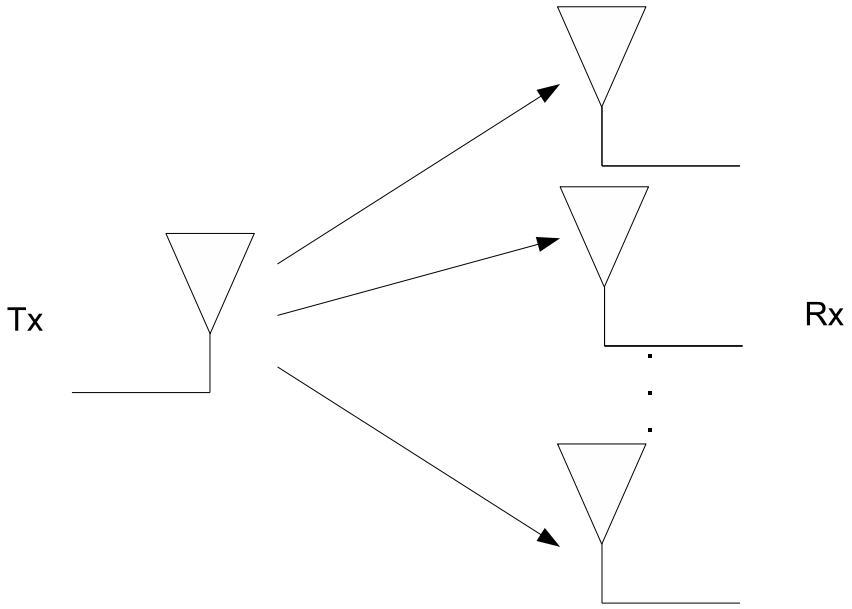

Figure 4.1: SIMO structure.

The transmitted signal utilizes multiple frequency bands. Therefore, the received signals at each of the receiver antennas has a dispersed spectrum structure,

as shown in Figure 2.1.

The baseband received signal at the kth band of the ith receiver antenna can be modeled as follows:

$$r_{ik}(t) = \alpha_{ik} e^{jw_k t} s_k(t-\tau) + n_{ik}(t) \ , \tag{4.1}$$

where $i = 1, \ldots, M$ is the index for the receiver antenna (M is the total number of receiver antennas) and $k = 1, \ldots, K$ is the index for the frequency band (K is the total number of frequency bands). Here, $\alpha_{ik} = a_{ik}\, e^{j\phi_{ik}}$ and w_k are the channel coefficient and the CFO of the corresponding receiver branch, respectively (a receiver branch is the transmission path from the transmitter to the receiver for a specific frequency band and a specific antenna). $s_k(t)$ is the baseband representation of the transmitted signal and τ is the time-delay of this signal. Additionally, $n_{ik}(t)$ represents the additive complex white Gaussian noise having independent components, each with spectral density σ_{ik}^2. Also, the noise processes at different antennas are modeled as independent from each other.

In this signal model, each of the signals, $s_k(t)$'s, are assumed to be narrowband signals. This facilitates the use of a single channel coefficient to denote the fading of each signal. Moreover, usage of narrowband signals makes the difference between time-delays of each received signal so small that the time-delays can be recognized as equal. Therefore, a single time-delay, τ, is used for each received signal.

If the separation distances between the receiver antennas are comparable to the signal wavelength, then the antennas are said to be sufficiently separated which implies that the channel coefficients can be considered as independent at different antennas.

4.2 CRLB Calculations

The estimation problem investigated in this chapter is the time-delay estimation in a cognitive SIMO system. As mentioned in Section 4.1, as a result of the narrowband assumption for each frequency band, there is a single unknown time-delay parameter. Since there is a separate channel coefficient α_{ik} for every receiver branch, there are two unknown parameters (a_{ik} and ϕ_{ik}) for each branch. w_k's are the CFOs of the frequency bands, so they are also among the unknown parameters. To sum up, the unknown signal parameters are given by the vector $\boldsymbol{\theta}$, which is described below:

$$\boldsymbol{\theta} = \begin{bmatrix} \tau & \boldsymbol{a} & \boldsymbol{\phi} & \boldsymbol{w} \end{bmatrix}, \tag{4.2}$$

where

$$\boldsymbol{a} = \begin{bmatrix} a_{11} & \dots & a_{1K} & a_{21} & \dots & a_{2K} & \dots & a_{M1} & \dots & a_{MK} \end{bmatrix}, \tag{4.3}$$

$$\boldsymbol{\phi} = \begin{bmatrix} \phi_{11} & \dots & \phi_{1K} & \phi_{21} & \dots & \phi_{2K} & \dots & \phi_{M1} & \dots & \phi_{MK} \end{bmatrix}, \tag{4.4}$$

$$\boldsymbol{w} = \begin{bmatrix} w_1 & \dots & w_K \end{bmatrix}. \tag{4.5}$$

If the received signal is observed in the time interval $[0, T]$, the log-likelihood function for $\boldsymbol{\theta}$ can be obtained from (4.1) as follows [49]:

$$\Lambda(\boldsymbol{\theta}) = c - \sum_{i=1}^{M} \sum_{k=1}^{K} \frac{1}{2\sigma_{ik}^2} \int_0^T \left| r_{ik}(t) - \alpha_{ik} e^{jw_k t} s_k(t-\tau) \right|^2 dt. \tag{4.6}$$

By using the log-likelihood expression in (4.6), the FIM is constructed, which

can be expressed as

$$\mathbf{I} = \begin{bmatrix} \mathrm{I}_{\tau\tau} & \mathbf{I}_{\tau a} & \mathbf{I}_{\tau\phi} & \mathbf{I}_{\tau w} \\ \mathbf{I}_{\tau a}^T & \mathbf{I}_{aa} & \mathbf{I}_{a\phi} & \mathbf{I}_{aw} \\ \mathbf{I}_{\tau\phi}^T & \mathbf{I}_{a\phi}^T & \mathbf{I}_{\phi\phi} & \mathbf{I}_{\phi w} \\ \mathbf{I}_{\tau w}^T & \mathbf{I}_{aw}^T & \mathbf{I}_{\phi w}^T & \mathbf{I}_{ww} \end{bmatrix} . \tag{4.7}$$

In order to calculate the FIM, the first derivatives of the log-likelihood function with respect to the unknown parameters are found and they are provided in Appendix A.

The submatrices of the FIM are provided below [1] [2] [3]:

$$\begin{aligned} \mathrm{I}_{\tau\tau} &= \mathrm{E}\left\{ \left(\frac{\partial \Lambda(\boldsymbol{\theta})}{\partial \tau} \right)^2 \right\} \\ &= \sum_{i=1}^{M} \sum_{k=1}^{K} \frac{a_{ik}^2}{\sigma_{ik}^2} \int_0^T |s_k^{'}(t-\tau)|^2 \, dt = \sum_{k=1}^{K} \tilde{E}_k \sum_{i=1}^{M} \frac{a_{ik}^2}{\sigma_{ik}^2} \end{aligned} \tag{4.8}$$

$$[\mathbf{I}_{aa}]_{\{ik\}\{ik\}} = \mathrm{E}\left\{ \left(\frac{\partial \Lambda(\boldsymbol{\theta})}{\partial a_{ik}} \right)^2 \right\} = \frac{1}{\sigma_{ik}^2} \int_0^T |s_k(t-\tau)|^2 \, dt = \frac{1}{\sigma_{ik}^2} E_k \tag{4.9}$$

$$[\mathbf{I}_{aa}]_{\{ik\}\{jl\}} = \mathrm{E}\left\{ \frac{\partial \Lambda(\boldsymbol{\theta})}{\partial a_{ik}} \frac{\partial \Lambda(\boldsymbol{\theta})}{\partial a_{jl}} \right\} = 0 \quad \text{for} \;\; i \neq j \text{ or } k \neq l \tag{4.10}$$

$$\begin{aligned} [\mathbf{I}_{\phi\phi}]_{\{ik\}\{ik\}} &= \mathrm{E}\left\{ \left(\frac{\partial \Lambda(\boldsymbol{\theta})}{\partial \phi_{ik}} \right)^2 \right\} = \frac{1}{\sigma_{ik}^2} \int_0^T a_{ik}^2 |s_k(t-\tau)|^2 \, dt \\ &= \frac{a_{ik}^2}{\sigma_{ik}^2} E_k \end{aligned} \tag{4.11}$$

$$[\mathbf{I}_{\phi\phi}]_{\{ik\}\{jl\}} = \mathrm{E}\left\{ \frac{\partial \Lambda(\boldsymbol{\theta})}{\partial \phi_{ik}} \frac{\partial \Lambda(\boldsymbol{\theta})}{\partial \phi_{jl}} \right\} = 0 \quad \text{for} \;\; i \neq j \text{ or } k \neq l \tag{4.12}$$

[1] $[\mathbf{X}]_{kl}$ denotes the element of matrix $\mathbf{X}$ in row k and column l.

[2] $[\mathbf{X}]_{\{ik\}\{jl\}}$ denotes the element of matrix $\mathbf{X}$ in row $(i-1)K+k$ and column $(j-1)K+l$.

[3] $[\mathbf{X}]_{\{ik\}\{l\}}$ denotes the element of matrix $\mathbf{X}$ in row $(i-1)K+k$ and column l.

$$[\mathbf{I}_{ww}]_{kk} = \mathrm{E}\left\{\left(\frac{\partial\Lambda(\boldsymbol{\theta})}{\partial w_k}\right)^2\right\} = \sum_{i=1}^{M}\frac{a_{ik}^2}{\sigma_{ik}^2}\int_0^T t^2|s_k(t-\tau)|^2\,dt \tag{4.13}$$

$$[\mathbf{I}_{ww}]_{kl} = \mathrm{E}\left\{\frac{\partial\Lambda(\boldsymbol{\theta})}{\partial w_k}\frac{\partial\Lambda(\boldsymbol{\theta})}{\partial w_l}\right\} = 0 \quad \text{for} \quad k{\neq}l \tag{4.14}$$

$$\begin{aligned}[\mathbf{I}_{\tau a}]_{ik} &= \mathrm{E}\left\{\left(\frac{\partial\Lambda(\boldsymbol{\theta})}{\partial\tau}\frac{\partial\Lambda(\boldsymbol{\theta})}{\partial a_{ik}}\right)\right\} \\ &= -\frac{1}{\sigma_{ik}^2}\int_0^T a_{ik}\mathcal{R}\left\{s_k^{'}(t-\tau)s_k^*(t-\tau)\right\} = \frac{-a_{ik}}{\sigma_{ik}^2}\hat{E}_k^{\mathrm{R}}\end{aligned} \tag{4.15}$$

$$\begin{aligned}[\mathbf{I}_{\tau\phi}]_{ik} &= \mathrm{E}\left\{\left(\frac{\partial\Lambda(\boldsymbol{\theta})}{\partial\tau}\frac{\partial\Lambda(\boldsymbol{\theta})}{\partial\phi_{ik}}\right)\right\} \\ &= \frac{-a_{ik}^2}{\sigma_{ik}^2}\int_0^T \mathcal{I}\left\{s_k^{'}(t-\tau)s_k^*(t-\tau)\right\} = \frac{-a_{ik}^2}{\sigma_{ik}^2}\hat{E}_k^{\mathrm{I}}\end{aligned} \tag{4.16}$$

$$\begin{aligned}[\mathbf{I}_{\tau w}]_{k} &= \mathrm{E}\left\{\left(\frac{\partial\Lambda(\boldsymbol{\theta})}{\partial\tau}\frac{\partial\Lambda(\boldsymbol{\theta})}{\partial w_k}\right)\right\} \\ &= \sum_{i=1}^{M}\frac{-a_{ik}^2}{\sigma_{ik}^2}\int_0^T \mathcal{I}\left\{ts_k^{'}(t-\tau)s_k^*(t-\tau)\right\} = \sum_{i=1}^{M}\frac{-a_{ik}^2}{\sigma_{ik}^2}G_k\end{aligned} \tag{4.17}$$

$$\begin{aligned}[\mathbf{I}_{a\phi}]_{\{ik\}\{ik\}} &= \mathrm{E}\left\{\left(\frac{\partial\Lambda(\boldsymbol{\theta})}{\partial a_{ik}}\frac{\partial\Lambda(\boldsymbol{\theta})}{\partial\phi_{ik}}\right)\right\} \\ &= -\frac{j}{4\sigma_{ik}^4}\int_0^T -2\sigma_{ik}^2a_{ik}|s_k(t-\tau)|^2 + 2\sigma_{ik}^2a_{ik}|s_k(t-\tau)|^2\,dt = 0\end{aligned} \tag{4.18}$$

$$[\mathbf{I}_{a\phi}]_{\{ik\}\{jl\}} = \mathrm{E}\left\{\left(\frac{\partial\Lambda(\boldsymbol{\theta})}{\partial a_{ik}}\frac{\partial\Lambda(\boldsymbol{\theta})}{\partial\phi_{jl}}\right)\right\} = 0 \quad \text{for} \quad i{\neq}j \text{ or } k{\neq}l \tag{4.19}$$

$$\begin{aligned}[\mathbf{I}_{aw}]_{\{ik\}\{k\}} &= \mathrm{E}\left\{\left(\frac{\partial\Lambda(\boldsymbol{\theta})}{\partial a_{ik}}\frac{\partial\Lambda(\boldsymbol{\theta})}{\partial w_k}\right)\right\} \\ &= -\frac{j}{4\sigma_{ik}^4}\int_0^T -t2\sigma_{ik}^2a_{ik}|s_k(t-\tau)|^2 + t2\sigma_{ik}^2a_{ik}|s_k(t-\tau)|^2\,dt = 0\end{aligned} \tag{4.20}$$

$$[\mathbf{I}_{aw}]_{\{ik\}\{l\}} = \mathrm{E}\left\{\left(\frac{\partial\Lambda(\boldsymbol{\theta})}{\partial a_{ik}}\frac{\partial\Lambda(\boldsymbol{\theta})}{\partial w_l}\right)\right\} = 0 \quad \text{for} \quad k{\neq}l \tag{4.21}$$

$$[\mathbf{I}_{\phi w}]_{\{ik\}\{l\}} = \mathrm{E}\left\{\left(\frac{\partial\Lambda(\boldsymbol{\theta})}{\partial \phi_{ik}}\frac{\partial\Lambda(\boldsymbol{\theta})}{\partial w_l}\right)\right\} = 0 \quad \text{for} \quad k{\neq}l \tag{4.22}$$

$$\begin{aligned}[\mathbf{I}_{\phi w}]_{\{ik\}\{k\}} &= \mathrm{E}\left\{\left(\frac{\partial\Lambda(\boldsymbol{\theta})}{\partial \phi_{ik}}\frac{\partial\Lambda(\boldsymbol{\theta})}{\partial w_k}\right)\right\} \\ &= -\frac{1}{4\sigma_{ik}^4}\int_0^T -2\sigma_{ik}^2 t a_{ik}^2|s_k(t-\tau)|^2 - 2\sigma_{ik}^2 t a_{ik}|s_k(t-\tau)|^2\,dt \\ &= \frac{a_{ik}^2}{\sigma_{ik}^2}\int_0^T t|s_k(t-\tau)|^2\,dt = \frac{a_{ik}^2}{\sigma_{ik}^2}\hat{F}_k\end{aligned} \tag{4.23}$$

The theoretical lower bound on the variance of an unbiased estimator is the CRLB. The problem investigated in this study is the time-delay estimation in a cognitive SIMO system; hence, the CRLB for the time-delay parameter must be found. The CRLB can be obtained from the inverse of the FIM. The CRLB for the time-delay parameter is the first element of the inverse of the FIM, which is $[\mathbf{I}^{-1}]_{11}$.

Before finding the CRLB, it is useful to observe that for any linear modulation in the form of $s_k(t) = \sum_n d_{k,n}p_k(t - nT_k)$, $\hat{E}_k^{\mathrm{I}} = 0$ and $G_k = 0$ (cf. Proposition 1 in [43]).

If the FIM is partitioned in the following form,

$$\mathbf{I} = \begin{bmatrix}\mathbf{A} & \mathbf{B} \\ \mathbf{B^T} & \mathbf{D}\end{bmatrix}, \tag{4.24}$$

where

$$\mathbf{A} = \begin{bmatrix}\mathbf{I}_{\tau\tau}\end{bmatrix}, \quad \mathbf{B} = \begin{bmatrix}\mathbf{I}_{\tau a} & \mathbf{I}_{\tau\phi} & \mathbf{I}_{\tau w}\end{bmatrix}, \quad \mathbf{D} = \begin{bmatrix}\mathbf{I}_{aa} & \mathbf{0} & \mathbf{0} \\ \mathbf{0} & \mathbf{I}_{\phi\phi} & \mathbf{I}_{\phi w} \\ \mathbf{0} & \mathbf{I}_{\phi w}^{\mathrm{T}} & \mathbf{I}_{ww}\end{bmatrix}, \tag{4.25}$$

then the CRLB, which is the first element of the inverse of the FIM, can be found in the following way:

$$\begin{aligned}\left[\mathbf{I}^{-1}\right]_{11} &= (\mathbf{A}-\mathbf{B}\mathbf{D}^{-1}\mathbf{B}^{\mathbf{T}})^{-1} \\ &= \left(\mathbf{I}_{\tau\tau}-\mathbf{I}_{\tau a}\mathbf{I}_{aa}^{-1}\mathbf{I}_{\tau a}^{\mathrm{T}}\right)^{-1} \\ &= \frac{1}{\sum_{k=1}^{K}\tilde{E}_k\sum_{i=1}^{M}\frac{a_{ik}^2}{\sigma_{ik}^2}-\frac{a_{ik}^2}{\sigma_{ik}^4}(\hat{E}_k^{\mathrm{R}})^2\frac{\sigma_{ik}^2}{E_k}} \\ &= \frac{1}{\sum_{k=1}^{K}\sum_{i=1}^{M}\frac{a_{ik}^2}{\sigma_{ik}^2}\left(\tilde{E}_k-\frac{(\hat{E}_k^{\mathrm{R}})^2}{E_k}\right)}\end{aligned} \tag{4.26}$$

Furthermore, if the linear modulation of the form $s_k(t)=\sum_n d_{k,n}p_k(t-nT_k)$ is with $|d_{k,n}|=|d_k|$ and $p_k(0)=p_k(T_i)$, then $\hat{E}^{\mathrm{R}}=0$ (cf. Proposition 2 in [43]). Finally, the CRLB becomes

$$\left[\mathbf{I}^{-1}\right]_{1x1}=\frac{1}{\sum_{k=1}^{K}\sum_{i=1}^{M}\frac{a_{ik}^2}{\sigma_{ik}^2}\tilde{E}_k}. \tag{4.27}$$

4.3 CRLB Calculations for Single Band and Single Antenna Systems

For a receiver branch, which means the channel between the transmitter and a receiver antenna for a single frequency band, the unknown parameter vector, $\boldsymbol{\theta}_{ik}$, can be described as

$$\boldsymbol{\theta}_{ik}=\begin{bmatrix}\tau_{ik} & a_{ik} & \phi_{ik} & w_{ik}\end{bmatrix}, \tag{4.28}$$

where the definitions of the parameters are the same as in Section 4.1.

The model for the baseband received signal is provided in (4.1). In our two-step approach for time-delay estimation, the unknown parameters for the received

signal is estimated separately at each branch. Therefore, the baseband received signal model can be modified to be as follows:

$$r_{ik}(t) = \alpha_{ik} e^{jw_{ik}t} s_k(t - \tau_{ik}) + n_{ik}(t) \ , \tag{4.29}$$

with the same definitions for the received and transmitted signals, and the noise process as in Section 4.1.

From (4.29), the log-likelihood function for $\boldsymbol{\theta}_{ik}$ can be expressed as follows:

$$\Lambda(\boldsymbol{\theta}_{ik}) = c - \frac{1}{2\sigma_{ik}^2} \int_0^T \left| r_{ik}(t) - \alpha_{ik} e^{jw_{ik}t} s_k(t - \tau_{ik}) \right|^2 dt, \tag{4.30}$$

assuming that the received signal is observed in the time interval $[0, T]$. Here, c is a constant that is independent of $\boldsymbol{\theta}_{ik}$.

The FIM for the time-delay estimation problem in a receiver branch, which is obtained from (4.30), is as follows:

$$\mathbf{I} = \begin{bmatrix} \mathrm{I}_{\tau\tau} & \mathbf{I}_{\tau a} & \mathbf{I}_{\tau\phi} & \mathbf{I}_{\tau w} \\ \mathbf{I}_{\tau a}^T & \mathbf{I}_{aa} & \mathbf{I}_{a\phi} & \mathbf{I}_{aw} \\ \mathbf{I}_{\tau\phi}^T & \mathbf{I}_{a\phi}^T & \mathbf{I}_{\phi\phi} & \mathbf{I}_{\phi w} \\ \mathbf{I}_{\tau w}^T & \mathbf{I}_{aw}^T & \mathbf{I}_{\phi w}^T & \mathbf{I}_{ww} \end{bmatrix} . \tag{4.31}$$

In order to calculate the FIM, the first derivatives of the log-likelihood function with respect to the unknown parameters are found and they are provided in Appendix B.

The submatrices of the FIM are provided below:

$$\begin{aligned} \mathbf{I}_{\tau\tau} = \mathrm{E}\left\{ \left(\frac{\partial \Lambda(\boldsymbol{\theta})}{\partial \tau_{ik}} \right)^2 \right\} &= \frac{1}{\sigma_{ik}^4} \int_0^T a_{ik}^2 \sigma_{ik}^2 |s_k'(t - \tau_{ik})|^2 \, dt \\ &= \frac{a_{ik}^2}{\sigma_{ik}^2} \tilde{E}_k \end{aligned} \tag{4.32}$$

$$\mathbf{I}_{aa} = \mathrm{E}\left\{\left(\frac{\partial\Lambda(\boldsymbol{\theta})}{\partial a_{ik}}\right)^2\right\} = \frac{1}{\sigma_{ik}^4}\int_0^T |s_k(t-\tau_{ik})|^2\sigma_{ik}^2\,dt$$
$$= \frac{1}{\sigma_{ik}^2}E_k \tag{4.33}$$

$$\mathbf{I}_{\phi\phi} = \mathrm{E}\left\{\left(\frac{\partial\Lambda(\boldsymbol{\theta})}{\partial \phi_{ik}}\right)^2\right\} = \frac{1}{\sigma_{ik}^4}\int_0^T a_{ik}^2|s_k(t-\tau_{ik})|^2\sigma_{ik}^2\,dt$$
$$= \frac{a_{ik}^2}{\sigma_{ik}^2}E_k \tag{4.34}$$

$$\mathbf{I}_{ww} = \mathrm{E}\left\{\left(\frac{\partial\Lambda(\boldsymbol{\theta})}{\partial w_{ik}}\right)^2\right\} = \frac{1}{\sigma_{ik}^4}\int_0^T t^2a_{ik}^2|s_k(t-\tau_{ik})|^2\sigma_{ik}^2\,dt$$
$$= \frac{a_{ik}^2}{\sigma_{ik}^2}\int_0^T t^2|s_k(t-\tau_{ik})|^2\,dt \tag{4.35}$$

$$\mathbf{I}_{\tau a} = \mathrm{E}\left\{\left(\frac{\partial\Lambda(\boldsymbol{\theta})}{\partial\tau_{ik}}\frac{\partial\Lambda(\boldsymbol{\theta})}{\partial a_{ik}}\right)\right\} = -\frac{1}{\sigma_{ik}^4}\int_0^T \sigma_{ik}^2a_{ik}\mathcal{R}\left\{s_k^{'}(t-\tau_{ik})s_k^*(t-\tau_{ik})\right\}$$
$$= \frac{-a_{ik}}{\sigma_{ik}^2}\hat{E}_k^{\mathrm{R}} \tag{4.36}$$

$$\mathbf{I}_{\tau\phi} = \mathrm{E}\left\{\left(\frac{\partial\Lambda(\boldsymbol{\theta})}{\partial\tau_{ik}}\frac{\partial\Lambda(\boldsymbol{\theta})}{\partial\phi_{ik}}\right)\right\} = \frac{-a_{ik}^2}{\sigma_{ik}^2}\int_0^T \mathcal{I}\left\{s_k^{'}(t-\tau_{ik})s_k^*(t-\tau_{ik})\right\}$$
$$= \frac{-a_{ik}^2}{\sigma_{ik}^2}\hat{E}_k^{\mathrm{I}} \tag{4.37}$$

$$\mathbf{I}_{\tau w} = \mathrm{E}\left\{\left(\frac{\partial\Lambda(\boldsymbol{\theta})}{\partial\tau_{ik}}\frac{\partial\Lambda(\boldsymbol{\theta})}{\partial w_{ik}}\right)\right\} = \frac{-a_{ik}^2}{\sigma_{ik}^2}\int_0^T \mathcal{I}\left\{ts_k^{'}(t-\tau_{ik})s_k^*(t-\tau_{ik})\right\}$$
$$= \frac{-a_{ik}^2}{\sigma_{ik}^2}G_k \tag{4.38}$$

$$\mathbf{I}_{a\phi} = \mathrm{E}\left\{\left(\frac{\partial\Lambda(\boldsymbol{\theta})}{\partial a_{ik}}\frac{\partial\Lambda(\boldsymbol{\theta})}{\partial\phi_{ik}}\right)\right\}$$
$$= -\frac{j}{4\sigma_{ik}^4}\int_0^T -2\sigma_{ik}^2a_{ik}|s_k(t-\tau_{ik})|^2 + 2\sigma_{ik}^2a_{ik}|s_k(t-\tau_{ik})|^2\,dt = 0 \tag{4.39}$$

$$\mathbf{I}_{aw} = \mathrm{E}\left\{\left(\frac{\partial\Lambda(\boldsymbol{\theta})}{\partial a_{ik}}\frac{\partial\Lambda(\boldsymbol{\theta})}{\partial w_{ik}}\right)\right\}$$
$$= -\frac{j}{4\sigma_{ik}^4}\int_0^T -t2\sigma_{ik}^2 a_{ik}|s_k(t-\tau_{ik})|^2 + t2\sigma_{ik}^2 a_{ik}|s_k(t-\tau_{ik})|^2\,dt = 0 \quad (4.40)$$

$$\mathbf{I}_{\phi w} = \mathrm{E}\left\{\left(\frac{\partial\Lambda(\boldsymbol{\theta})}{\partial \phi_{ik}}\frac{\partial\Lambda(\boldsymbol{\theta})}{\partial w_{ik}}\right)\right\}$$
$$= -\frac{1}{4\sigma_{ik}^4}\int_0^T -2\sigma_{ik}^2 t a_{ik}^2|s_k(t-\tau_{ik})|^2 - 2\sigma_{ik}^2 t a_{ik}|s_k(t-\tau_{ik})|^2\,dt$$
$$= \frac{a_{ik}^2}{\sigma_{ik}^2}\int_0^T t|s_k(t-\tau_{ik})|^2\,dt = \frac{a_{ik}^2}{\sigma_{ik}^2}\hat{F}_k \quad (4.41)$$

The FIM can be written as $\mathbf{I} = \begin{bmatrix}\mathbf{A} & \mathbf{B}\\ \mathbf{B^T} & \mathbf{D}\end{bmatrix}$ where $\mathbf{A} = \begin{bmatrix}\mathbf{I}_{\tau\tau} & \mathbf{I}_{\tau a}\\ \mathbf{I}_{\tau a}^T & \mathbf{I}_{aa}\end{bmatrix}$, $\mathbf{B} = \begin{bmatrix}\mathbf{I}_{\tau\phi} & \mathbf{I}_{\tau w}\\ 0 & 0\end{bmatrix}$, and $\mathbf{D} = \begin{bmatrix}\mathbf{I}_{\phi\phi} & \mathbf{I}_{\phi w}\\ \mathbf{I}_{\phi w}^T & \mathbf{I}_{ww}\end{bmatrix}$. The first 2-by-2 block of $\mathbf{I}$ can be calculated as $\left[\mathbf{I}^{-1}\right]_{2\times 2} = (\mathbf{A} - \mathbf{B}\mathbf{D}^{-1}\mathbf{B}^{\mathbf{T}})^{-1}$.

If $\hat{E}_k = 0$, then $\mathbf{I}_{\tau a} = 0$, and $\mathbf{I}_{\tau\phi} = 0$. If also $\mathbf{I}_{\tau w} = 0$ is satisfied, then

$$\left[\mathbf{I}^{-1}\right]_{2\times 2} = \begin{bmatrix}\frac{\sigma_{ik}^2}{a_{ik}^2\tilde{E}_k} & 0\\ 0 & \frac{\sigma_{ik}^2}{E_k}\end{bmatrix} \quad (4.42)$$

becomes valid.

This result leads us to the following lemma on the delay and channel amplitude estimates at high SNRs.

Lemma 2: *Consider any linear modulation of the form* $s_k(t) = \sum_n d_{k,n}p_k(t - nT_k)$*, where* $d_{k,n}$ *denotes the complex data for the* n*th symbol of signal* k*, and* $p_k(t)$ *represents a pulse with duration* T_k*. Assume that* $\int_{-\infty}^{\infty} s_k'(t-\tau)s_k^*(t-\tau)\mathrm{d}t = 0$ *for* $k = 1, \ldots, K$*. Then, for the signal model in (4.1), the delay estimate in (4.48)*

and the channel amplitude estimate in (4.49) can be modeled, at high SNR, as

$$\hat{\tau}_{ik} = \tau + \nu_{ik} \ , \tag{4.43}$$

$$\hat{a}_{ik} = a_{ik} + \eta_{ik} \ , \tag{4.44}$$

for $k = 1, \ldots, K$ *and* $i = 1, \ldots, M$*, where* ν_{ik} *and* η_{ik} *are independent zero mean Gaussian random variables with variances* $\sigma_{ik}^2/(\tilde{E}_k\, a_{ik}^2)$ *and* σ_{ik}^2/E_k*, respectively. In addition,* ν_{ik} *and* ν_{jl} *(*η_{ik} *and* η_{jl}*) are independent for* $i \neq j$ *and* $k \neq l$*.*

4.4 Two-Step Time-Delay Estimation

The optimal solution for the time-delay estimation is the parameter vector that maximizes the log-likelihood function given in (4.6). This solution, which is the ML estimate, can be expressed as follows:

$$\hat{\boldsymbol{\theta}} = \arg\max_{\boldsymbol{\theta}} \left\{ c - \sum_{i=1}^{M} \sum_{k=1}^{K} \frac{1}{2\sigma_{ik}^2} \int_0^T \left| r_{ik}(t) - \alpha_{ik} e^{jw_k t} s_k(t-\tau) \right|^2 dt \right\}. \tag{4.45}$$

This ML estimate includes an optimization over $2MK + K + 1$ variables, which has huge computational complexity. To avoid such a complex method, an alternative two-step solution is proposed to this problem.

In the first step, using the received signal, the ML estimate for the time-delay parameter is found for every receiver branch (If there are M receiver antennas and K frequency branches, then there are $M \times K$ branches.). The weighted combination of the time-delay estimates obtained from each branch is the second step of the time-delay estimation process. The weights used in this step determines the complexity and accuracy of the estimator. The two-step approach is depicted in Figure 4.2.

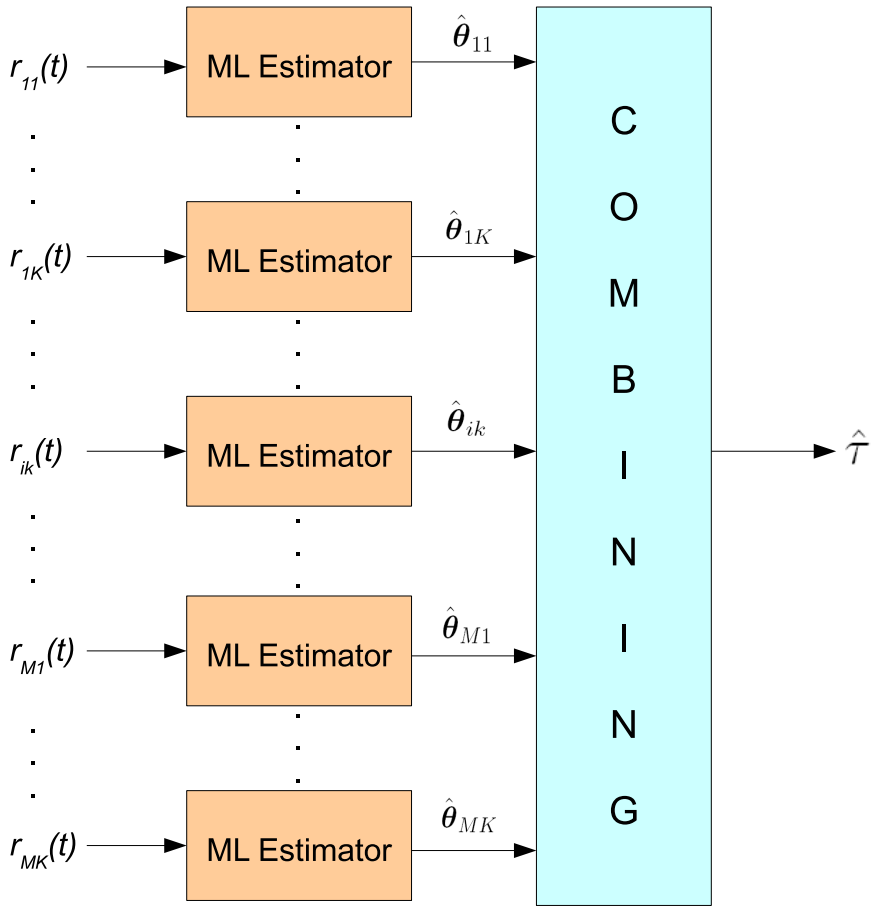

Figure 4.2: Illustration of the two-step time-delay estimation algorithm for a cognitive SIMO system.

4.4.1 First Step: Maximum Likelihood Estimation at Each Branch

The unknown parameters at each branch are denoted by vector $\boldsymbol{\theta}_{ik}$, as mentioned in (4.28). The ML estimate for these unknown parameters is the set of parameter values that maximize the log-likelihood function in (4.30); that is,

$$\hat{\boldsymbol{\theta}}_{ik} = \arg\max_{\boldsymbol{\theta}_{ik}} \left\{ c - \frac{1}{2\sigma_{ik}^2} \int_0^T \left| r_{ik}(t) - \alpha_{ik} e^{jw_{ik}t} s_k(t-\tau_{ik}) \right|^2 dt \right\}, \tag{4.46}$$

which is equivalent to

$$\hat{\boldsymbol{\theta}}_{ik} = \arg\min_{\boldsymbol{\theta}_{ik}} \int_0^T \left| r_{ik}(t) - \alpha_{ik} e^{jw_{ik}t} s_k(t-\tau_{ik}) \right|^2 dt \ . \tag{4.47}$$

At each branch, the unknown parameters are estimated separately and they are denoted by the unknown parameter vector $\hat{\boldsymbol{\theta}}_{ik} = \left[\hat{\tau}_{ik} \quad \hat{a}_{ik} \quad \hat{\phi}_{ik} \quad \hat{w}_{ik}\right]$. The expression in (4.47) is separable into two parts, so is the ML estimation process. Therefore, the optimization problem in (4.47) can be performed in two steps as follows:

$$\left[\hat{\tau}_{ik} \ \hat{\phi}_{ik} \ \hat{\omega}_{ik}\right] = \arg \max_{\tau_{ik},\omega_{ik},\phi_{ik}} \left| \int_0^T \mathcal{R}\left\{ r_{ik}(t)\, \mathrm{e}^{-j(\omega_{ik}t+\phi_{ik})} s_{ik}^*(t-\tau_{ik}) \right\} \mathrm{d}t \right| \tag{4.48}$$

and

$$\hat{a}_{ik} = \frac{1}{E_{ik}} \int_0^T \mathcal{R}\left\{ r_{ik}(t)\, \mathrm{e}^{-j(\hat{\omega}_{ik}t+\hat{\phi}_{ik})} s_{ik}^*(t-\hat{\tau}_{ik}) \right\} \mathrm{d}t \ . \tag{4.49}$$

In this way, the optimization process over $2MK + K + 1$ variables that the ML estimation in (4.45) requires is avoided and this process in handled by MK optimizations each of which are over 3 variables.

If it is assumed that the CFOs (w_{ik}'s) are zero, which means that the carrier frequencies are known, then the w_{ik}'s in (4.48) and (4.49) will be omitted and the equations will become as follows:

$$\left[\hat{\tau}_{ik}\ \hat{\phi}_{ik}\right] = \arg\max_{\tau_{ik},\phi_{ik}} \left| \int_0^T \mathcal{R}\left\{ r_{ik}(t)\, \mathrm{e}^{-j\phi_{ik}} s_{ik}^*(t-\tau_{ik}) \right\} \mathrm{d}t \right| \tag{4.50}$$

and

$$\hat{a}_{ik} = \frac{1}{E_{ik}} \int_0^T \mathcal{R}\left\{ r_{ik}(t)\, \mathrm{e}^{-j\hat{\phi}_{ik}} s_{ik}^*(t-\hat{\tau}_{ik}) \right\} \mathrm{d}t\ . \tag{4.51}$$

4.4.2 Second Step: Combining Time-Delay Estimates from Different Branches

1. Optimal Combining: In this combining method, the time-delay estimates obtained from each receiver branch are combined. This is performed by finding the weighted average of MK time-delay estimates. The weight determined for each branch is expressed as

$$\beta_{ik} = \frac{\hat{a}_{ik}^2 \tilde{E}_{ik}}{\sigma_{ik}^2}\ . \tag{4.52}$$

Using these weights, the combining is performed as follows:

$$\hat{\tau} = \frac{\sum_{i=1}^{M}\sum_{k=1}^{K} \beta_{ik}\hat{\tau}_{ik}}{\sum_{i=1}^{M}\sum_{k=1}^{K} \beta_{ik}}\ . \tag{4.53}$$

By a similar discussion to the one provided in Section 2.3.2 about the effective bandwidth component in the weights used in optimal combining, the weights used here also means to combine the time-delay estimates of different branches in proportion to the multiplication of the SNR estimate and the effective bandwidth of that branch, which means that the optimal combining considers both the SNR and the effective bandwidth of the branches while calculating the weighted average of time-delay estimates.

2. SNR Combining: In this combining method, the weights assigned to each time-delay estimate obtained from the branches are as follows:

$$\mu_{ik} = \frac{\hat{a}_{ik}^2 E_{ik}}{\sigma_{ik}^2} \ . \tag{4.54}$$

These weights are used for combining the estimates as

$$\hat{\tau} = \frac{\sum_{i=1}^{M} \sum_{k=1}^{K} \mu_{ik} \hat{\tau}_{ik}}{\sum_{i=1}^{M} \sum_{k=1}^{K} \mu_{ik}} \ . \tag{4.55}$$

The difference between this estimator and the optimal combining estimator is that SNR combining only weights the branches according to their SNR values, whereas optimal combining considers both the SNR and effective bandwidth values. SNR combining omits the effective bandwidth term in the weights.

3. Selection Combining 1: In the previous two combining methods, the weighted average of the estimates are used as the final time-delay estimate. In selection combining, the best branch is used as the final time-delay estimate.

In selection combining 1, the definition of the best branch is in terms of the weights that are used in the optimal combining method. The time-delay of the branch that has the maximum β_{ik} is selected as the final time-delay estimate; that is,

$$\hat{\tau} = \hat{\tau}_{jl} \ , \tag{4.56}$$

with

$$\begin{aligned} \{j, l\} &= \arg \max_{i \in \{1,\ldots,M\},\ k \in \{1,\ldots,K\}} \{\beta_{ik}\} \\ &= \arg \max_{i \in \{1,\ldots,M\},\ k \in \{1,\ldots,K\}} \left\{ \frac{\hat{a}_{ik}^2 \tilde{E}_{ik}}{\sigma_{ik}^2} \right\}, \end{aligned} \tag{4.57}$$

where j and l are the i and k indices of the branch that have the maximum β_{ik}.

4. Selection Combining 2: In selection combining 2, the best branch is selected by using the SNR values of the receiver branches. The SNR value of each branch is as it is defined in the "SNR combining" method, that is $\mu_{ik} = \hat{a}_{ik}^2 E_{ik}/\sigma_{ik}^2$. Hence, the selection combining method 2 is performed as follows:

$$\hat{\tau} = \hat{\tau}_{jl} \ , \tag{4.58}$$

with

$$\begin{aligned} \{j,l\} &= \arg \max_{i\in\{1,\ldots,M\},\ k\in\{1,\ldots,K\}} \{\mu_{ik}\} \\ &= \arg \max_{i\in\{1,\ldots,M\},\ k\in\{1,\ldots,K\}} \left\{ \frac{\hat{a}_{ik}^2 E_{ik}}{\sigma_{ik}^2} \right\} \ . \end{aligned} \tag{4.59}$$

5. Equal Combining: In this combining method, the time-delay estimates from different branches are combined regardless of their "importance". That is, in equal combining, all of the time-delay estimates are assigned equal weights

$$\hat{\tau} = \frac{1}{MK} \sum_{i=1}^{M} \sum_{k=1}^{K} \hat{\tau}_{ik} \ . \tag{4.60}$$

4.5 Optimality of the Two-Step Estimator

The rule for the two-step estimator that employs optimal combining is

$$\hat{\tau} = \frac{\sum_{i=1}^{M} \sum_{k=1}^{K} \beta_{ik} \hat{\tau}_{ik}}{\sum_{i=1}^{M} \sum_{k=1}^{K} \beta_{ik}} \ , \tag{4.61}$$

where

$$\beta_{ik} = \frac{\hat{a}_{ik}^2 \tilde{E}_k}{\sigma_{ik}^2} \ , \tag{4.62}$$

as mentioned before.

It can be shown that

$$\mathrm{E}\left\{\hat{\tau}|\hat{a}_{ik}...\right\} = \frac{\sum_{i=1}^{M}\sum_{k=1}^{K}\beta_{ik}E\{\hat{\tau}_{ik}|\hat{a}_{ik}...\}}{\sum_{i=1}^{M}\sum_{k=1}^{K}\beta_{ik}} = \frac{\sum_{i=1}^{M}\sum_{k=1}^{K}\beta_{ik}E\{\hat{\tau}_{ik}|\hat{a}_{ik}\}}{\sum_{i=1}^{M}\sum_{k=1}^{K}\beta_{ik}} \tag{4.63}$$

$$= \tau = \mathrm{E}\{\hat{\tau}\} \tag{4.64}$$

Hence, the estimator is unbiased. (The equality of the above expression to τ results from Lemma 2)

On the other hand, the conditional variance can be expressed as

$$\mathrm{Var}\left\{\hat{\tau}|\hat{a}_{ik}...\right\} = \frac{\sum_{i=1}^{M}\sum_{k=1}^{K}\beta_{ik}^2 \mathrm{Var}\{\hat{\tau}_{ik}|\hat{a}_{ik}...\}}{\left(\sum_{i=1}^{M}\sum_{k=1}^{K}\beta_{ik}\right)^2} \ . \tag{4.65}$$

From the same lemma, $\mathrm{Var}\left\{\hat{\tau}|\hat{a}_{ik}...\right\} = \mathrm{Var}\left\{\hat{\tau}|\hat{a}_{ik}\right\} = \frac{\sigma_{ik}^2}{a_{ik}^2 \tilde{E}_k}$. Then

$$\mathrm{Var}\left\{\hat{\tau}|\hat{a}_{ik}...\right\} = \frac{\sum_{i=1}^{M}\sum_{k=1}^{K}\frac{\hat{a}_{ik}^4 \tilde{E}_k^2}{\sigma_{ik}^4}\frac{\sigma_{ik}^2}{a_{ik}^2 \tilde{E}_k}}{\left(\sum_{i=1}^{M}\sum_{k=1}^{K}\frac{\hat{a}_{ik}^2 \tilde{E}_k}{\sigma_{ik}^2}\right)^2} \ . \tag{4.66}$$

According to the lemma; at high SNRs, $\hat{a}_{ik}$ is distributed as a Gaussian random variable with mean a_{ik} and variance σ_{ik}^2/E_k.

$$\mathrm{Var}\left\{\hat{\tau}|\hat{a}_{ik}...\right\} \approx \frac{1}{\sum_{i=1}^{M}\sum_{k=1}^{K}\frac{a_{ik}^2}{\sigma_{ik}^2}\tilde{E}_k} \ , \tag{4.67}$$

which is equal to the CRLB. Hence, the estimator is approximately optimal at high SNRs.

Optimality of the estimator can also be proved when the other combining techniques are used. An example of such proof for SNR combining can be carried out similar to the proof in Section 2.4.

4.6 Simulation Results

Simulations are performed in order to compare the performance of the various combining methods proposed in Section 4.4. The performance evaluation of these methods is carried out by comparing them with each other and with the theoretical bound, the CRLB.

In the simulations, the signal at each branch, $s_k(t)$ in (4.1), is modeled by the Gaussian doublet which can be expressed as follows:

$$s_k(t) = A_k \left(1 - \frac{4\pi(t - 1.25\,\zeta_k)^2}{\zeta_k^2}\right) e^{-2\pi(t-1.25\zeta_k)^2/\zeta_k^2}\ , \tag{4.68}$$

where A_k is the parameter that adjusts the energy of the pulse. In the following simulations, the pulses are adjusted to have unit-energy. ζ_k is the parameter that adjusts the pulse width which can be approximately expressed as $\zeta_k \approx 1/(2.5\,B_k)$ in terms of the bandwidth B_k of the signal $s_k(t)$ [25].

For all the simulations, the time-delay, τ, is uniformly distributed over the observation interval. The distribution of ϕ_{ik} is also the same for all the simulations, which is uniform distribution in the interval $[0, 2\pi)$. For different branches, the spectral density of the noise process is assumed to be the same. Additionally, the definition of the SNR is the same for all the simulation scenarios, which is $\text{SNR} = 10\log_{10}\left(\frac{\sum_{i=1}^{M}\sum_{k=1}^{K} E_{ik}}{2\,\sigma_{ik}^2}\right)$.

In Figure 4.3, the first simulation result is presented. It depicts the performance of the estimators in terms of the RMSE as the SNR increases. The distribution of the magnitude of each channel coefficient, a_{ik}, is assumed to be Rayleigh distributed with an average power of 1, i.e. $\text{E}\{|\alpha_{ik}^2|\} = \text{E}\{a_{ik}^2\} = 1$. There are 2 antennas ($M = 2$) and 3 spectrum bands ($K = 3$) with different bandwidths, i.e. 100 kHz, 200 kHz, and 400 kHz.

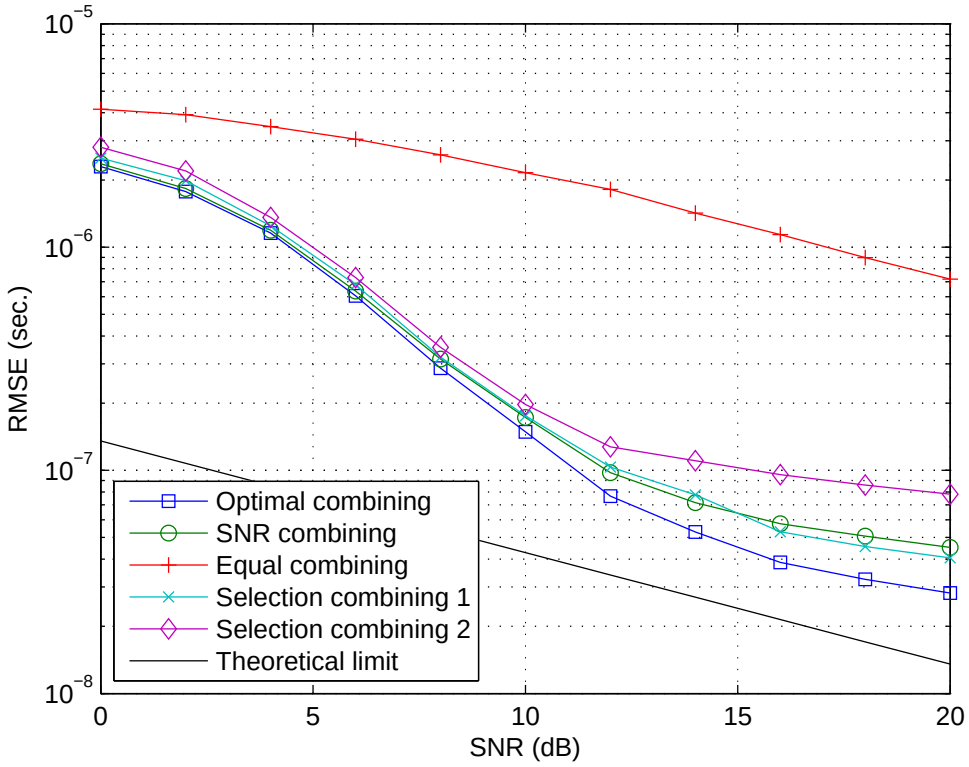

Figure 4.3: The performances of the estimators, RMSE vs. SNR, and the theoretical limit (CRLB). There are 2 receive antennas, 3 dispersed bands with 100 kHz, 200 kHz, and 400 kHz bandwidths under Rayleigh fading condition.

As observed from Figure 4.3, in this simulation scenario, the best performance is achieved by the optimal combining estimator. Selection combining 1 is the second best after optimal combining. SNR combining has worse performance than optimal combining and selection combining 1. Selection combining 2, which selects the best branch in terms of the SNR values of the branches, has worse performance than SNR combining, which takes the weighted average of the time-delays by using their SNRs. Equal combining has the worst performance among all of the estimators, since it takes the average of the time-delay estimates

regardless of the "importances" of the branches.

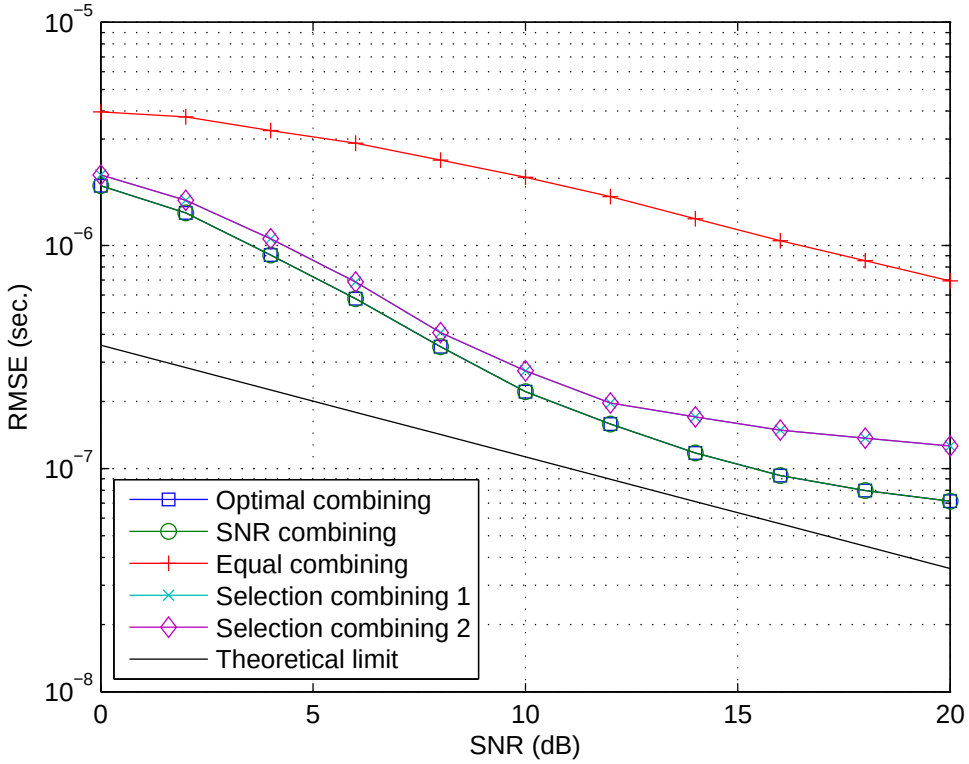

Figure 4.4: The performances of the estimators, RMSE vs. SNR, and the theoretical limit (CRLB). There are 2 receive antennas, 3 dispersed bands each with 100 kHz bandwidth under Rayleigh fading condition.

Figure 4.4 provides the performance of the estimators under the same scenario as in Figure 4.3, except for the bandwidths of the frequency bands. The bandwidths are the same for all bands, which is 100 kHz for each band.

As mentioned before, the optimal combining algorithm uses $\beta_{ik} = \hat{a}_{ik}^2 \tilde{E}_{ik}/\sigma_{ik}^2$ and the SNR combining uses $\mu_{ik} = \hat{a}_{ik}^2 E_{ik}/\sigma_{ik}^2$ as the weights for each branch. In this case, since the bandwidths for all the bands are the same, the energies of the signals at different branches will be equal to each other. Similarly, the energies of

the signal derivatives will also be equal at all the branches. Therefore, for both optimal combining and SNR combining, the time-delays of different branches will be combined effectively by using $\hat{a}_{ik}^2/\sigma_{ik}^2$, which means the omission of $\tilde{E}_{ik}$ and E_{ik} from β_{ik} and μ_{ik}, respectively. This leads to the same final time-delay estimates for SNR and optimal combining methods, as seen in Figure 4.4. Since selection combining methods are based on selecting the time-delays of the best branches by using the same criteria as the optimal and SNR combining, they also give the same final estimate. The best performance is achieved by optimal/SNR combining pair, as expected. The selection combining is worse than this pair. Equal combining is the worst, as before.

The results of the simulations which test the estimators' RMSE performance as the number of spectrum bands increases are depicted in Figure 4.5. The number of antennas is two ($M = 2$). The bandwidths of the signals at different bands are all equal to 100 kHz. The spectral density of the noise processes is the same at each branch, as mentioned before. The distributions of the channel parameters are selected to be the same as in the previous simulations.

Since the bandwidths of the frequency bands are the same, the SNR combining and the optimal combining methods show the same performance, like the selection combining methods do. As before, the estimators are ranked in following order depending on their performances: Optimal combining, selection combining, and equal combining. It is notable that when the number of bands reaches 5, the return of the selection combining becomes negligible as the number of bands continues increasing. Another point is that the return of the equal combining increases as the number of bands increases.

The next simulation scenario has 3 frequency bands with 100 kHz, 200 kHz,

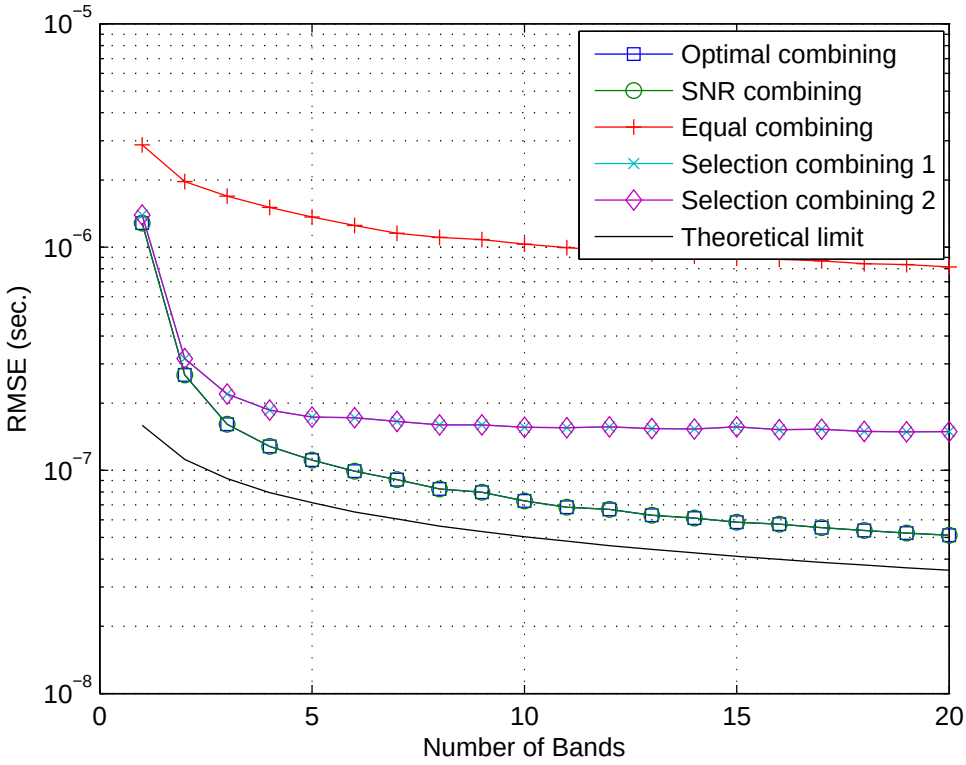

Figure 4.5: The performances of the estimators, RMSE vs. number of bands, and the theoretical limit (CRLB). There are 2 receive antennas under Rayleigh fading condition.

and 400 kHz bandwidths. In this case, the performance analysis is carried out as the number of receive antennas is increased. The other simulation parameters are the same as in the previous simulations. In Figure 4.6, the results of this simulation can be observed.

The best performance result again belongs to optimal combining. The SNR combining and selection combining 1 methods are so close to each other, which come after optimal combining. Selection combining 2 performs worse than these estimators. The performance of equal combining is way worse than the others

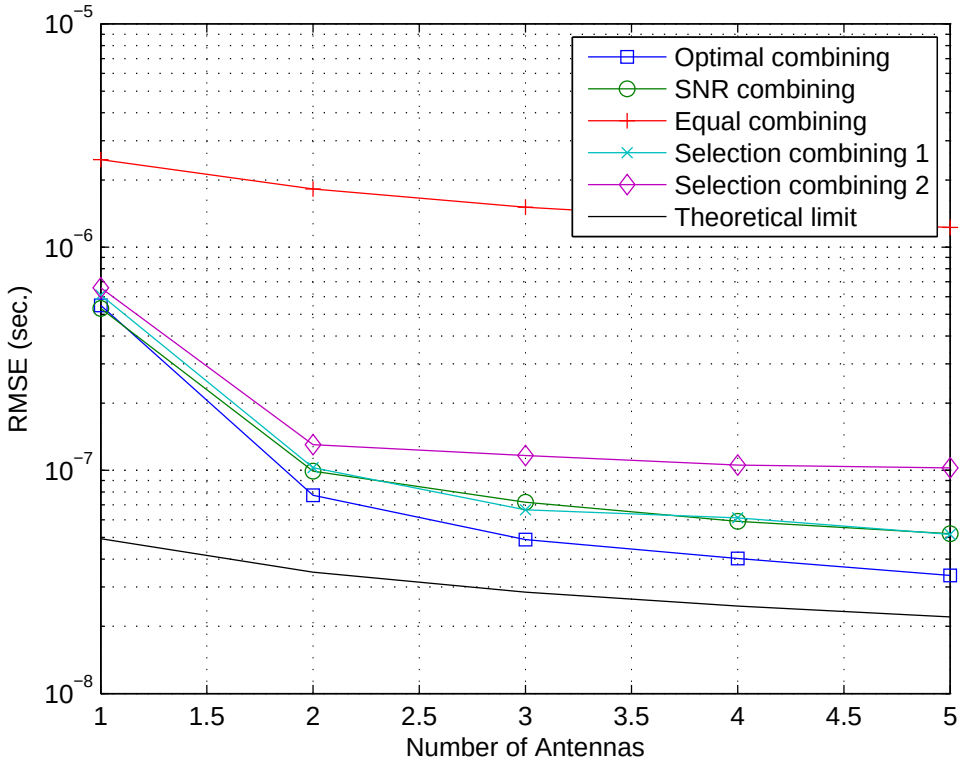

Figure 4.6: The performances of the estimators, RMSE vs. number of antennas, and the theoretical limit (CRLB). There are 3 dispersed bands with 100 kHz, 200 kHz, and 400 kHz bandwidths under Rayleigh fading condition.

but it comes closer as the number of bands increases.

Figure 4.7 illustrates the results of a similar simulation scenario as the previous one, the only difference being the same bandwidth usage for all frequency bands; i.e., 100 kHz instead of using different bandwidths.

Similar to the simulation results depicted in Figure 4.6, the optimal combining is the best, followed by the selection combining and the equal combining. Moreover, as in the simulation results in Figure 4.4, the optimal combining has the same performance as the SNR combining, and selection combining methods

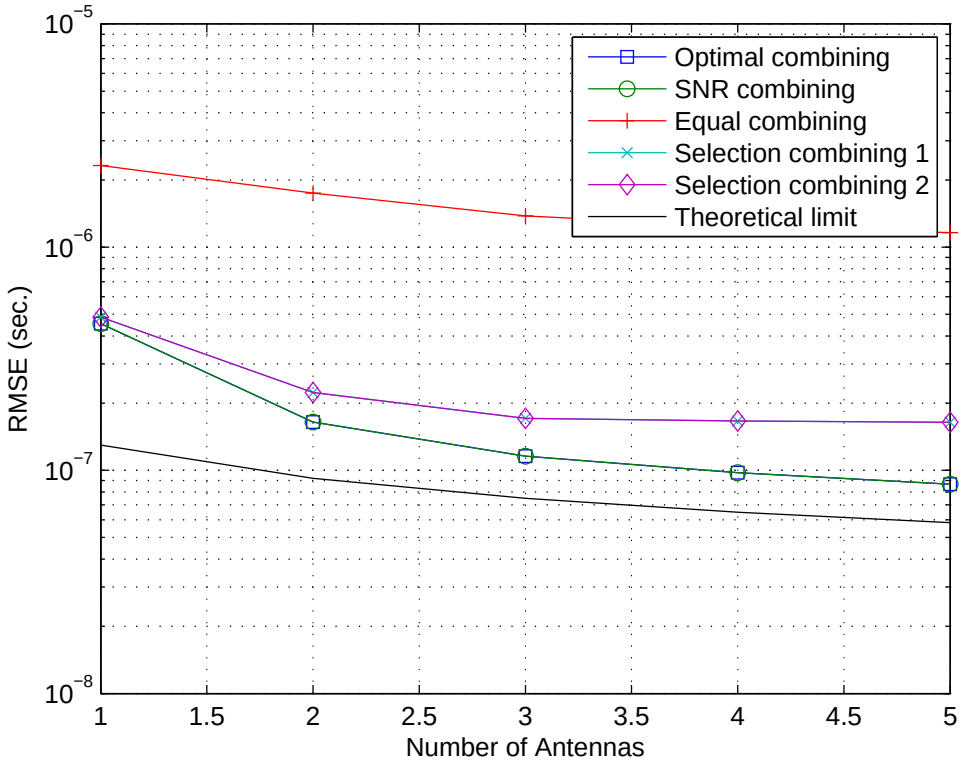

Figure 4.7: The performances of the estimators, RMSE vs. number of antennas, and the theoretical limit (CRLB). There are 3 dispersed bands each with 100 kHz bandwidth under Rayleigh fading condition.

are also the same in terms of the RMSE performance.

In the following set of simulations, the distribution of the magnitude of the channel coefficients is selected as Rician distribution with an average power of 1, i.e. $\mathrm{E}\{|a_{ik}^2|\} = 1$. The K factor of Rician distribution is selected as 5. Rician fading assumption replaces the Rayleigh fading assumption in the first 5 simulations. The simulation pairs that use the same simulation scenarios other than the Rician-Rayleigh fading replacement are as follows: Figure 4.3-Figure 4.8, Figure 4.4-Figure 4.9, Figure 4.5-Figure 4.10, Figure 4.6-Figure 4.11, and

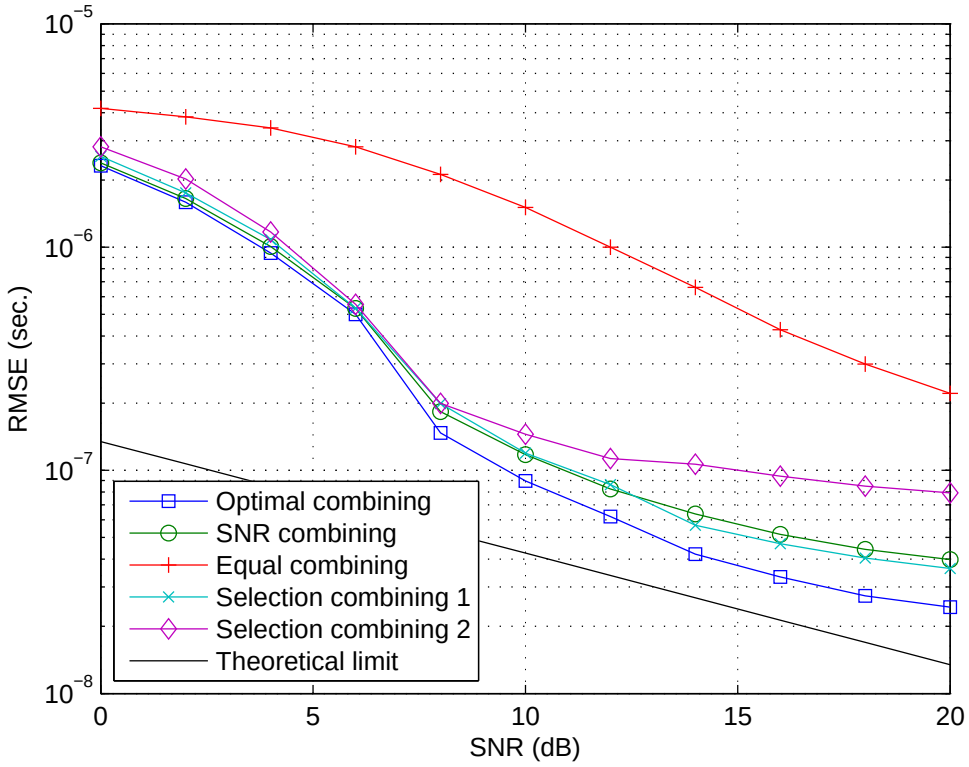

Figure 4.8: The performances of the estimators, RMSE vs. SNR, and the theoretical limit (CRLB). There are 2 receive antennas, 3 dispersed bands with 100 kHz, 200 kHz, and 400 kHz bandwidths under Rician fading condition.

Figure 4.7-Figure 4.12.

In Figure 4.8, the relative performances of the algorithms are the same as in Figure 4.3. The biggest difference between the two simulations is the improvement in the performance of equal combining algorithm in Rician fading scenario. The performance of equal combining gets closer to the other algorithms under Rician fading, whereas it is worse in Rayleigh fading channel. This can be bound to the fact that in Rician fading channel, there is a LOS component that improves the performance of the estimator. Since the other algorithms are already close to

the theoretical limit, they are affected much from this performance improvement. Therefore, the biggest change is observed in equal combining estimator.

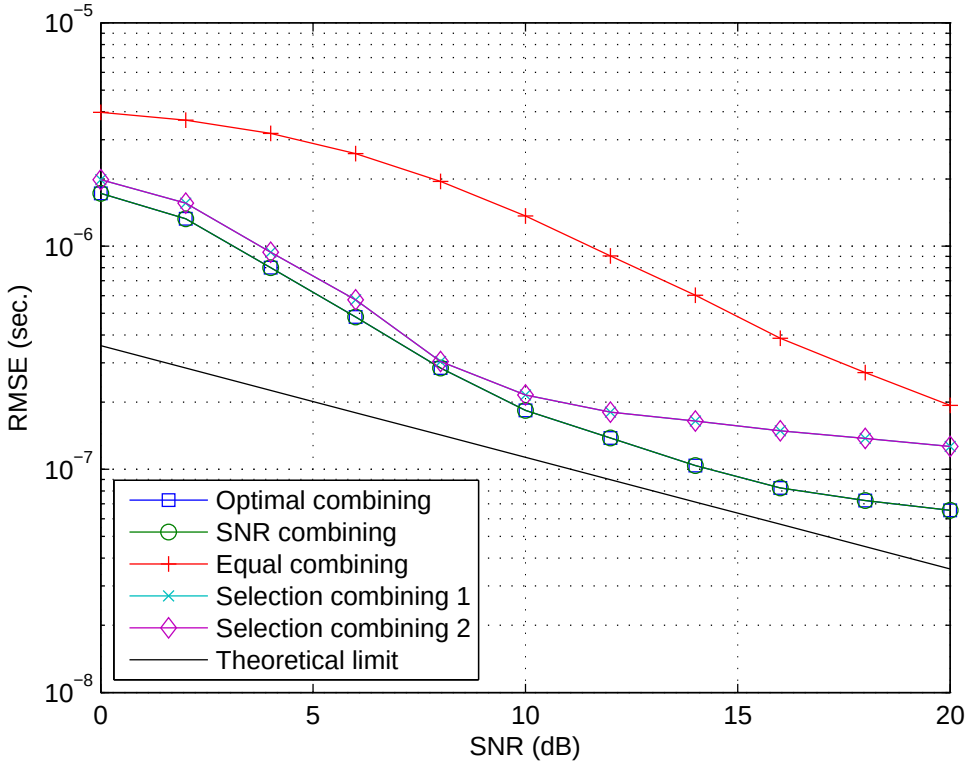

Figure 4.9: The performances of the estimators, RMSE vs. SNR, and the theoretical limit (CRLB). There are 2 receive antennas, 3 dispersed bands each with 100 kHz bandwidth under Rician fading condition.

In Figure 4.9, the combining weights of the SNR combining and optimal combining methods reduce to the same weights, like in Figure 4.4. Therefore SNR combining and optimal combining perform exactly the same, so do the selection combining methods. Equal combining has better performance compared to the Rayleigh fading scenario, but still worse than the other algorithms'.

In Figure 4.10, it can observed that the performance of optimal combining

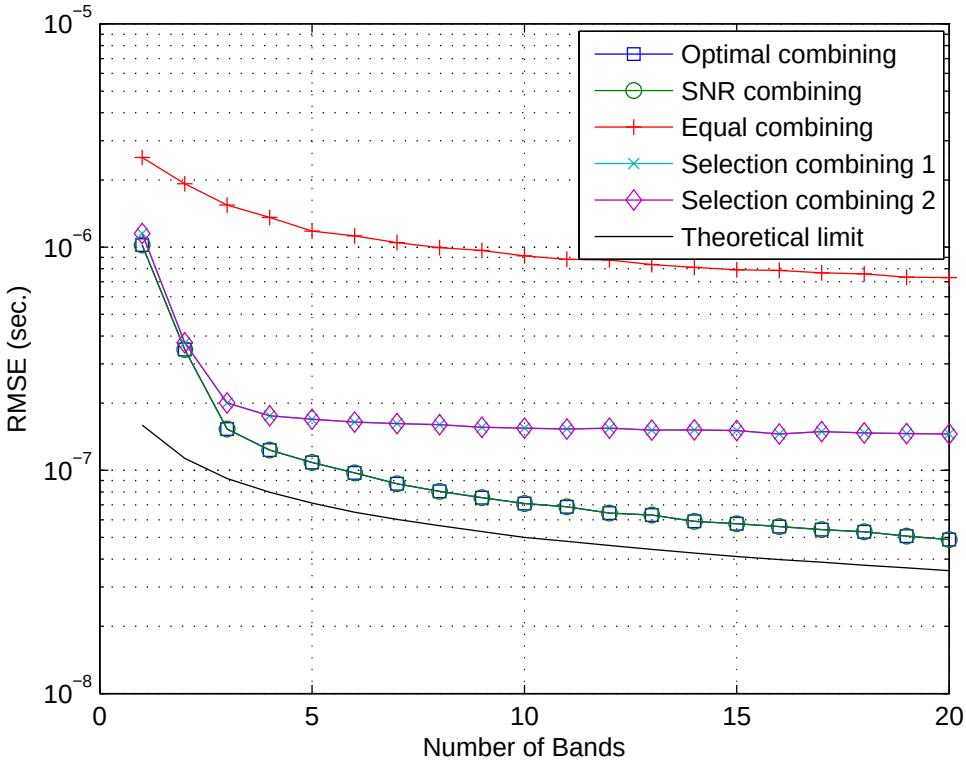

Figure 4.10: The performances of the estimators, RMSE vs. number of bands, and the theoretical limit (CRLB). There are 2 receive antennas under Rician fading condition.

stays close to the CRLB as the number of bands increases, whereas the selection combining methods exhibit a diminishing return, that is after 5 bands there is almost no improvement. The equal combining performs the worst of all. There is no significant difference in performance between Rayleigh fading (cf. Figure 4.5) and Rician fading versions (cf. Figure 4.10).

In Figure 4.11, it can be observed that as the number of antennas increases, the performances of the algorithms increase. Here, again, the best performance belongs to the optimal combining, which becomes closer to the CRLB as the

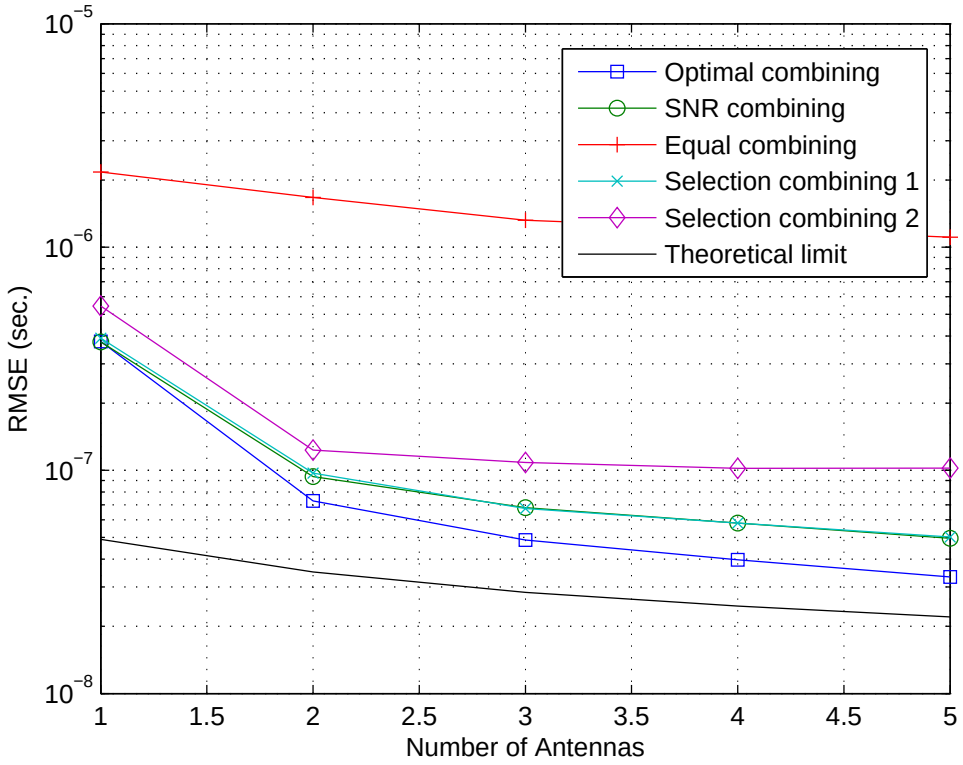

Figure 4.11: The performances of the estimators, RMSE vs. number of antennas, and the theoretical limit (CRLB). There are 3 dispersed bands with 100 kHz, 200 kHz, and 400 kHz bandwidths under Rician fading condition.

number of antennas increases. Selection combining 1 and SNR combining perform almost the same. Similar to the previous simulation, under Rayleigh fading and Rician fading assumptions, the algorithms perform almost the same.

In Figure 4.12, the performances of the algorithms are similar to the previous simulation (cf. Figure 4.11), the only difference being the same weight usage in SNR and optimal combining algorithms, and so in selection combining algorithms.

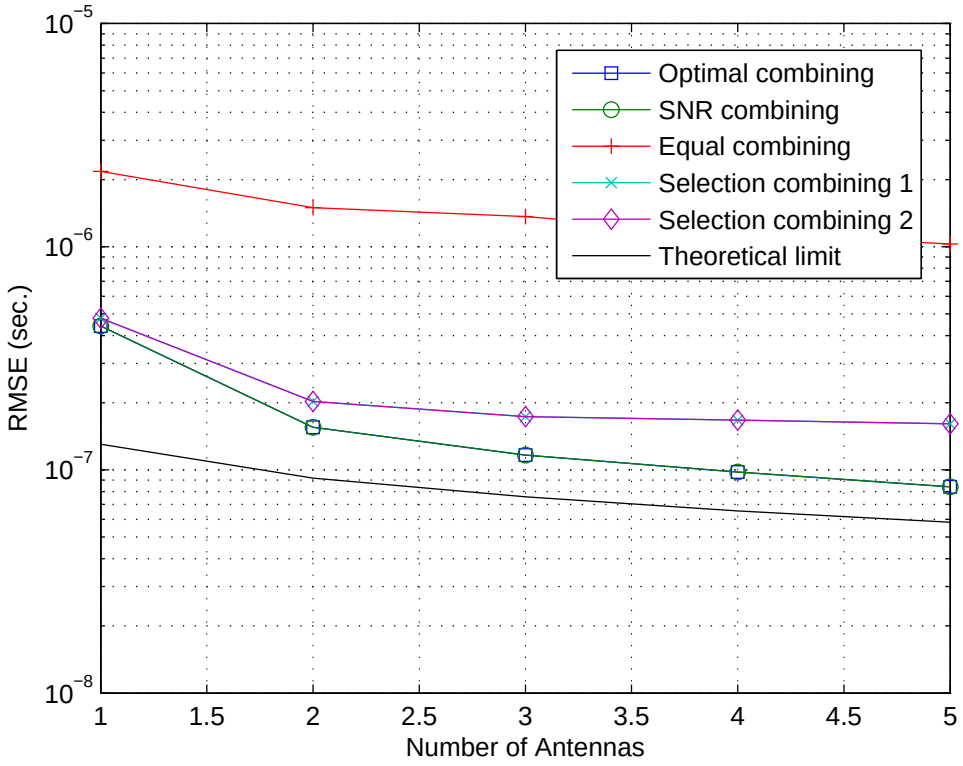

Figure 4.12: The performances of the estimators, RMSE vs. number of antennas, and the theoretical limit (CRLB). There are 3 dispersed bands each with 100 kHz bandwidth under Rician fading condition.

Chapter 5

Conclusions

In this thesis, the time-delay estimation problems in cognitive radio systems, MISO systems, and cognitive SIMO systems have been studied.

In time-delay estimation for dispersed spectrum cognitive radio systems, after the investigation of the ML estimator and the CRLBs, a two-step approach has been proposed to obtain accurate time-delay estimates with reasonable computational complexity. In the first step of the proposed approach, an ML estimator is used at each branch of the receiver in order to estimate the unknown parameters of the received signal at that branch. Then, in the second step, a number of diversity combining approaches have been studied. In the optimal combining technique, both the SNRs and the bandwidths of the signals at different branches are considered to obtain the time-delay estimate, whereas the SNR combining technique obtains the time-delay estimate according to the estimated SNR values only. In addition, two selection combining techniques, as well as the equal combining technique, have been investigated. It has been shown that the optimal combining technique can approximate the CRLB at high SNRs, whereas the

equal combining technique has the worst performance since it does not make use of any information about signal bandwidths and/or the SNRs. Simulation results have been presented to verify the theoretical analysis.

In the time-delay estimation for MISO systems study, the expression for the theoretical limit (CRLB) has been found. The ML estimator achieves the CRLB under certain conditions; however, it can have very high computational complexity. To avoid this, a genetic global optimization algorithm has been used to obtain the ML estimate with lower computational complexity. It has been observed that DE can find the ML estimate much more rapidly than the exhaustive search method, and that the parameters of DE are crucial in terms of obtaining the optimum point that maximizes the log-likelihood function. The optimum parameter values have been selected for DE and applied in the algorithm. In addition, this study has emphasized the importance of space diversity for the time-delay estimation problem in MISO systems. It has been stated that the transmit diversity can be utilized by using signals with orthogonal derivatives. Finally, the performance of DE has been tested under various channel conditions. It has been observed that the DE based ML algorithm converges to the CRLB at lower SNRs in the Rician fading channel than in the Rayleigh fading one. However, in both of the scenarios, the algorithm reaches the CRLB at sufficiently high SNRs by utilizing the transmit diversity, with much lower computational complexity than the ML estimator via an exhaustive search.

In the last study of this thesis, which is the analysis of the time-delay estimation problem in cognitive SIMO systems, the approach is similar to the one in the estimation problem in cognitive radio systems. The CRLB has been found and the two-step time-delay estimation has been proposed. The performance analysis

of the algorithms applied in the second step of this two-step approach has been carried out. It has been observed in the simulations that optimal estimator has the best performance among all estimators. The effective bandwidth property of the signals has not been taken into account in SNR combining algorithm, although it has been done so in optimal combining. Therefore, SNR combining performs a little bit worse than the optimal combining. Selection combining algorithms select the time-delay estimate of the "best" branch, which trade off simplicity with performance. Equal combining is the simplest and the worst of all. Changing the fading assumption from Rayleigh fading to Rician fading is shown to significantly improve the estimator performance of equal combining in some simulations.

Finally, joint analysis of the time-delay estimation problems of MISO systems and cognitive SIMO systems leads to the analysis of the same problem in cognitive MIMO systems. This follows from the fact that a MIMO system can be perceived as multiple MISO systems connected to each receiver antenna of a SIMO system. The inclusion of dispersed spectrum structure to a MIMO system results in a cognitive MIMO system, which can be handled in analysis belonging to the cognitive SIMO systems. Therefore, the most general scenario, the time-delay estimation problem in a system with space diversity both at the receiver and the transmitter, and with frequency diversity, is developed and analyzed in the framework in this thesis.

Appendix A

Assuming the received signal is observed in the time interval $[0, T]$, from Eq. (4.1), the log-likelihood function for $\boldsymbol{\theta}$ can be found as follows [49]:

$$\begin{aligned}
\Lambda(\boldsymbol{\theta}) =& c - \sum_{i=1}^{M}\sum_{k=1}^{K} \frac{1}{2\sigma_{ik}^2} \int_0^T \left| r_{ik}(t) - \alpha_{ik} e^{jw_k t} s_k(t-\tau) \right|^2 dt \\
=& c - \sum_{i=1}^{M}\sum_{k=1}^{K} \frac{1}{2\sigma_{ik}^2} \int_0^T \left\{ r_{ik}(t) - a_{ik} e^{j\phi_{ik} + jw_k t} s_k(t-\tau) \right\} \\
& \left\{ r_{ik}^*(t) - a_{ik} e^{-j\phi_{ik} - jw_k t} s_k^*(t-\tau) \right\} dt \\
=& c - \sum_{i=1}^{M}\sum_{k=1}^{K} \frac{1}{2\sigma_{ik}^2} \int_0^T |r_{ik}(t)|^2 - r_{ik}(t) a_{ik} e^{-j\phi_{ik} - jw_k t} s_k^*(t-\tau) \\
& - r_{ik}^*(t) a_{ik} e^{j\phi_{ik} + jw_k t} s_k(t-\tau) + a_{ik}^2 |s_k(t-\tau)|^2 \, dt
\end{aligned} \tag{A.1}$$

The first derivatives of the log-likelihood function are provided in equations

(A.2), (A.3), (A.4), and (A.5).

$$\begin{aligned}
\frac{\partial \Lambda(\boldsymbol{\theta})}{\partial \tau} =& -\sum_{i=1}^{M}\sum_{k=1}^{K}\frac{1}{2\sigma_{ik}^2}\int_0^T r_{ik}(t)a_{ik}e^{-j\phi_{ik}-jw_kt}s_k^{'*}(t-\tau) \\
&+ r_{ik}^*(t)a_{ik}e^{j\phi_{ik}+jw_kt}s_k^{'}(t-\tau) \\
&- a_{ik}^2 s_k(t-\tau)s_k^{'*}(t-\tau) - a_{ik}^2 s_k^{'}(t-\tau)s_k^*(t-\tau)\,dt \\
=& -\sum_{i=1}^{M}\sum_{k=1}^{K}\frac{1}{2\sigma_{ik}^2}\int_0^T \alpha_{ik}^*\Big(r_{ik}(t)-\alpha_{ik}e^{jw_kt}s_k(t-\tau)\Big)s_k^{'*}(t-\tau)e^{-jw_kt} \\
&+ \alpha_{ik}\Big(r_{ik}^*(t)-\alpha_{ik}^*e^{-jw_kt}s_k^*(t-\tau)\Big)s_k^{'}(t-\tau)e^{jw_kt}\,dt \\
=& -\sum_{i=1}^{M}\sum_{k=1}^{K}\frac{1}{2\sigma_{ik}^2}\int_0^T \alpha_{ik}^* n_{ik}(t)e^{-jw_kt}s_k^{'*}(t-\tau) \\
&+ \alpha_{ik}n_{ik}^*(t)e^{jw_kt}s_k^{'}(t-\tau)\,dt
\end{aligned} \tag{A.2}$$

$$\begin{aligned}
\frac{\partial \Lambda(\boldsymbol{\theta})}{\partial a_{ik}} =& \frac{1}{2\sigma_{ik}^2}\int_0^T r_{ik}(t)e^{-j\phi_{ik}-jw_kt}s_k^*(t-\tau) \\
&+ r_{ik}^*(t)e^{j\phi_{ik}+jw_kt}s_k(t-\tau) - 2a_{ik}|s_k(t-\tau)|^2\,dt \\
=& \frac{1}{2\sigma_{ik}^2}\int_0^T s_k^*(t-\tau)e^{-j\phi_{ik}-jw_kt}\Big(r_{ik}(t)-\alpha_{ik}e^{jw_kt}s_k(t-\tau)\Big) \\
&+ s_k(t-\tau)e^{j\phi_{ik}+jw_kt}\Big(r_{ik}^*(t)-\alpha_{ik}^*e^{-jw_kt}s_k^*(t-\tau)\Big)\,dt \\
=& \frac{1}{2\sigma_{ik}^2}\int_0^T s_k^*(t-\tau)e^{-j\phi_{ik}-jw_kt}n_{ik}(t) + s_k(t-\tau)e^{j\phi_{ik}+jw_kt}n_{ik}^*(t)\,dt
\end{aligned} \tag{A.3}$$

$$\begin{aligned}
\frac{\partial \Lambda(\boldsymbol{\theta})}{\partial \phi_{ik}} =& -\frac{1}{2\sigma_{ik}^2}\int_0^T jr_{ik}(t)a_{ik}e^{-j\phi_{ik}-jw_kt}s_k^*(t-\tau) \\
&- jr_{ik}^*(t)a_{ik}e^{j\phi_{ik}+jw_kt}s_k(t-\tau)\,dt \\
=& \frac{-j}{2\sigma_{ik}^2}\int_0^T \Big(\alpha_{ik}e^{jw_kt}s_k(t-\tau)+n_{ik}(t)\Big)a_{ik}e^{-j\phi_{ik}-jw_kt}s_k^*(t-\tau) \\
&- \Big(\alpha_{ik}^*e^{-jw_kt}s_k^*(t-\tau)+n_{ik}^*(t)\Big)a_{ik}e^{j\phi_{ik}+jw_kt}s_k(t-\tau)\,dt \\
=& \frac{-j}{2\sigma_{ik}^2}\int_0^T n_{ik}(t)\alpha_{ik}^*e^{-jw_kt}s_k^*(t-\tau) - n_{ik}^*(t)\alpha_{ik}e^{jw_kt}s_k(t-\tau)\,dt
\end{aligned} \tag{A.4}$$

$$\begin{aligned}\frac{\partial \Lambda(\boldsymbol{\theta})}{\partial w_k} &= -\sum_{i=1}^{M} \frac{1}{2\sigma_{ik}^2} \int_0^T jtr_{ik}(t) a_{ik} e^{-j\phi_{ik} - jw_k t} s_k^*(t-\tau) \\ &\quad - jtr_{ik}^*(t) a_{ik} e^{j\phi_{ik} + jw_k t} s_k(t-\tau)\, dt \\ &= -\sum_{i=1}^{M} \frac{j}{2\sigma_{ik}^2} \int_0^T tn_{ik}(t) \alpha_{ik}^* e^{-jw_k t} s_k^*(t-\tau) - tn_{ik}^*(t) \alpha_{ik} e^{jw_k t} s_k(t-\tau)\, dt\end{aligned} \tag{A.5}$$

Appendix B

Assuming the received signal is observed in the time interval $[0, T]$, from Eq. (4.29), the log-likelihood function for $\boldsymbol{\theta}_{ik}$ can be found as follows [49]:

$$\begin{aligned}\Lambda(\boldsymbol{\theta}_{ik}) =& c - \sum_{i=1}^{M}\sum_{k=1}^{K}\frac{1}{2\sigma_{ik}^2}\int_0^T \left|r_{ik}(t) - \alpha_{ik}e^{jw_{ik}t}s_k(t-\tau_{ik})\right|^2 dt \\ =& c - \sum_{i=1}^{M}\sum_{k=1}^{K}\frac{1}{2\sigma_{ik}^2}\int_0^T \left\{r_{ik}(t) - a_{ik}e^{j\phi_{ik}+jw_{ik}t}s_k(t-\tau_{ik})\right\} \\ & \left\{r_{ik}^*(t) - a_{ik}e^{-j\phi_{ik}-jw_{ik}t}s_k^*(t-\tau_{ik})\right\} dt\end{aligned} \tag{B.1}$$

The first derivatives of the log-likelihood function are as follows:

$$\begin{aligned}\frac{\partial\Lambda(\boldsymbol{\theta}_{ik})}{\partial\tau_{ik}} =& -\frac{1}{2\sigma_{ik}^2}\int_0^T \alpha_{ik}^* n_{ik}(t)e^{-jw_{ik}t}s_k'^*(t-\tau) \\ & + \alpha_{ik}n_{ik}^*(t)e^{jw_{ik}t}s_k'(t-\tau)\,dt\end{aligned} \tag{B.2}$$

$$\begin{aligned}\frac{\partial\Lambda(\boldsymbol{\theta}_{ik})}{\partial a_{ik}} =& \frac{1}{2\sigma_{ik}^2}\int_0^T s_k^*(t-\tau_{ik})e^{-j\phi_{ik}-jw_{ik}t}n_{ik}(t) \\ & + s_k(t-\tau_{ik})e^{j\phi_{ik}+jw_{ik}t}n_{ik}^*(t)\,dt\end{aligned} \tag{B.3}$$

$$\begin{aligned}\frac{\partial\Lambda(\boldsymbol{\theta}_{ik})}{\partial\phi_{ik}} =& \frac{-j}{2\sigma_{ik}^2}\int_0^T n_{ik}(t)\alpha_{ik}^*e^{-jw_{ik}t}s_k^*(t-\tau_{ik}) \\ & - n_{ik}^*(t)\alpha_{ik}e^{jw_{ik}t}s_k(t-\tau_{ik})\,dt\end{aligned} \tag{B.4}$$

$$\frac{\partial \Lambda(\boldsymbol{\theta}_{ik})}{\partial w_{ik}} = \frac{-j}{2\sigma_{ik}^2} \int_0^T t n_{ik}(t) \alpha_{ik}^* e^{-jw_{ik}t} s_k^*(t - \tau_{ik}) - t n_{ik}^*(t) \alpha_{ik} e^{jw_{ik}t} s_k(t - \tau_{ik})\, dt \tag{B.5}$$

Bibliography

[1] J. Mitola and G. Q. Maguire, "Cognitive radio: Making software radios more personal," vol. 6, no. 4, pp. 13–18, Aug. 1999.

[2] S. Haykin, "Cognitive radio: Brain-empowered wireless communications," *IEEE J. Select Areas Commun.*, vol. 23, no. 2, pp. 201–220, Feb. 2005.

[3] Z. Quan, S. Cui, H. V. Poor, and A. H. Sayed, "Collaborative wideband sensing for cognitive radios," *IEEE Signal Process. Mag.*, vol. 25, no. 6, pp. 60–73, Nov. 2008.

[4] Q. Zhao and B. Sadler, "A survey of dynamic spectrum access," *IEEE Signal Process. Mag.*, vol. 24, no. 3, pp. 79–89, May 2007.

[5] N. Devroye, M. Vu, and V. Tarokh, "Cognitive radio networks," *IEEE Signal Process. Mag.*, vol. 25, no. 6, pp. 12–23, Nov. 2008.

[6] G. Scutari, D. Palomar, and S. Barbarossa, "Cognitive MIMO radio," *IEEE Signal Process. Mag.*, vol. 25, no. 6, pp. 46–59, Nov. 2008.

[7] I. Budiarjo, H. Nikookar, and L. Ligthart, "Cognitive radio modulation techniques," *IEEE Signal Process. Mag.*, vol. 25, no. 6, pp. 24–34, Nov. 2008.

[8] H. Arslan (ed.), *Cognitive Radio, Software Defined Radio, and Adaptive Wireless Systems*. New York: Springer, Sep. 2007.

[9] J. O. Neel, "Analysis and design of cognitive radio networks and distributed radio resource management algorithms," Ph.D. dissertation, Virginia Polytechnic Institute and State University, Blacksburg, VA, Sept. 2006.

[10] H. Celebi and H. Arslan, "Enabling location and environment awareness in cognitive radios," *Elsevier Computer Communications (Special Issue on Advanced Location-Based Services)*, vol. 31, no. 6, pp. 1114–1125, April 2008.

[11] R. V. Prasad, P. Pawelczak, J. A. Hoffmeyer, and H. S. Berger, "Cognitive functionality in next generation wireless networks: Standardization efforts," *IEEE Communications Magazine*, vol. 46, no. 4, pp. 72–78, Apr. 2008.

[12] Federal Communications Commission (FCC), "Facilitating opportunities for flexible, efficient, and reliable spectrum use employing cognitive radio technologies," *ET Docket No. 03-108*, Mar. 2005.

[13] M. Wellens, J. Wu, and P. Mahonen, "Evaluation of spectrum occupancy in indoor and outdoor scenario in the context of cognitive radio," in *Proc. International Conference on Cognitive Radio Oriented Wireless Networks and Communications (CROWNCOM)*, Orlando, FL, Aug. 2007.

[14] `http://www.cmpe.boun.edu.tr/WiCo/doku.php?id=research`.

[15] E. Biglieri, A. Constantinides, R. Calderbank, A. Goldsmith, A. Paulraj, and H. V. Poor, *MIMO Wireless Communications*. Cambridge Univ. Press, 2007.

[16] R. W. Heath and A. Paulraj, "Switching between diversity and multiplexing in MIMO systems," *IEEE Transactions on Communications*, vol. 53, no. 6, pp. 962–968, June 2005.

[17] R. Zhang and Y. C. Liang, "Exploiting multi-antennas for opportunistic spectrum sharing in cognitive radio networks," *IEEE Journal on Selected Topics in Signal Processing*, vol. 2, no. 1, pp. 88–102, Feb. 2008.

[18] I. Budiarjo, M. K. Lakshmanan, and H. Nikookar, "Cognitive radio dynamic access techniques," *Wireless Personal Communications*, vol. 45, pp. 293–324, Feb. 2008.

[19] E. Baccarelli, M. Biagi, C. Pelizzoni, and N. Cordeschi, "Cognitive MIMO radio: An emerging paradigm for enhancing wireless access capability," *International Journal of Communication Networks and Distributed Systems*, vol. 2, no. 2–3, pp. 302–330, 2009.

[20] G. Scutari, D. P. Palomar, and S. Barbarossa, "Cognitive MIMO radio," *IEEE Signal Processing Magazine*, vol. 25, no. 6, pp. 46–59, Nov. 2008.

[21] Y. Zeng, Y. C. Liang, A. T. Hoang, and R. Zhang, "A review on spectrum sensing for cognitive radio: Challenges and solutions," *EURASIP Journal on Advances in Signal Processing*, pp. Article ID 381 465, 15 pages, 2010.

[22] F. Kocak, H. Celebi, S. Gezici, K. A. Qaraqe, H. Arslan, and H. V. Poor, "Time-delay estimation in dispersed spectrum cognitive radio systems," *EURASIP Journal on Advances in Signal Processing, Special Issue on Advanced Signal Processing for Cognitive Radio Networks*, pp. Article ID 675 959, 10 pages, 2010.

[23] S. Gezici, "A survey on wireless position estimation," *Wireless Personal Communications, Special Issue on Towards Global and Seamless Personal Navigation*, vol. 44, no. 3, pp. 263–282, Feb. 2008.

[24] J. J. Caffery, *Wireless Localization in CDMA Cellular Radio Systems.* Boston: Kluwer, 2000.

[25] Z. Sahinoglu, S. Gezici, and I. Guvenc, *Ultra-Wideband Positioning Systems: Theoretical Limits, Ranging Algorithms, and Protocols.* Cambridge, UK: Cambridge University Press, 2008.

[26] "IEEE 15-03-0489-03-004a-application-requirement-analysis-031127 v0.4.[online]," `http://www.ieee802.org/15/pub/TG4.html`.

[27] A. Goldsmith, *Wireless Communications.* Cambridge: UK: Cambridge University Press, 2005.

[28] E. Fishler, A. Haimovich, R. Blum, L. Cimini, D. Chizhik, and R. Valenzuela, "MIMO radar: An idea whose time has come," in *Proc. IEEE Int. Conf. on Radar*, Philadelphia, PA, Apr. 2004.

[29] J. Li and P. Stoica, "MIMO radar - diversity means superiority," in *Proc. 14th Adaptive Sensor Array Process. Workshop (ASAP'06, Invited)*, MIT Lincoln Laboratory, Lexington, MA, Jun. 2006.

[30] L. Xu, J. Li, and P. Stoica, "Radar imaging via adaptive MIMO techniques," in *Proc. 14th European Signal Processing Conf. (invited)*, Florence, Italy, Sept. 2006.

[31] S. Gezici and Z. Sahinoglu, "Ranging in a single-input multiple-output (SIMO) system," *IEEE Commun. Lett.*, vol. 12, no. 3, pp. 197–199, Mar. 2008.

[32] S. Haykin, "Cognitive radar: A way of the future," *IEEE Sig. Processing Mag.*, vol. 23, no. 1, pp. 30–40, Jan. 2006.

[33] Y. Zhao, H. H. Reed, S. Mao, and K. K. Bae, "Overhead analysis for radio environment mapenabled cognitive radio networks," in *Proc. IEEE Workshop on Networking Technologies for Software Defined Radio Networks*, Reston, VA, Sep. 2006, pp. 18–25.

[34] H. Celebi and H. Arslan, "Utilization of location information in cognitive wireless networks," *IEEE Wireless Commun. Mag.-Special issue on Cognitive Wireless Networks*, vol. 14, no. 4, pp. 6–13, Aug. 2007.

[35] S. Yarkan and H. Arslan, "Exploiting location awareness towards improved wireless system design in cognitive radio," vol. 46, no. 1, pp. 128–136, Jan. 2008.

[36] H. Celebi and H. Arslan, "Cognitive positioning systems," vol. 6, no. 12, pp. 4475–4483, Dec. 2007.

[37] P. Mahonen, M. Petrova, and J. Riihijarvi, "Applications of topology information for cognitive radios and networks," in *Proc. IEEE Symposium on New Frontiers in Dynamic Spectrum Access Networks (DySpan)*, Dublin, Ireland, Apr. 2007, pp. 103–114.

[38] H. Celebi and H. Arslan, "Adaptive positioning systems for cognitive radios," in *Proc. IEEE Symposium on New Frontiers in Dynamic Spectrum Access Networks (DySpan)*, Dublin, Ireland, Apr. 2007, pp. 78–84.

[39] ——, "Utilization of location information in cognitive wireless networks," *IEEE Wireless Comm.*, vol. 14, no. 4, pp. 6–13, Aug. 2007.

[40] R. Storn and K. Price, "Differential evolution - A simple and efficient heuristic for global optimization over continuous spaces," *Journal of Global Optimization*, vol. 11, pp. 341–359, 1997.

[41] R. Gamperle, S. D. Muller, and P. Koumoutsakos, "A parameter study for differential evolution," in *Advances in Intelligent Systems, Fuzzy Systems, Evolutionary Computation*, WSEAS Press, 2002, pp. 293–298.

[42] S. Gezici, Z. Tian, G. B. Giannakis, H. Kobayashi, A. F. Molisch, H. V. Poor, and Z. Sahinoglu, "Localization via UWB radios," vol. 22, no. 4, pp. 70–84, July 2005.

[43] S. Gezici, H. Celebi, H. V. Poor, and H. Arslan, "Fundamental limits on time delay estimation in dispersed spectrum cognitive radio systems," *IEEE Trans. Wireless Commun.*, vol. 8, no. 1, pp. 78–83, Jan. 2009.

[44] C. Williams, S. McLaughlin, and M. A. Beach, "Exploiting multiple antennas for synchronization," *IEEE Trans. Vehicular Technology*, vol. 58, no. 2, pp. 773–787, Feb. 2009.

[45] F. Kocak, H. Celebi, S. Gezici, K. A. Qaraqe, H. Arslan, and H. V. Poor, "Time delay estimation in cognitive radio systems," in *IEEE International*

Workshop on Computational Advances in Multi-Sensor Adaptive Processing (CAMSAP 2009), Dec. 2009, pp. 400–403.

[46] T. A. Weiss and F. K. Jondral, "Spectrum pooling: An innovative strategy for the enhancement of spectrum efficiency," vol. 42, no. 3, pp. 8–14, March 2004.

[47] S. Brandes, I. Cosovic, and M. Schnell, "Reduction of out-of-band radiation in OFDM based overlay systems," vol. 10, no. 6, pp. 420–422, June 2006.

[48] H. Mahmoud and H. Arslan, "Sidelobe suppression in OFDM-based spectrum sharing systems using adaptive symbol transition," vol. 12, no. 2, pp. 133–135, Feb. 2008.

[49] H. V. Poor, *An Introduction to Signal Detection and Estimation.* New York: Springer-Verlag, 1994.

[50] S. Gezici, Z. Sahinoglu, A. F. Molisch, H. Kobayashi, and H. V. Poor, "Two-step time of arrival estimation for pulse based ultra-wideband systems," *EURASIP Journal on Advances in Signal Processing*, vol. 2008, 2008.

[51] T.-H. Kim and I.-C. Park, "Two-step approach for coarse time synchronization and frequency offset estimation for IEEE 802.16D systems," in *Proc. IEEE Workshop on Signal Processing Systems*, Shanghai, China, Oct. 2007, pp. 193–198.

[52] A. Goldsmith, *Wireless Communications.* Cambridge, UK: Cambridge University Press, 2005.

[53] J. Kennedy and R. C. Eberhart, "Particle swarm optimization," in *Proceedings of IEEE International Conference on Neural Networks*, Piscataway, NJ., 1995, pp. 1942–1948.

[54] J. Vesterstrøm and R. Thomsen, "A comparative study of differential evolution, particle swarm optimization, and evolutionary algorithms on numerical benchmark problems," in *Congress on Evolutionary Computation (CEC2004)*, vol. 2, 2004, pp. 1980–1987.

[55] R. Storn and K. Price, *Differential evolution - A simple and efficient adaptive scheme for global optimization over continuous spaces*, Berkeley, 1995.

[56] F. Neri and V. Tirronen, "Recent advances in differential evolution: A survey and experimental analysis," *Artificial Intelligence Review*, vol. 33, no. 1-2, pp. 61–106, 2010.

[57] A. K. Qin and P. N. Suganthan, "Self-adaptive differential evolution algorithm for numerical optimization," in *Proc. IEEE Congress on Evolutionary Computation*, vol. 2, 2005, pp. 1785–1791.

[58] R. Mallipeddi and P. N. Suganthan, "Empirical study on the effect of population size on differential evolution algorithm," in *Proc. IEEE congress on Evolutionary Computation*, 2008, pp. 3663–3670.

[59] D. Wolpert and W. Macready, "No free lunch theorems for optimization," *IEEE Transactions on Evolutionary Computation*, vol. 1, no. 1, pp. 67–82, April 1997.

[60] J. Liu and J. Lampinen, "On setting the control parameter of the differential evolution algorithm," in *Proc. 8th International Mendel Conference on Soft Computing*, 2002, pp. 11–18.

[61] J. Rokkonen, S. Kukkonen, and K. V. Price, "Real-parameter optimization with differential evolution," in *Proc. IEEE International Conference on Evolutionary Computation*, vol. 1, pp. 506–513.

[62] H. Harada, K. Ikemoto, and R. Kohno, "Modulation and hopping using modified hermite pulses for UWB communications," in *Proc. IEEE Conference of Ultra Wideband Systems and Technologies (UWBST 2004)*, Kyoto, Japan, May 2004, pp. 336–340.

[63] C. Mitchell and R. Kohno, "High data rate transmissions using orthogonal modified hermite pulses in UWB communications," in *International Conferences on Telecommunications, ICT 2003*, vol. 2, March 2003, pp. 1278–1283.

[64] D. Tse and P. Viswanath, *Fundamentals of Wireless Communication*. Cambridge Univ. Press, 2005.